Deutsches Biomasseforschungszentrum
gemeinnützige GmbH

DBFZ REPORT NR. 53

Hydrothermal Conversion of Hemicellulose Sugars for the Production of Furfural

Doctoral thesis

Jakob Köchermann

With support from
Federal Ministry
of Food
and Agriculture
by decision of the
German Bundestag

IMPRINT

Publisher:
DBFZ Deutsches Biomasseforschungszentrum
gemeinnützige GmbH
Torgauer Straße 116
04347 Leipzig
Phone: +49 (0)341 2434-112
info@dbfz.de

Funding:
DBFZ Deutsches Biomasseforschungszentrum gemeinnützige GmbH, Leipzig, an enterprise of the German Government with funding from the Federal Ministry of Food and Agriculture pursuant to a resolution by the German Bundestag.

With support from
Federal Ministry
of Food
and Agriculture

by decision of the
German Bundestag

General Management:
Prof. Dr. mont. Michael Nelles
(Scientific Managing Director)
Dr. Christoph Krukenkamp
(Administrative Managing Director)

DBFZ Report Nr. 53
Hydrothermal Conversion of Hemicellulose Sugars
for the Production of Furfural
Leipzig: DBFZ, 2025
ISSN: 2197-4632 (Online)
ISBN: 978-3-949807-26-8
DOI: 10.48480/ecn9-4k74

Author:
Jakob Köchermann

Pictures:
If not indicated on the image: DBFZ, Stefanie Bader (Map)
Frontpage: freepik

Date of Publication:
3/4/2025

DIRECTIONS

By train: Arrival Leipzig main station; streetcar line 3/3E (direction Taucha/Sommerfeld) to stop Bautzner Straße; cross the street, leave the parking lot on the right and use the main entrance of the DBFZ (house 1, Torgauer Str. 116). Please register at the reception

By car: on the A 14 motorway. Exit at Leipzig Nord-Ost; follow signs for Taucha; then follow signs for Leipzig; then follow signs for Zentrum, Innenstadt. Turn off left after the “bft” filling station (see “By train” for further directions).

By tram: line 3/3 E towards Taucha/Sommerfeld; Bautzner Strasse stop (see “By train” for further directions)

The German National Library lists these publications in the German National Bibliography; detailed bibliographic data are available on the Internet at the address www.dnb.de.

Hydrothermal Conversion of Hemicellulose Sugars for the Production of Furfural

vorgelegt von
Dipl.-Ing.
Jakob Köchermann
ORCID: 0000-0002-0957-4743

an der Fakultät II – Mathematik und Naturwissenschaften
der Technischen Universität Berlin
zur Erlangung des akademischen Grades

Doktor der Ingenieurwissenschaften
- Dr.-Ing. -

genehmigte Dissertation

Promotionsausschuss:

Vorsitzender: Prof. Dr. Michael Gradzielski
Gutachter: Prof. Dr. Reinhard Schomäcker
Gutachterin: Prof. Dr. Andrea Kruse
Gutachter: Prof. Dr. Michael Nelles

Tag der wissenschaftlichen Aussprache: 05. Februar 2025

Berlin 2025

Danksagung

Diese Arbeit entstand während meiner Zeit am Deutschen Biomasseforschungszentrum und war geprägt von vielen Höhen und Tiefen. Deshalb möchte ich mich an dieser Stelle bei allen Menschen bedanken, die schlussendlich zum Gelingen der Arbeit beigetragen haben.

Zunächst möchte ich Herrn Prof. Dr. Reinhard Schomäcker meinen aufrichtigen Dank für die Übernahme der akademischen Betreuung und das mir entgegengebrachte Vertrauen aussprechen. Mein besonderer Dank gilt auch Frau Prof. Dr. Andrea Kruse und Herrn Prof. Dr. Michael Nelles für die Übernahme der Zweitgutachten. Ebenso danke ich Herrn Prof. Dr. Michael Gradzielski herzlich für die Übernahme des Vorsitzes des Prüfungsausschusses.

Besonderer Dank gebührt meinem Betreuer und Mentor, Dr. Marco Klemm, der mir die Chance eröffnete, diese Dissertation zu verfassen. Ich bin dir zutiefst dankbar für die inspirierenden Diskussionen und die Freiheit, die du mir für die Entwicklung eigener Ideen gewährt hast. Ein zusätzlicher Dank gebührt Dr. Franziska Müller-Langer für das entgegengebrachte Vertrauen sowie die motivierenden Impulse, die mich ermutigt haben, meine Komfortzone zu verlassen.

Weiterhin möchte ich mich ganz besonders bei Alexander Feist für die unfassbare Unterstützung beim Aufbau und der Erweiterung der Versuchsanlagen bedanken. Ohne seine Hilfe wäre vieles unmöglich geblieben. In gleicher Weise möchte ich mich bei Jessica Pester, Martin Apelt, Igor Adolf, Jana Mühlenberg und Kati Görsch für die Unterstützung bei der Probenanalytik bedanken. Mein Dank gilt auch Benjamin Herklotz, Roy Nitzsche, Paul Körner, Matthis Kurth, Sebastian Dietrich und Arne Gröngröft für die zahlreichen fachlichen Diskussionen, Anregungen und Motivationen. Ein besonderer Dank gilt zudem allen Studierenden, insbesondere Janine Schreiber, Raphael al Diban und Paulina Schulze, für ihre tatkräftige Unterstützung. Nicht zu vergessen sind meine Kolleginnen und Kollegen aus dem Bereich Bioraffinerien – danke für die unvergesslichen Mittagspausen, Geburtstagsfeiern, Diskussionen, Bereichsausflüge und Weihnachtsfeiern. All das und euch werde ich für immer in Erinnerung behalten und mit meiner Zeit am DBFZ verbinden.

Ein inniger Dank gilt meiner Familie, ohne die all dies nie möglich gewesen wäre. Ich danke meinen Eltern für ihre bedingungslose Unterstützung und Hilfe während

meines gesamten Studiums und der Zeit dieser Promotion. Philipp, danke, dass du immer an mich geglaubt und mich motiviert hast. Mein Dank gilt auch Rainer und Kerstin, die mir auf vielfältige Weise zur Seite standen.

Zu guter Letzt möchte ich meinen tiefsten Dank an Nadine, Hilda und Käthe richten. Danke für eure unendliche Geduld, für die Motivation, die ihr mir in schwierigen Zeiten geschenkt habt, und für die Freude, die wir in den schönen Momenten geteilt haben. Eure Aufmunterungen und euer Glaube an mich haben mir Kraft gegeben, auch in den anstrengendsten Phasen weiterzumachen. Ihr alle habt einen unschätzbaren Beitrag zu dieser Arbeit geleistet.

Leipzig, Februar 2025

Abstract

In the context of climate change and international efforts to achieve climate neutrality, the chemical industry is increasingly turning to renewable carbon sources. Existing renewable options such as recyclable plastics or CO_2 capture from the atmosphere are not sufficient or are too energy-intensive, giving biogenic resources a key role in the future supply of raw materials. Due to the global decline in agricultural land per capita and the desire not to compete with food production, biogenic residues from agriculture and forestry are becoming increasingly important. Lignocellulose biorefineries make it possible to efficiently break down biomass into its main components (cellulose, lignin, and hemicellulose). However, the use of hemicellulose, which can account for up to 35 % of the mass of biomass, remains commercially underrepresented.

The conversion of hemicellulose, primarily composed of pentoses, into furfural, a versatile platform chemical, holds significant potential. There are over 80 known applications in various industries based on furfural. However, furfural production presents several challenges. A recurring issue is the formation of humins, which not only reduce yield but can also lead to process-related problems such as blockages. For this reason, the aim of this work was to carry out reaction kinetic investigations using model substances and an organosolv-based hemicellulose hydrolysate and then to investigate and optimize new process approaches for furfural production.

The reaction kinetic studies were carried out in a continuous tubular reactor at temperatures of 160 to 200 °C, based on three reaction models. In addition to considering furfural degradation to include self-polymerization, the results were compared with existing literature. The models revealed differences in D-xylose conversion and furfural formation, with model 3, which includes a xylose intermediate, agreeing best with the experimental data.

It has been shown that short-chain alcohols such as ethanol can effectively reduce the formation of humins during furfural production. The study of acid-catalyzed conversion of xylose in water/ethanol mixtures showed that ethanol can significantly increase the furfural yield from 36-52 % to up to 90 %, while humin formation decreases by an average of 60 %. However, when Organosolv hemicellulose was used instead of xylose, no increase in furfural yield was observed, and an ethanol content of 50 % even led to a lower yield, which can be attributed to the reduced hydrolysis capacity due to the high ethanol content. Nevertheless, ethanol also contributed to the reduction of the humins formed.

Another method investigated in this work is hydrothermal reactive distillation (HRD). In this process, furfural is continuously removed via the vapor phase to prevent its degradation and the associated polymerization. Two biomasses and their hydrolysates were treated at temperatures of 170 to 210 °C using a steam releasing batch reactor. Analysis of the condensate and sump samples for reactants, products and by-products showed an outstanding efficiency of the HRD in terms of furfural yield (approx. 83 mol%) and purity, with no detection of residual sugars or humins in the condensate. The main by-products in the condensate were acetic acid and formic acid, while non-volatile substances such as levulinic acid and 5-hydroxymethylfurfural were enriched in the sump with a yield of up to 23 mol%.

Kurzfassung

Angesichts des Klimawandels und der internationalen Bestrebungen hin zur Klimaneutralität richtet die Chemieindustrie ihr Augenmerk zunehmend auf erneuerbare Kohlenstoffquellen. Vorhandene erneuerbare Optionen wie recycelbare Kunststoffe oder die CO_2-Abscheidung aus der Atmosphäre reichen jedoch nicht aus oder sind zu energieintensiv, was biogenen Ressourcen eine Schlüsselrolle in der zukünftigen Rohstoffversorgung zuweist. Die weltweit abnehmende landwirtschaftliche Nutzfläche pro Kopf und das Bestreben, keine Konkurrenz zur Nahrungsmittelproduktion zu schaffen, lassen biogene Reststoffe aus der Land- und Forstwirtschaft zunehmend an Bedeutung gewinnen. Lignocellulose-Bioraffinerien ermöglichen die effiziente Zerlegung von Biomasse in ihre Hauptbestandteile (Cellulose, Lignin und Hemicellulose). Die Nutzung von Hemicellulose, die bis zu 35 % der Biomasse ausmachen kann, bleibt jedoch bisher kommerziell unterrepräsentiert.

Die Umwandlung von Hemicellulose, primär bestehend aus Pentosen, zu Furfural, einer vielseitig einsetzbaren Plattformchemikalie, birgt erhebliches Potenzial. Es sind über 80 Anwendungen in verschiedenen Industriezweigen bekannt, die auf Furfural basieren. Trotz dieser vielversprechenden Aussichten stehen der Furfuralproduktion jedoch diverse Herausforderungen gegenüber. Eine häufig auftretende Problematik ist die Entstehung von Huminstoffen, die nicht nur die Ausbeute mindern, sondern auch zu prozesstechnischen Schwierigkeiten wie Verblockungen führen können. Aus diesem Grund sollten im Rahmen dieser Arbeit zunächst reaktionskinetische Untersuchungen anhand von Modellsubstanzen sowie eines organosolvbasierten Hemicellulose-Hydrolysats durchgeführt werden, um anschließend neue Verfahrensansätze zur Furfuralproduktion zu untersuchen und zu optimieren.

Die reaktionskinetischen Studien wurden in einem kontinuierlichen Rohrreaktor bei Temperaturen von 160 bis 200 °C durchgeführt, basierend auf drei Reaktionsmodellen. Neben der Betrachtung des Furfuralabbaus zur Berücksichtigung von Selbstpolymerisation wurden die Ergebnisse mit der bestehenden Literatur verglichen. Auf Grundlage der Modelle konnten Unterschiede im D-Xylose-Umsatz und in der Furfuralbildung aufgezeigt werden, wobei Modell 3, das ein Xylose-Zwischenprodukt berücksichtigt, am besten mit den experimentellen Daten übereinstimmte.

Es hat sich herausgestellt, dass kurzkettige Alkohole wie Ethanol effektiv die Bildung von Huminstoffen während der Furfuralproduktion reduzieren können. Die Untersuchung der säurekatalysierten Umwandlung von D-Xylose in Wasser/Ethanol-Gemischen zeigte, dass Ethanol die Furfuralausbeute signifikant von 36 – 52 mol% auf bis zu 90 mol% steigern kann, während die Huminstoffbildung um durchschnittlich 60 % abnimmt. Bei der Verwendung von Organosolv-Hemicellulose anstelle von D-Xylose wurde jedoch keine Erhöhung der Furfuralausbeute festgestellt, und ein Ethanolgehalt von 50 % führte sogar zu einer geringeren Ausbeute. Dies könnte auf die verminderte Hydrolysefähigkeit aufgrund des hohen Ethanolgehalts zurückgeführt werden. Dennoch trug Ethanol auch in diesem Fall zur Verringerung der sich bildenden Huminstoffe bei.

Eine weitere Methode, die in dieser Arbeit untersucht wurde, ist die hydrothermale Reaktivdestillation (HRD). Dabei wird Furfural kontinuierlich über die Dampfphase entfernt, um dessen Abbau und die damit einhergehende Polymerisation zu verhindern. Zwei Arten von Biomasse sowie deren Hydrolysate wurden bei Temperaturen von 170 bis 210 °C in einem Batch-Reaktor mit Dampfabscheidung behandelt. Die Analyse der Kondensat- und Sumpfproben hinsichtlich Reaktanten, Produkten und Nebenprodukten ergab eine herausragende Effizienz der HRD in Bezug auf die Furfuralausbeute (ca. 83 mol%) und Reinheit, ohne Nachweis von Restzucker oder Huminstoffen im Kondensat. Die Hauptnebenprodukte im Kondensat waren Essig- und Ameisensäure, während im Sumpf nichtflüchtige Stoffe wie Lävulinsäure und 5-Hydroxymethylfurfural mit einer Ausbeute von bis zu 23 mol% angereichert wurden.

Erklärung zur Dissertation

Ich erkläre hiermit, dass ich meine Promotionsabsicht bisher an keiner anderen Hochschule oder Fakultät beantragt habe. Die vorliegende kumulative Dissertation wurde bereits in Form von wissenschaftlichen Publikationen veröffentlicht (PAPER 1-4). Es handelt sich dabei um die folgenden Artikel, die chronologisch anhand des Publikationsdatums aufgelistet sind. Für alle in dieser Arbeit vorkommenden veröffentlichten Artikel liegen die entsprechenden Genehmigungen der Verlage zur Zweitpublikation (reprint permissions) vor.

PAPER 1: Kinetics of Hydrothermal Furfural Production from Organosolv Hemicellulose and D-Xylose
Jakob Köchermann, Jana Mühlenberg, Marco Klemm
Industrial & Engineering Chemical Research (2018), 57 (43), S. 14417–14427

In diesem Artikel wird die kinetische Untersuchung der hydrothermalen Furfuralproduktion aus Organosolv-Hemicellulose sowie dem Modellsubstrat D-Xylose behandelt. Hierfür wurden drei unterschiedliche Reaktionsmechanismen bzw. kinetische Modelle entwickelt und mittels experimentell erhobener Daten hinsichtlich ihrer Vorhersagegenauigkeit evaluiert. Die analysierten Reaktionsmechanismen berücksichtigen die Hydrolyse von Oligopentosen und unterscheiden sich in den spezifischen Mechanismen hinsichtlich der Furfuralbildung und -zersetzung. Um den Effekt der Selbstpolymerisation von Furfural einzubeziehen, wurden zusätzliche kinetische Untersuchungen durchgeführt, deren Ergebnisse in die Modelle integriert wurden. Diese methodische Herangehensweise ermöglicht eine detaillierte Bewertung der Genauigkeit verschiedener Modelle zur Vorhersage der Reaktionsabläufe unter diversen Bedingungen und leistet somit einen wesentlichen Beitrag zur Optimierung des Furfuralherstellungsprozesses.

Die konzeptionelle Entwicklung dieser Studie, die Modifizierung der Versuchsanlage, die Planung und Durchführung der Experimente sowie die Berechnung und Auswertung der kinetischen Daten wurden von mir durchgeführt. Jana Mühlenberg war verantwortlich für die Entwicklung und Durchführung der Probenanalyse mittels HPLC. Das Manuskript, mit Ausnahme des Analytikteils, sowie sämtliche Diagramme und Abbildungen wurden eigenständig von mir erstellt. Marco Klemm übernahm die Projektleitung und leistete einen entscheidenden Beitrag zur Interpretation der Ergebnisse und trug somit zur Fertigstellung und Überarbeitung des Manuskripts bei.

PAPER 2: Conversion of D-Xylose and Hemicellulose in Water/Ethanol Mixtures
Jakob Köchermann, Janine Schreiber, Marco Klemm
ACS Sustainable Chemistry Engineering (2019), 7 (14), S. 12323–12330

Die zweite Studie konzentrierte sich zunächst auf die Untersuchung des Ethanol-Einflusses auf den Furfuralherstellungsprozess unter Verwendung von D-Xylose als Modellsubstrat. Dazu wurden Experimente mit unterschiedlichen Ethanol-Wasser-Mischverhältnissen durchgeführt und deren Ergebnisse mit solchen aus ethanolfreien Versuchen verglichen. Ziel war es, den spezifischen Einfluss von Ethanol durch die Ermittlung und den Vergleich kinetischer Daten zu charakterisieren, insbesondere in Bezug auf die Bildung von unlöslichen Huminen. Weiterhin wurde die Tauglichkeit einer realen Hemicelluloselösung (Organosolv-Hemicellulose) für diesen spezifischen Prozess evaluiert.

Die Idee und die wissenschaftliche Fragestellung dieser Studie stammen von mir. Auch der Aufbau der Versuchsanlage, die Etablierung der Versuchsmethodik sowie die Versuchsplanung wurden von mir übernommen. Im Rahmen ihrer Masterarbeit führte Janine Schreiber sämtliche Experimente sowie die Analysen der Proben mittels HPLC durch. Die Anfertigung des Manuskripts und die damit verbundene Erstellung von Diagrammen und Abbildungen erfolgten eigenständig durch mich. An der Interpretation der Ergebnisse waren neben Janine Schreiber auch Marco Klemm maßgeblich beteiligt. Die kinetischen Auswertungen wurden von mir vorgenommen. Darüber hinaus war Marco Klemm an der Überarbeitung und Fertigstellung des Manuskripts beteiligt.

PAPER 3: Platform and fine chemicals from woody biomass. Demonstration and assessment of a novel biorefinery
Roy Nitzsche, Arne Gröngröft, **Jakob Köchermann**, Kathleen Meisel, Hendrik Etzold, Marlen Verges, Moritz Leschinsky, Julian Bachmann, Bodo Saake, Sandra Torkler, Katja Patzsch, Björn Rößiger, Daniela Pufky-Heinrich, Gerd Unkelbach
Biomass Conversion and Biorefinery (2021), 11, S. 2369-2385

Das Ziel dieser Studie war es, eine neu entwickelte Lignocellulose-Bioraffinerie experimentell zu demonstrieren und zu evaluieren. Diese Raffinerie konzentriert sich auf die Integration von Produkten auf Buchenholzbasis, die sowohl als Plattform- als auch als Spezialchemikalien dienen. Der Prozess umfasste den Organosolv-Aufschluss, gefolgt von der Bleiche des Zellstoffs, der hydrothermalen Umwandlung von Hemicellulose in Xylose und deren Aufreinigung, der Fermentation von Xylose zu Äpfelsäure sowie der basenkatalysierten Depolymerisation von Lignin.
Die konzeptionelle Entwicklung dieser Veröffentlichung wurde in Zusammenarbeit mit Roy Nitzsche, Arne Gröngröft, Hendrik Etzold und Kathleen Meisel realisiert. Die Planung, Durchführung, Auswertung und Verschriftlichung der experimentellen Ergebnisse zur hydrothermalen Valorisierung von Hemicellulose wurden von mir übernommen. Die weiterhin aufgeführten experimentellen Arbeiten wurden von Roy Nitzsche, Marlen Verges, Moritz Leschinsky, Julian Bachmann, Bodo Saake, Sandra Torkler, Katja Patzsch, Björn Rößiger und Daniela Pufky-Heinrich ausgeführt. Die techno-ökonomische sowie ökologische Analyse wurde durch Hendrik Etzold und Kathleen Meisel durchgeführt. Die Gesamtergebnisse dieser Studie wurden gemeinsam mit allen Co-Autoren diskutiert, evaluiert und interpretiert.

PAPER 4: Hydrothermal Reactive Distillation of Biomass and Biomass Hydrolysates for the Recovery and Separation of Furfural and Its Byproducts
Jakob Köchermann, Marco Klemm
Industrial & Engineering Chemical Research (2023), 62 (18), S. 6886–6896

In dieser Studie wurde die kontinuierliche Abtrennung von Furfural aus zwei lignocellulosehaltigen Biomassen (Dinkelspelzen und Buchenholz) sowie aus deren hemicellulosereichen Hydrolysaten über die Dampfphase mittels hydrothermaler Reaktivdestillation (HRD) untersucht. Diese Methode zielt darauf ab, die Nebenreaktionen bei der Furfuralproduktion zu verhindern und so die Ausbeute und Reinheit des Zielproduktes zu steigern. Gleichzeitig sollten etwaige Nebenprodukte identifiziert werden, die ebenfalls über die Dampfphase abgeleitet werden könnten.

Auch die Zuordnung der im Sumpf verbleibenden Nebenstoffe war Gegenstand der Untersuchung.

Die Entwicklung des Konzepts sowie die Anpassungen am Versuchsstand, die Planung und die Durchführung der Experimente lagen in meiner Verantwortung. Die Vorhydrolysen zur Erzeugung des Dinkelspelzenhydrolysats wurden von Stefan Römerscheid (Labortechniker) ausgeführt. Jessica Pester (Laborantin) übernahm in Absprache mit Jana Mühlenberg (Leitung Analytiklabor) die Durchführung der HPLC-Analysen. Martin Apelt (Laborant) führte die GC-FID-Analysen, ebenfalls in Koordination mit Jana Mühlenberg, durch. Die Borat-AEC-Analysen zur Ermittlung der biopolymeren Zusammensetzung der eingesetzten Biomassen wurden von Herrn Prof. Bodo Saake am Institut für Holzwissenschaften der Universität Hamburg im Rahmen eines Unterauftrages durchgeführt. Die Erstellung des Manuskripts sowie aller Abbildungen und Diagramme oblag mir. Marco Klemm spielte eine entscheidende Rolle bei der Dateninterpretation sowie beim Abschluss- und Überarbeitungsprozess des Dokuments.

List of Publications

1. **Köchermann, Jakob**; Mühlenberg, Jana; Klemm, Marco (2018): Kinetics of Hydrothermal Furfural Production from Organosolv Hemicellulose and D-Xylose. In: Ind. Eng. Chem. Res. 57 (43), S. 14417–14427. DOI: 10.1021/acs.iecr.8b03402.

2. **Köchermann, Jakob;** Schreiber, Janine; Klemm, Marco (2019): Conversion of D-Xylose and Hemicellulose in Water/Ethanol Mixtures. In: ACS Sustain. Chem. Eng. 7 (14), S. 12323–12330. DOI: 10.1021/acssuschemeng.9b01697.

3. Nitzsche, Roy; Gröngröft, Arne; **Köchermann, Jakob**; Meisel, Kathleen; Etzold, Hendrik; Verges, Marlen; Leschinsky, Moritz; Bachmann, Julian; Saake, Bodo; Torkler, Sandra; Patzsch, Katja; Rößiger, Björn; Pufky-Heinrich, Daniela; Unkelbach, Gerd (2021): Platform and fine chemicals from woody biomass. Demonstration and assessment of a novel biorefinery. In: Biomass Conv. Bioref. 11 (6), S. 2369–2385. DOI: 10.1007/s13399-020-00769-z.

4. **Köchermann, Jakob;** Klemm, Marco (2023): Hydrothermal Reactive Distillation of Biomass and Biomass Hydrolysates for the Recovery and Separation of Furfural and Its Byproducts. In: Ind. Eng. Chem. Res. 62 (18), S. 6886-6896. DOI: 10.1021/acs.iecr.3c00259.

Further Publications during this Work

Listed below in chronological order are all other publications that were published during my time at the DBFZ Deutsches Biomasseforschungszentrum, in the Biorefineries Department, as part of my doctorate, but which were not included in this thesis.

5. **Köchermann, Jakob**; Görsch, Kati; Wirth, Benjamin; Mühlenberg, Jana; Klemm, Marco (2018): Hydrothermal carbonization: Temperature influence on hydrochar and aqueous phase composition during process water recirculation. In: J. Environ. Chem. Eng. 6 (4), S. 5481–5487. DOI: 10.1016/j.jece.2018.07.053

6. **Köchermann, Jakob**; Klüpfel, Christian; Klemm, Marco (2020): Brønsted/Lewis-Acid Combinations for Hydrothermal Production of Levulinic Acid from Starch Residues. In: P. Mauguin, Nicolae Scarlat, A. Grassi und P. Helm (Hg.): Papers of the 28th European Biomass Conference. Bioeconomy's role in the post-pandemic economic recovery. Extracted from the Proceedings of the International Conference held virtually. 6 – 9 July 2020. 28th European Biomass Conference and Exhibition. [online], 06.-09.07.2020. Florenz (Italien): ETA-Florence Renewable Energies, S. 515–519. DOI: 10.5071/28thEUBCE2020-3AO.9.4.

7. Pujan, Robert; Nitzsche, Roy; **Köchermann, Jakob**; Preisig, Heinz A. (2020): Modelling Ontologies for Biorefinery Processes – A Case Study. In: Sauro Pierucci, Flavio Manenti, Giulia Luisa Bozzano und Davide Manca (Hg.): 30th European Symposium on Computer Aided Process Engineering, Bd. 48: Elsevier (Computer Aided Chemical Engineering), S. 1963–1968. DOI: 10.1016/B978-0-12-823377-1.50283-4.

8. Nitzsche, Roy; **Köchermann, Jakob;** Gröngröft, Arne; Kraume, Matthias (2021): Nanofiltration of Organosolv Hemicellulose Hydrolyzate. Influence of Hydrothermal Pretreatment and Membrane Characteristics on Filtration Performance and Fouling. In: Ind. Eng. Chem. Res. 60 (2), S. 916–930. DOI: 10.1021/acs.iecr.0c03256.

List of Figures and Schemes

Figures

Schemes

List of Tables

Table of Contents

Nomenclature

Abbreviations

2G	Second generation
AA	Acetic acid
AEC	Anion exchange chromatography
AISI	American Iron and Steel Institute
ANOVA	Analysis of variance
Ara	Arabinose
BMIM	1-Butyl-3-methylimidazolium
BV	Ball valve
BWS	Beech wood shavings
C5	Pentose sugars
C6	Hexose sugars
CBP	Chemical-Biotechnological Processes
CCF	Face-centered central composite design
CIMV	Compagnie Industrielle de la Matière Végétale
CoP	Condensation products
CPME	Cyclopentyl methyl ether
CTR	Continuous tube reactor without plug flow
CW	Cool water
CyH	Cyclohexane
DAD	Diode array detector
DB-FFAP	Durable bonded free fatty acid phase
DMSO	Dimethyl Sulfoxide
DOE	US Department of Energy
DSTR	Discontinuous stirred tank reactors
EMIM	1-Ethyl-3-methylimidazolium
FA	Formic acid
FID	Flame ionization detector
Fu	Furfural
Gal	Galactose
GC	Gas chromatograph
GVL	Gamma-Valerolactone
hb	High boiling point
HMF/5-HMF	5-Hydroxymethylfurfural
HPLC	High-performance liquid chromatography
HRD	Hydrothermal reactive distillation

HT	Hydrothermal treatment
HYP	Hypothesis
Int	Intermediate
LA	Levulinic acid
lb	Low boiling point
M	Motor
Man	Mannose
MCM	Mobil Composition of Matter
MIBK	Methyl Isobutyl Ketone
MTC	Multi-Turbine-Column
MTHF	2-Methyltetrahydrofuran
NRTL	Non-Random Two-Liquid
NV	Needle valve
OHC	Organosolv hemicellulose
PFR	Plug flow reactor
PI	Pressure indicator
PR	Pressure regulator
PTFE	Polytetrafluorethylene
ReP	Resinification products
Rha	Rhamnose
RID	Refractive index detector
RSM	Response surface methodology
SA	Sulfuric acid
SBA	Santa Barbara Amorphous
SH	Spelt husks
SHH	Spelt husk hydrolysate
TC	Temperature controller
THF	Tetrahydrofuran
USY	Ultra-stable Y zeolite
Xos	Xylooligosaccharide
Xy	Xylose
ZSM	Zeolite Socony Mobil

Symbols, Subscripts, and Superscripts

Symbol	Unit	Description
A	Depending on order	Pre-exponential factor
$[\mathrm{Ara}]$	mol L^{-1}	Arabinose concentration
$[\mathrm{BP}]$	mol L^{-1}	By-product concentration
β	mol%	Regression coefficient
c	g L^{-1}	Concentration
$\hat{c}$	g L^{-1}	Predicted concentration by regression model
$[\mathrm{CE}]$	mol L^{-1}	Cellulose concentration
E	J mol^{-1}	Activation energy
$[\mathrm{Fu}]$	mol L^{-1}	Furfural concentration
$[\mathrm{Glu}]$	mol L^{-1}	Glucose concentration
$[\mathrm{H}^{+}]$	mol L^{-1}	Hydrogen ion concentration
$[\mathrm{HC}]$	mol L^{-1}	Hemicellulose concentration
$[\mathrm{Hex}]$	mol L^{-1}	Hexose concentration
$[\mathrm{Int}]$	mol L^{-1}	Intermediate product concentration
k	s^{-1}	Rate constant
K	-	Dissociation constant
m	g	Mass
n	-	Number of experimental data
R	J mol^{-1} K^{-1}	Universal gas constant
R^2	-	Coefficient of determination
S	%	Selectivity
t	min	Time
T	°C	Temperature
V	mL	Volume
x	-	Variables
X	mol%	Conversion
$[\mathrm{Xos}]$	mol L^{-1}	Xylooligosaccharide concentration
$[\mathrm{Xy}]$	mol L^{-1}	Xylose concentration
Y	mol%	Yield
$\hat{Y}$	mol%	Predicted yield by regression model

Subscript	Unit	Description
0	-	Before the reaction
1	-	After the reaction
BP	-	By-product
C5	-	Pentose
F	-	Furfural
Feed	-	Feedstock
Fu	-	Furfural
Glu	-	Glucose
H2O	-	Water
HC	-	Hemicellulose

max	-	Maximum
Pred	-	Predicted
R	-	Reaction
S	-	Sump
t	-	Reaction time
T	-	Temperature
W	-	Water
Xy	-	Xylose
Ymax	-	Maximum yield
i	-	Continuous index (i = 1, 2, ...)
j	-	Running index

Superscript	**Unit**	**Description**
m	-	Acid concentration exponent

1 Introduction

1.1 Background

Climate change, primarily caused by the start of industrialization and the associated burning of fossil resources such as coal, oil, and gas, has motivated the international community to set climate neutrality targets. These targets aim to limit global warming to a maximum of 2 °C by the middle of the century.[1] Against this backdrop, the chemical industry, which is responsible for 18 % of global annual industrial CO_2 emissions,[2] is facing the most extensive transformation in its history. The carbon-based chemical industry is dependent on the use of fossil resources. Accordingly, only three feedstocks are available for the defossilization of carbon-based chemistry: Recyclable plastics, CO_2 from the atmosphere, and biomass. While the amount of recyclable plastics is not sufficient to cover the carbon requirements of the chemical industry alone, the direct air capture of CO_2 is highly energy-intensive.[3] For this reason, a significant proportion of renewable carbon must come from biogenic resources in the future.

Biomass is a globally available resource. However, global arable land per capita is constantly decreasing due to population growth, land sealing, and the influence of climate change.[4] For this reason, the use of biomass must adhere to a so-called cascade utilization, whereby food provision has the highest priority.[5] Against this background, biogenic residues from agriculture, forestry, and the pulp and paper industry are of crucial importance, as they do not compete directly with food production. These biogenic residues are primarily composed of lignocellulosic biomass, which is divided into three main constituents: cellulose, hemicellulose, and lignin. While cellulose and hemicellulose are biopolymers consisting of C6 (hexoses) and C5 (pentoses) sugars, respectively, lignin is a polymer made up of aromatic building blocks. These fractions are made available in so-called lignocellulose biorefineries through pulping processes.

The quality and yield of the lignocellulose fractions depends on both the pulping process and the biomass used.[6] One process that has received a lot of attention in recent years is the organosolv process.[7–10] In this process, lignocellulose is decomposed by means of a water-organic solvent mixture at temperatures of 130 – 200 °C and pressures up to 40 bar, in the presence or absence of acid and alkali catalysts such as sulfuric acid and sodium hydroxide.[8] The hemicellulose and lignin fractions are dissolved from the cellulose. By successively reducing the solvent content, the lignin is then separated from the hemicellulose through precipitation. The hemicellulose remains in dissolved form in the aqueous hydrolysate. Thus, the organosolv process offers the possibility of obtaining all three lignocellulose fractions in particularly high purity.

The economic success of such an organosolv biorefinery concept heavily depends on the development of effective value chains for the individual lignocellulose fractions. There are already a wide range of utilization paths for cellulose, for example, as cellulose pulp for the paper industry[11,12] or dissolving pulp for textile[13,14] industry. Further applications include the provision of hexoses[15] for fermentation processes (bioethanol, lactic acid, etc.)[16,17] In contrast, hemicellulose and lignin have only a few commercial fields of application to date. Lignin, characterized by its high calorific value,[18] is therefore often used for process heat recovery. More recently, the industrial use of lignin as a functional filler in various plastics and rubber applications has become established.[19] So far, the commercial use of hemicellulose has received little attention, although various utilization strategies have been developed. One promising approach is the production of furfural from hemicellulose.

Furfural is a versatile chemical with an estimated annual global market volume of 365,000 tons in 2022, and it is expected to grow to nearly 500,000 tons by 2030.[20] Due to its wide array of application capabilities, furfural is considered one of the platform chemicals. In 2004, the US Department of Energy (DOE) classified furfural as one of the Top 10 bio-based platform chemicals.[21] To date, it serves as a precursor or direct component in the synthesis of over 80 chemicals across diverse sectors, including plastics, pharmaceuticals, agrochemicals, solvents, and biofuels..[22]

Furfural is conventionally produced directly from hemicellulose-rich biomass, such as corn cobs or bagasse. The process is very simple and has barely changed since its commercial introduction in 1921.[23,24] The biomass is first impregnated with mineral acids, usually sulfuric acid, and then treated with large quantities of superheated steam (16.2 tons/ton of furfural).[25] The resulting furfural is discharged via the steam fraction. The acid-contaminated biomass residue is then neutralized and subjected to thermal disposal. During neutralization, substantial amounts of salt fractions are generated, which must be disposed of.[26] Furthermore, the value-added path of this process is limited to the hemicellulose, with up to 70 % of the biomass remaining unused.

On the other hand, the production of furfural from hemicellulose fractions obtained through lignocellulose biorefinery processes, such as the organosolv process, represents promising optimization potential. The advantage lies in the hemicellulose being already isolated. As a result, there are fewer interactions with other components and degradation products of the lignin or cellulose fraction during the conversion to furfural. This also makes the pentoses more accessible, potentially accelerating the reaction process. Utilizing all lignocellulose fractions leads to significantly higher overall material utilization of the biomass. Given that hemicellulose from biorefinery processes is present in an aqueous phase, hydrothermal processes, in which water under subcritical conditions acts as both solvent and reaction medium, offer great potential, especially as no additives need to be added to the process.

However, so far, the production of furfural from aqueous hemicellulose fractions has been limited to a research context.[27–32] Accompanying substances and impurities found in such hemicellulose fractions lead to issues with furfural yields and purity. For this reason, various investigations have been conducted on different hemicellulose hydrolysates in recent years to identify problematic accompanying substances and other interfering factors. These methods can be broadly divided into four approaches: (1) the use and development of homogeneous[33,34] and heterogeneous[35,36] catalysts, (2) reactive extraction using biphasic systems,[37–39] (3) monophasic solvent mixtures consisting of water and an organic solvent,[40,41] and (4) reactive distillation using steam or nitrogen.[42,43]

1.2 Aim of this Thesis

In light of the aforementioned considerations, the overall objective of this dissertation was to enhance the efficiency and yield of furfural production from biomass-derived feedstocks, with a particular focus on organosolv hemicellulose. This was achieved by investigating a variety of chemical engineering processes and conditions. For this purpose, a real organosolv hemicellulose solution based on beech wood was available. Starting from this basis, the following three hypotheses were to be investigated:

(HYP-1) The use of advanced kinetic models, which consider sugar oligomers and furfural degradation, will significantly improve the ability to accurately predict furfural production from D-xylose and organosolv hemicellulose, leading to more effective process control and optimization.

(HYP-2) The introduction of ethanol as a co-solvent in the acid-catalyzed conversion of D-xylose and organosolv hemicellulose to furfural is expected to lead to a substantial increase in furfural yield while simultaneously reducing the formation of humins.

(HYP-3) Hydrothermal reactive distillation (HRD) as a separation technique will significantly enhance furfural yield and purity by effectively minimizing side reactions during production. The continuous stripping of furfural from the reaction mixture via the vapor phase will prevent the accumulation of undesirable by-products.

The initial aim of the kinetic investigations (**Paper 1**) was to identify a suitable reaction model that accurately represents the reaction process. To study the degradation of furfural without the influence of other accompanying substances, furfural degradation studies were conducted under hydrothermal conditions using a continuous tubular reactor. For this study, no catalysts or other additives were added to the organosolv hemicellulose. Ultimately, the goal was to identify the ideal reaction conditions based on the kinetic model.

The introduction of ethanol as a co-solvent was carried out in a discontinuous stirred tank reactor. The aim of this study (**Paper 2**) was to investigate the influence of alcohol proportion on D-xylose conversion, furfural yield, and humin formation, using a D-xylose solution or organosolv hemicellulose liquor, respectively. Therefore, different water/ethanol mixtures were used to investigate the influence of the alcohol content on furfural synthesis and to evaluate the impact on the formation of humins. Results were compared with experiments without the addition of ethanol. Based on the determination of the kinetic parameters, using a simplified reaction mechanism, an objective evaluation of the ethanol influence could be made. Finally, a hemicellulose liquor made from an ethanol-based organosolv process was used to observe the behavior of a real feedstock under the given conditions.

For the investigation of hydrothermal reactive distillation (**Paper 4**), a stirred tank reactor was equipped with a reflux condenser. The study aimed to investigate the suitability of phosphoric acid, as well as the temperature behavior on furfural yield and on the enrichment of byproducts in the sump and condensate, using real biogenic feedstocks. For this purpose, two types of biomasses, spelt husks (SH) and beech wood shavings (BWS), along with a hydrothermally produced spelt husk hydrolysate and a beechwood-based organosolv hydrolysate, were used.

1.3 Outline

In order to investigate the aforementioned hypotheses, the work is structured as schematically shown in Figure 1.1 below.

Chapter 2 provides a comprehensive overview of the current state of scientific knowledge, starting with a detailed explanation of the structure of hemicellulose, the starting material for furfural production. This is followed by a detailed description of the target product, furfural, highlighting its physical properties, current areas of application, and economic conditions. The formation and degradation mechanisms of furfural are then described in detail, before concluding the chapter with a comprehensive overview of various furfural production methods.

Chapter 3 provides a detailed description of all the materials and methods required for this thesis, including precise explanations of the experimental equipment, kinetic modeling, and calculations used to achieve the research objectives.

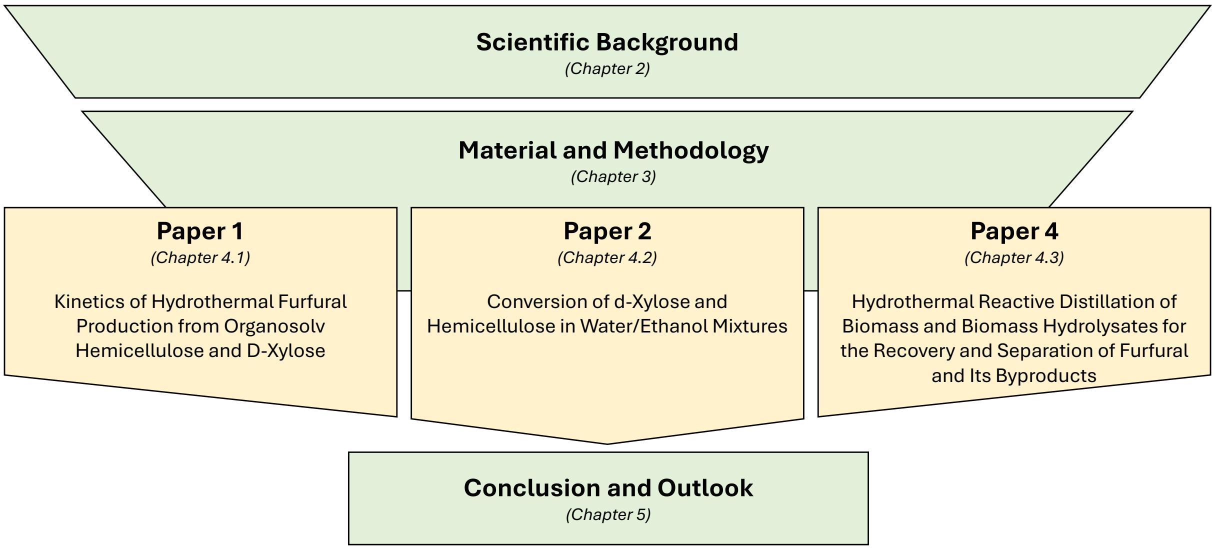

Figure 1.1 Schematic overview of the thesis structure.

Chapter 4 represents the main part of this cumulative dissertation and highlights the key findings from three scientific papers published in established peer-reviewed journals. It first examines in detail the kinetic study of furfural production from organosolv hemicellulose and D-xylose, investigates the efficiency of converting D-xylose and organosolv hemicellulose to furfural using water/ethanol mixtures, and discusses the benefits of hydrothermal reactive distillation for processing biomass and biomass hydrolysates.

Finally, **Chapter 5** summarizes the main results and findings, critically evaluating them with regard to potential weaknesses and limitations of the studies. To conclude, an outlook for future studies, based on the knowledge gained in this thesis, is provided.

2 Scientific Background

2.1 Hemicellulose

Hemicellulose is the world's second most abundant carbohydrate, after cellulose, with an estimated annual production of 45 billion tonnes.[44] This diverse polymer primarily consists of pentoses (xylose, arabinose), hexoses (glucose, mannose, galactose), uronic acids (glucuronic and 4-O-methyl-glucuronic acids), and acetyl groups (Figure 2.1). Unlike cellulose, hemicellulose does not form a crystalline structure, which is due to its heterogeneously structured and branched polymer chains. While cellulose consists of 500 to 15,000 glucose units, polymers of hemicellulose are shorter, containing only about 50 to 200 sugar monomers. Nonetheless, hemicelluloses are classified according to their repeated sugar units in the main chain as xylans (xylose), mannans (mannose), or galactans (galactose). However, the structure and composition of hemicelluloses significantly vary depending on the plant species (Table 2.1). In hardwoods, hemicellulose consists mainly of xylans, while in softwoods mannans and xylans dominate. Furthermore, softwood hemicellulose is characterized by a lower proportion of acetyl groups. Grasses, such as wheat or maize, also contain hemicelluloses, but with a higher proportion of arabinoxylans. [44,45]

Table 2.1 Distribution of hemicellulose polysaccharides in different plant species. Data adopted from [44,46,47]

Species	Xyl	Ara	Man	Gal	Rha	Uronic acid	Acetylated
				(wt%)			
Softwood	3-8	1-2	8-14	1-6	< 0.3	1.8-5	< 1.6
Hardwood	15-25	0.4-1	1-4	0.7-1.5	< 0.6	3.5-6	3-4
Grasses	4-17	2-4	1-3	0.1-2	-	2-3.6	0.5-3

Due to its heterogeneity, amorphous structure, and lower degree of polymerization, hemicellulose is much more soluble in water and alkali solutions than cellulose. Generally, hemicelluloses from hardwoods are less resistant to alkali hydrolysis compared to those from softwoods, due to their structure and composition.

This is partly because hemicelluloses from hardwoods often have a higher number of substituents, such as O-acetyl groups and 4-O-methylglucuronic acid, which tend to be more easily degraded at alkaline pH. In softwoods, the removal of reducing ends of xylans, such as galacturonic acid, contributes to the stabilization of hemicellulose. This property is essential for its processing and extraction from biomass, especially in the context of furfural production.[46]

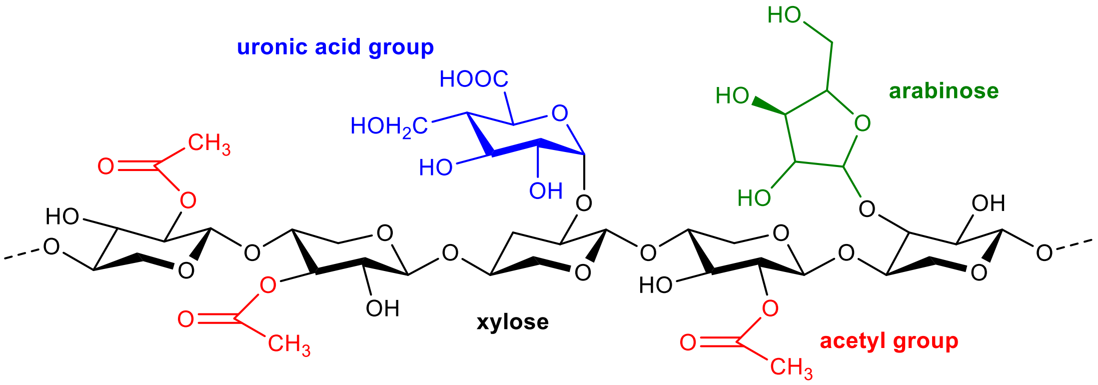

Figure 2.1 Simplified structure of hemicellulose with D-xylose backbone.

Furfural is typically produced from hemicellulose through a dehydration process, often carried out in the presence of an acid catalyst. Initially, hemicellulose undergoes hydrolysis to break down its polysaccharide structure into smaller sugar units, including D-xylose. Then, under acidic or autocatalytic conditions and at elevated temperatures, D-xylose undergoes dehydration to form furfural, along with water as a byproduct (Figure 2.2).

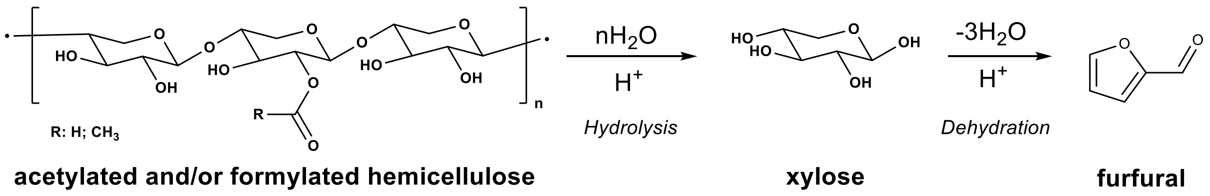

Figure 2.2 Reaction path of furfural from hemicellulose over D-xylose.

Not only the internal composition of the hemicellulose differs depending on the biomass species, but also the total proportion of hemicellulose. For this reason, biomass with a high hemicellulose content is typically used for the production of furfural (Figure 2.3). Consequently, most industrial processes utilize corncobs or oat hulls. In regions where sugar cane is cultivated, the fibrous remains, known as bagasse, are also utilized, primarily in the Dominican Republic and South Africa. Looking ahead, with an increasing number of lignocellulosic biorefineries, the direct utilization of hemicellulose, also known as biomass hydrolysates, could become a promising feedstock for furfural production. The crucial advantage of these new feedstocks lies in the abundant availability of hemicellulose. In contrast, in established processes, hemicellulose remains bound within the lignocellulosic matrix and must be released prior to use. In addition, the utilization of hemicellulose, such as for furfural production, has the potential to enhance the economic viability of lignocellulose biorefinery processes. Interesting entry points are, for instance, so-called 2G ethanol plants. These facilities utilize lignocellulose residues such as wheat straw or bagasse to fractionate the biomass into its constituents, after which the cellulose and hemicellulose then being fermented into ethanol. Another approach involves integrating hemicellulose utilization into wood pulp production, where hydrolysate can be derived through pretreatment processes and further converted into furfural. The pulp and paper industry alone offer enormous potential for hemicellulose utilization, as over 300 million tons of woody biomass (mainly softwood) are utilized annually.[50] Approximately 50 % of this biomass, containing pentosans (8.5 %), hexosans (12 – 12.8 %), and lignin (27 – 28.6 %), is currently used for energy recovery in the pulping process.[44,50] New biorefinery projects, such as that of the Finnish company UPM in Leuna (Germany), use beech wood residues to produce monoethylene and propylene glycol derived from the cellulose fraction. The refinery aims to process up to 500,000 tons of beech wood annually by the end of 2024.[51] Additionally, for the first time, lignin will be utilized in this biorefinery. However, strategies for commercializing the resulting hemicellulose have not yet been published.[52]

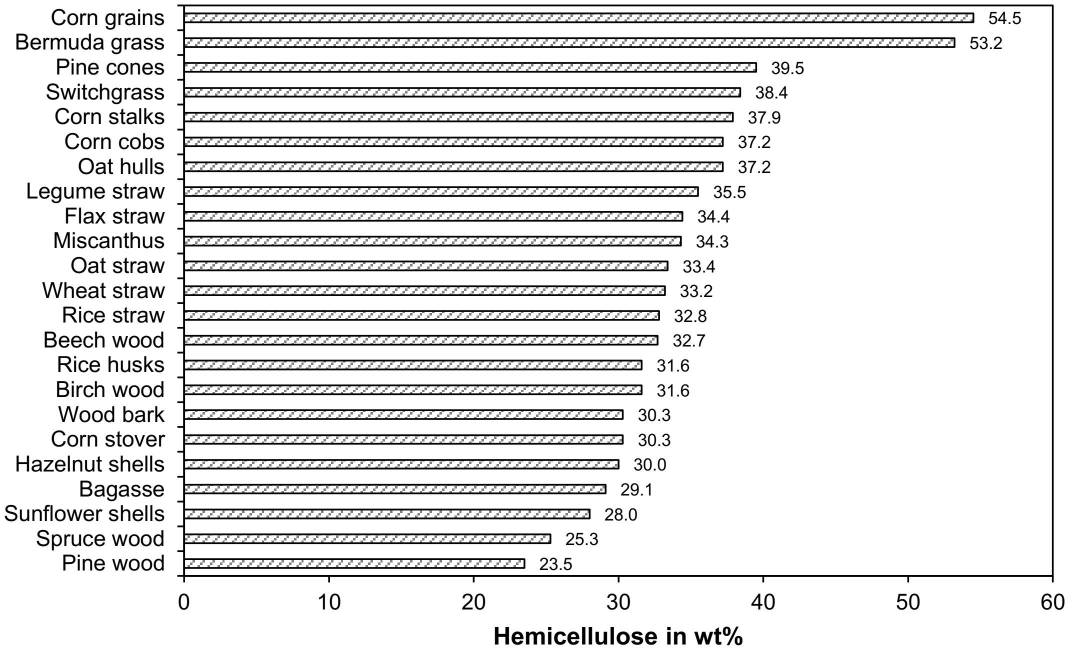

Figure 2.3 Hemicellulose content of various lignocellulosic raw materials on dry ash-free basis and normalized to 100 %. Data adopted from [48,49].

2.2 Hydrothermal Treatment

2.2.1 Properties of Hydrothermal Conditions

Hydrothermal treatment (HT) takes place in subcritical water at temperatures ranging from 100 to 374 °C (the critical point), under the respective vapor pressures. Due to the high pressures, water remains in the liquid phase. Under these conditions, water serves both as a solvent and as a reaction medium. However, the physical and chemical properties of water change significantly with temperature and can therefore influence reactions. As the temperature increases, the vapor pressure of water rises exponentially, while the density decreases (Figure 2.4).

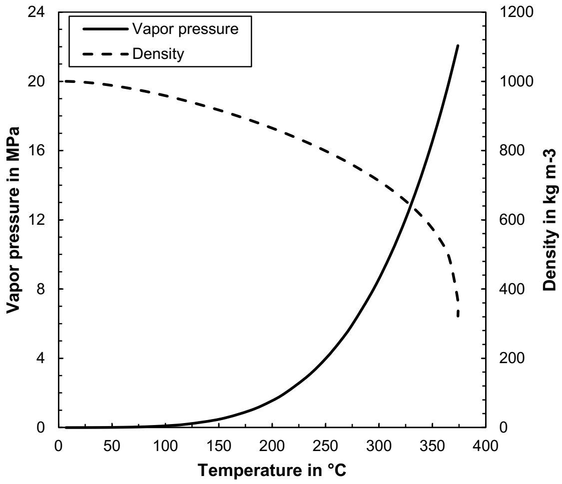

Figure 2.4 Density of liquid water at saturation along the vapor pressure curve. Data from Brunner (2014).[45]

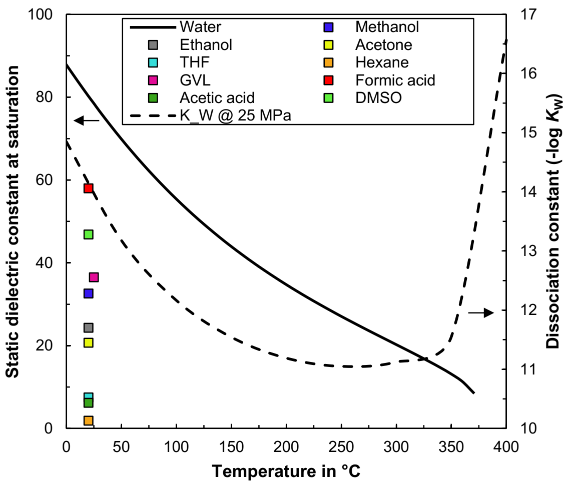

Figure 2.5 Static dielectric constant for saturated water in comparison with several organic solvents and dissociation constant of water (K_W) for 25 MPa. Data from Brunner (2014)[45], Aparicio and Alcalde (2009)[53], and Kato et al. (2013).[54]

The dynamic viscosity of water depends on both temperature and pressure, with temperature having a more pronounced influence. An increase in pressure leads in a slight increase in viscosity, while higher temperatures result in a significant reduction in viscosity. The reduced viscosity can lead to an increase in diffusion rates, which, for example, can improve accessibility to catalysts or facilitate penetration into solid biomass structures, thus accelerating the rate of chemical reactions.[55] Simultaneously, decreasing viscosity also promotes heat transfer, leading to a more homogeneous temperature distribution in the reaction system. The static dielectric constant of water describes its ability to be polarized by an electric field. A higher dielectric constant correlates with a greater capacity to dissolve polar compounds. Due to its polarity and molecular association through hydrogen bonds, liquid water has a higher dielectric constant than most other liquids. However, with increasing temperatures, the movement of water molecules increases, reducing the dielectric isolating ability, accompanied by a decreasing dielectric constant (Figure 2.5). Consequently, water changes from a polar to a less polar solvent, which improves the solubility of non-polar substances, while salts may precipitate at higher temperatures.

$$2H_2O \rightleftarrows H_3O^+ + OH^- \tag{2-1}$$

Another temperature-dependent property of water is its dissociation into hydronium (H_3O^+) and hydroxide (OH^-) ions (Eq. (2-1)), which increases up to a temperature of 250 °C and then decreases above this temperature (Figure 2.5). For instance, the concentration of hydronium ions in water at 250 °C is equivalent to a pH of around 5.5.

2.2.2 Processing of Hemicellulose under Hydrothermal Conditions

Due to the aforementioned properties of hydrothermal water, hydrothermal treatment (HT) has received significant attention in recent years, as it is able to convert moist biogenic residues or aqueous sugar solutions into various valuable products without the use of additives.[56,57] Hemicellulose is particularly suitable for this process because, in contrast to the linear, crystalline structure of cellulose, it has a branched, amorphous structure as already explained in section 2.1. This heterogeneity of hemicellulose results in fewer intramolecular interactions, such as hydrogen bonds, thereby facilitating the penetration of water molecules into the hemicellulose structure.[58] Another important role of water is its involvement in the hydrolytic cleavage of hemicellulose. In order to cleave the glycosidic bonds between monosaccharides, the participation of a water molecule is required, as illustrated by the general reaction equation for a hydrolysis reaction (Eq. (2-2)).

$$(X - O - X)_n + nH_2O \rightarrow 2nX - OH \tag{2-2}$$

In the scientific literature, studies usually focus on the release of hemicellulose sugars from lignocellulosic biomass, such as agricultural waste or wood. Boussarsar et al. (2009) compared the production of D-xylose from sugarcane bagasse by hydrothermal treatment with acid hydrolysis. The results showed that under hydrothermal conditions, D-xylose can be extracted with a high yield of 55 wt%. However, by adding 1 % sulfuric acid, the yield could be increased to 88 wt%, while at the same time, the reaction time was reduced from 4 h to 20 min and the temperature from 170 to 150 °C. However, the authors pointed out that delayed neutralization when using H_2SO_4 can lead to degradation of the sugar monomers and thus to a reduced yield.[59] Garrote et al. showed that under mild hydrothermal conditions (145 – 190 °C, reaction times of up to 7.5 h), mainly D-xylose and xylooligosaccharides could be obtained from wood (eucalyptus) with total yields of 71 – 80 wt%.[58] Similar results were also found by Nitsos et al., who compared the extraction of hemicellulose sugars from hardwood (poplar and grapevine) and softwood (pine). A maximum xylan yield of 60 wt% was achieved for all substrates studied.[60]

The extraction of hemicellulose under hydrothermal conditions always leads to the production of furfural, as shown in all referenced studies. It has been observed that harsher reaction conditions or the addition of acids promote furfural formation. Therefore, hydrothermal environments create optimal conditions for the efficient production of furfural, both directly from biomass and from biomass hydrolysates.

2.3 Furfural

2.3.1 Properties

Furfural, an aromatic heterocyclic aldehyde produced from hemicellulose-rich biomasses, is an oily and, in its pure state, colorless liquid with a distinctive almond-like odor. In contact with air, furfural quickly starts to react with oxygen, forming polymeric compounds, which is accompanied by an amber discoloration. Furfural is soluble in a wide range of polar organic solvents, such as ethanol or acetone. However, the solubility in water is limited to 83 g L^{-1} at 20 °C. Furthermore, it forms an azeotrope with water at a proportion of approx. 35 wt% furfural. Since the mixture separates into a two-phase mixture at the azeotrope in the liquid phase, it is classified as a heteroazeotrope. Up to the miscibility gap, furfural reduces the boiling temperature of the mixture from 100 to 97.8 °C (Figure 2.6). [61,62]

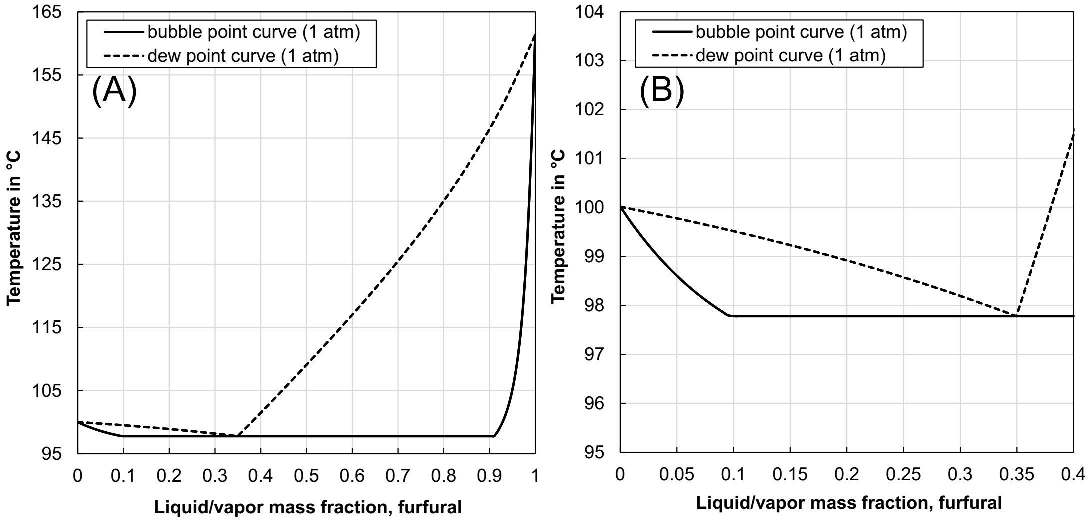

Figure 2.6 T-x,y diagrams for water furfural at atmospheric pressure (A) in the entire concentration range and (B) in detail up to the azeotrope. The diagrams were created using ASPEN Properties V10 on the basis of NRTL property method.

2.3.2 Uses and Economics of Furfural

Furfural has versatile applications and is thus also referred to as a platform chemical. The production of furfural is 100 % bio-based and already commercial since 1921.[23,63] The first industrial process was developed and established by the Quaker Oats Company whereas oat hulls are heated with continuous steam injection after mixing with sulfuric acid. The formed furfural is then removed by continuous vapor passaging. This process is still the most common today in a slightly modified form.[24] Over the last century, several new processes have been developed and, in some cases, implemented on an industrial scale. An overview of these processes can be seen in Table 2.2.

Table 2.2 Overview of industrial processes developed for the production of furfural.

Process	**Operation mode**	**Reaction condition**	**Furfural yield**	**Ref.**
Quaker Oats 1921	semi-batch	H_2SO_4, stripping (153 °C) at high pressure	40–52 %	23
Quaker Oats 1997	continuous	H_2SO_4, 184 °C at 11 bar	55 %	24
Chinese batch	batch	H_2SO_4, stripping (160-165 °C) at high pressure	50 %	24
Agrifurane	batch	H_2SO_4, 177–161 °C at 6–9 bar	14.5 %[a]	24,64
Escher Wyss	continuous	H_2SO_4, 170 °C	< 60 %	24,65
Rosenlew	continuous	Autocatalysis, 180 °C at 10 bar	40-60 %	24,66
Supratherm	continuous	H_2SO_4, 200–240 °C	/	24
Stake	continuous	Acids formed in situ, 230 °C at 27.7 bar	66 %	24
Suprayield	batch	H_3PO_4/CH_3COOH, 170–230 °C at high pressure	70 %	24,65
Biofine	continuous	H_2SO_4, 1st reactor 220 °C, 2nd reactor 200 °C	70 %	67
Vedernikovs	continuous	H_2SO_4, 188 °C	75 %	68
CIMV[b]	continuous	Organic acids,	/	69
MTC[c]	continuous	$H_2SO_4/NaCl$, stripping (180 °C)	86 %	69

[a] based on the used raw material (corn cobs)
[b] Compagnie Industrielle de la Matière Végétale
[c] Multi-Turbine-Column

So far, more than 80 chemicals are known in the fields of plastics, pharmaceuticals, agrochemicals, solvents, and biofuels, which can be directly or indirectly synthesized from it (Figure 2.7).[22] However, the production conditions for furfural are not very sustainable due to the high energy demand and the large quantities of mineral acids required for its production. Furthermore, the total yield of furfural, at about 10.3 wt% in relation to the applied biomass, is quite low.[66] Therefore, most of the production plants are located in countries with low environmentally standards as well as energy costs. Highest production capacities are in China (>70 %), followed by Dominican Republic, South Africa, Europe, and India.[70] Simultaneously, the demand for furfural in Europe is expected to increase from 50 kt today to 200 kt by 2030, driven by its eco-friendly and renewable nature, along with its potential to replace conventional fossil-based chemicals. However, the production capacity in Europe today is only 6.5 kt/a, although many potential biogenic residues would be available for furfural production.[71] From this perspective, environmentally friendly, energy-saving, and as cost-effective point of view, environmentally friendly, energy-saving as well as cost-effective manufacturing processes for furfural are required to satisfy the growing demand in Europe and countries with high environmental standards. One opportunity to reduce production costs is the combination with other processes, such as cellulose ethanol production or wood pulp production.[71] Here, it is possible to discharge pentosan-rich hydrolysates in order to subsequently make them available for the production of furfural.

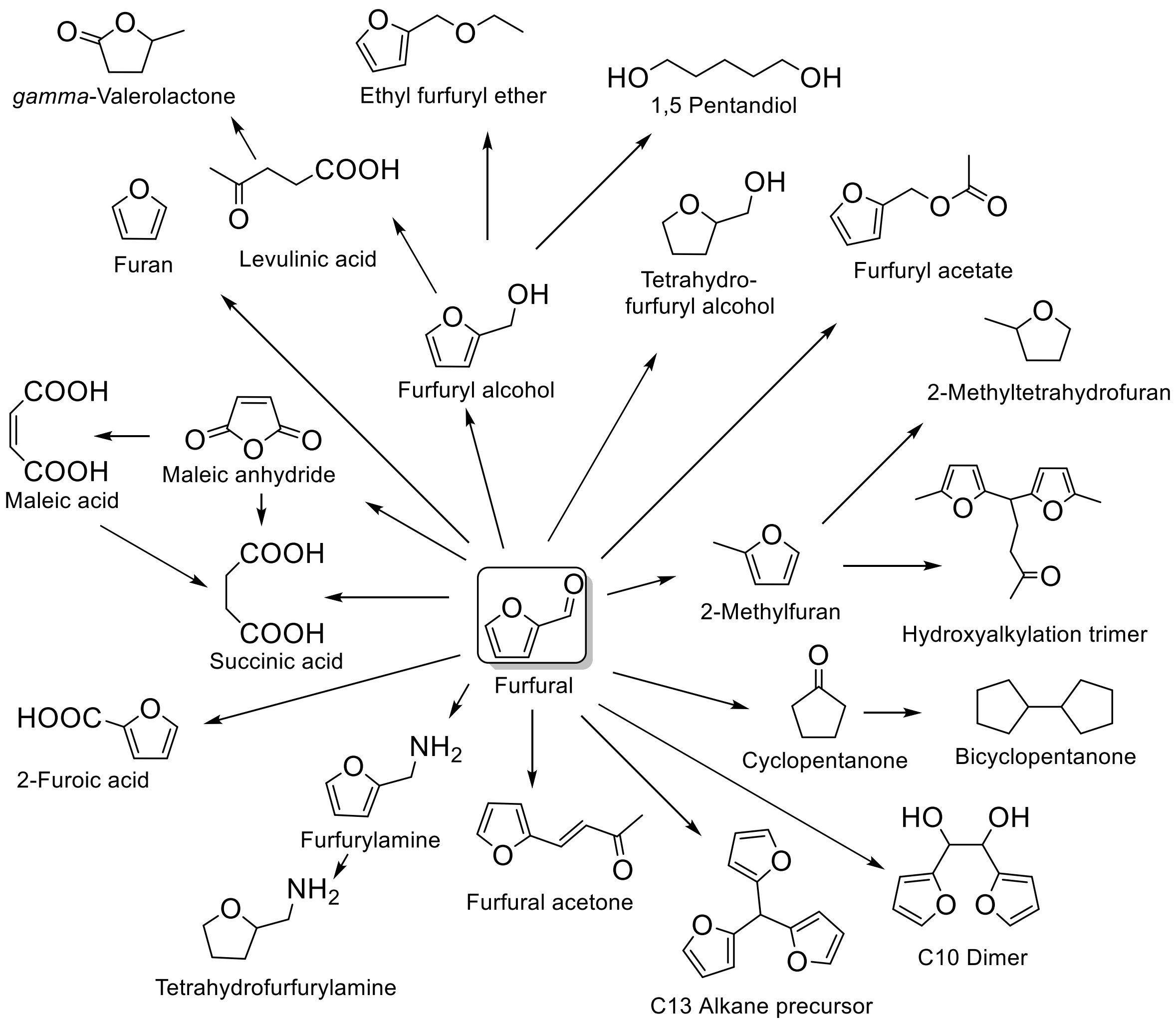

Figure 2.7 Overview of furfural applications based on Kabbour and Luque (2020).[72]

2.3.3 Reaction Mechanism of Furfural Formation

The formation of furfural from pentoses like D-xylose or D-arabinose is a typical acid-catalyzed dehydration reaction. In the literature, several reaction mechanisms have been discussed over time. Initially, it was proposed that the formation of furfural proceeds from the acyclic form of pentoses via a 1,2-enediol intermediate[73,74] or directly from the α, β-unsaturated aldehyde[75,76], followed by dehydration to furfural. Later, intramolecular hydrogen transfer reactions were detected[77], which led to new mechanisms, starting from the cyclic form of the pentose (furanose and pyranose) and protonation of the hydroxyl groups at various positions[74,78,79]. These have subsequently become established in the literature and can be summarized according to the following steps.

(1) Protonation of the hydroxyl group by an acid catalyst

(2) Formation of an unstable carbocation by intermolecular rearrangement leading to the elimination of a water molecule

(3) The carbocation undergoes a cyclization by attack of the ether bonded ring oxygen forming the reactive intermediate 2,5-anhydroxylose.

(4) In the final step, the two remaining hydroxyl groups are eliminated, resulting in the formation of furfural. This final dehydration stabilizes the molecule in its characteristic furan structure.

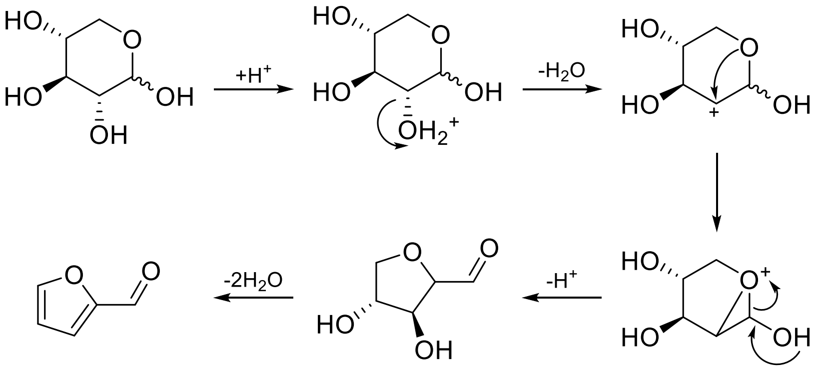

Figure 2.8 Reaction mechanism for the acid-catalyzed dehydration of pentose to furfural based on Nimlos et al. (2006).[79]

These advancements in understanding have highlighted the complexity of the furfural formation process, suggesting that multiple pathways might coexist, depending on the reaction conditions such as pH, temperature, and the nature of the acid catalyst used. Moreover, the discovery of these mechanisms has stimulated further research into optimizing reaction conditions to improve furfural yields and to reduce the formation of unwanted by-products. The interaction between different reactive intermediates suggests that the pathway to furfural can be fine-tuned by varying reaction parameters, leading to more efficient and sustainable production processes.

2.3.4 Furfural Decomposition

The formation of furfural from pentoses always involves the formation of insoluble solids, commonly called humins. These humins can be formed in two ways during the reaction:

I) The polymerization of furfural molecules with themselves, also called furfural resinification or self-polymerization(Figure 2.9).

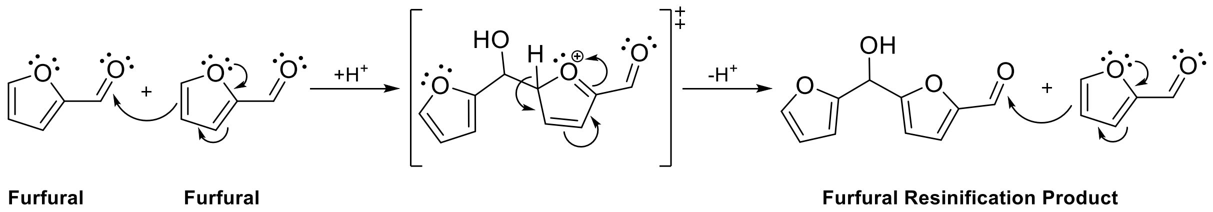

Figure 2.9 Proposed reaction pathway for furfural resinification according to Enslow et al. (2015).[80]

II) The polymerization of furfural with a reactive intermediate (carbocation), also called furfural condensation or cross-polymerization (Figure 2.10).

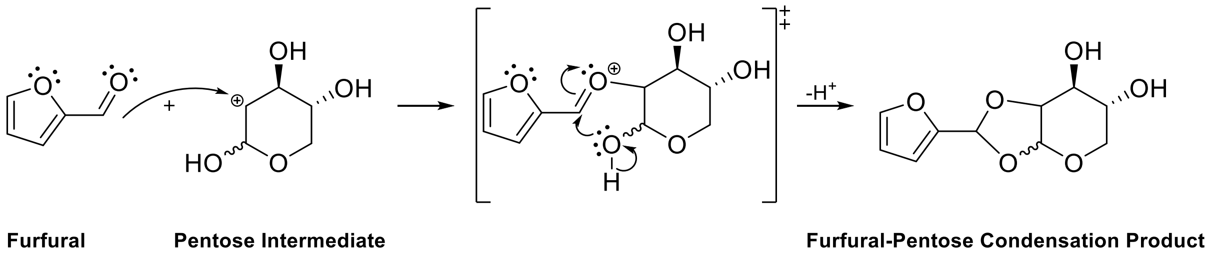

Figure 2.10 Proposed reaction pathway for furfural condensation via a pentose intermediate according to Zeitsch (2000).[24]

From the literature, it is known that the loss of furfural over the condensation with a sugar intermediate is much more relevant than the self-polymerization. This could be proven by furfural destruction experiments in absence of any pentoses. In contrast to experiments starting with sugars, the degradation of furfural was significantly lower and cannot explain the overall loss.[81] Furthermore, Enslow et al. were able to demonstrate that the condensation must take place through an pentose intermediate since D-xylose conversion is not influenced in the presence of an initial furfural concentration.[80]

Since furfural is consumed in both cases, these reactions are also summarized as loss reactions. These loss reactions are strongly dependent on the chosen reaction conditions as well as the catalysts or solvents used. For this reason, reducing furfural degradation is a central focus of nearly all studies. However, preventing degradation not only leads to higher yields of furfural but also reduces the formation of insoluble humins, which can cause blockages in subsequent processes due to deposits. The use of heterogeneous catalysts is also complicated by the formation of humins, as it can lead to rapid deactivation due to deposits on the catalyst surface.

2.3.5 Overview of Advanced Production Routes of Furfural

In recent years, several research groups have been intensively working on new production methods for furfural, which can be grouped in summary into four different approaches:

(1) Addition and development of homogeneous and heterogeneous catalysts,

(2) Reactive extraction by biphasic systems,

(3) Monophasic solvent mixtures consisting of water and an organic or ionic solvent, and

(4) Reactive distillation of furfural by means of steam or nitrogen.

2.3.5.1 Homogenous and Heterogeneous Catalyzed Reactions

As described in section 2.3.3, the dehydration of pentoses to furfural is acid-catalyzed. The removal of hydroxyl groups can only occur in the presence of a proton-donating acid (Brønsted acids). Nevertheless, studies have successfully demonstrated that omitting an acid catalyst can still yield substantial furfural quantities (45 – 50 mol%).[26,82] This can be attributed in part to the enhanced dissociation potential of water within the subcritical range (100 – 374 °C) and the formation of formic acid from subsequent or side reactions.[26,33,45,83] In the context of biomass or biomass hydrolysates, the cleavage of formyl and acetyl groups present in hemicellulose (Figure 2.1) also contributes to the generation of formic and acetic acid,[84,85] thereby promoting the autocatalytic reaction. Kinetic studies have shown, however, that the use of acid catalysts can significantly reduce the activation energy for the formation of furfural from D-xylose.[82] This can greatly increase the reaction rate and thus also reduce the reaction time or temperature. Concurrently, an elevated potential for furfural degradation has been noted, attributable to the increased production of highly reactive carbocations (Figure 2.8). For this reason, various catalysts have been considered in the literature in the past. These can be classified into homogeneous and heterogeneous acid catalysts.

Homogeneous Acid Catalysts

Homogeneous catalysts are completely dissolved in the reaction mixture and are in the same phase as the reactants, which enables a uniform reaction environment and efficient interactions.

Mineral Acids

Mineral acids, such as sulfuric, hydrochloric, or phosphoric acid, are the most commonly used and studied catalysts in the production of furfural (Figure 2.11). They are cost-effective and available in large quantities. Often, their use is combined with various production methods, such as metal salts[86], mono-[41] and biphasic[87] reactions, or reactive distillation[88].

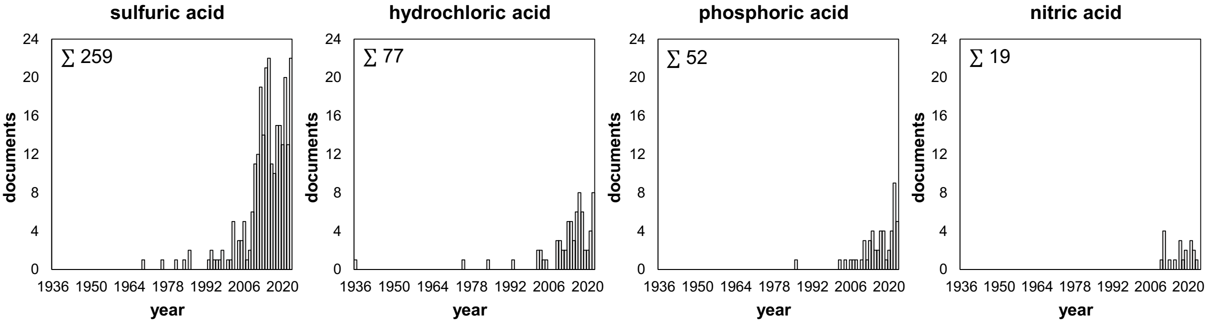

Figure 2.11 Number of publications per year (1936 – 2024) exploring the application of homogeneous acid catalysts (sulfuric, hydrochloric, phosphoric and nitric acid) in furfural production. Source: Scopus

For the first time, Yemiş and Mazza carried out a comprehensive investigation of the influence of homogeneous Brønsted acids on the production of furfural from D-xylose and xylan.[33] In their study, they examined at various mineral and organic Brønsted acid catalysts and compared them with each other. At constant pH (1.12), the following order was identified with regard to the highest furfural yield based on D-xylose:

$$HCl > H_2SO_4 > H_3PO_4 > HCOOH > CH_3COOH > HNO_3 > H_2O$$

On the basis of xylan, a different order was found, particularly with regard to nitric acid:

$$HCl > H_2SO_4 \sim HNO_3 > H_3PO_4 > HCOOH > CH_3COOH >> H_2O$$

Furthermore, they investigated the influence of acid concentration (c_{HCl}: 0.01 – 1 M) on furfural yield and identified the best results (54 – 56 mol%) at a concentration of 0.1 M (pH 1.12). This can be attributed, among other factors, to the increased formation of insoluble solids (humins), which occurred more frequently with rising acid concentrations. The two control experiments without a catalyst confirmed, on the one hand, that furfural can be autocatalytically produced from D-xylose and, on the other hand, that the polysaccharide xylan is not sufficiently autocatalytically hydrolyzed. Therefore, no D-xylose could be released and no furfural produced. Marcotullio and Jong, who compared HCl and H_2SO_4 in their study, came to similar conclusions.[34]

However, the dissolved mineral acids are difficult to separate and reuse after the reaction. For this reason, the acidic solutions obtained after the reaction must be neutralized. This process generates large amounts of salt-containing waste products that need to be disposed of.[26] Furthermore, mineral catalysts, especially HCl and H_2SO_4, are highly corrosive to stainless steels. This requires the use of special materials in the construction of corresponding industrial reactors.

Table 2.3 Overview of reported furfural yields for homogeneous mineral and organic acid catalysts.

Catalyst	Substrate	Solvent	T (°C)	t_R (min)	X_{C5} (mol%)	Y_{Fu} (mol%)	Ref.
HCl (0.1 M)	Xylose (1 wt%)	H_2O	145	300	76	28.8	89
HCl (0.05 M)	Xylose (0.5 wt%)	H_2O	200	68.7	86	68.7	34
HCl (0.1 M)	Xylose (1 wt%)	H_2O	180	30	-	56	33
HCl (0.1 M)	Xylan (1 wt%)	H_2O	180	30	-	54	33
H_2SO_4 (0.1 M)	Xylose (1 wt%)	H_2O	180	30	-	50	33
H_2SO_4 (0.1 M)	Xylan (1 wt%)	H_2O	180	30	-	45	33
H_2SO_4 (0.05 M)	Xylose (0.5 wt%)	H_2O	200	61.4	87	61.4	34
H_2SO_4 (0.04 M)	Hydrolysate (3.5 wt%)	H_2O	170	100	86	48.4	90
H_2SO_4 (0.08 M)	Xylose (8 wt%)	H_2O	155	330	-	62	88
H_2SO_4 (0.05 M)	Hydrolysate (8 wt%)	MIBK/H_2O (2:1 v/v)	170	20	96	80.1	87
H_2SO_4 (0.05 M)	Hydrolysate (8 wt%)	toluene/H_2O (2:1 v/v)	170	30	98	76.6	87
H_2SO_4 (0.05 M)	Hydrolysate (8 wt%)	CyH/H_2O (2:1 v/v)	170	20	91	73.8	87
H_3PO_4 (0.08 M)	Xylose (8 wt%)	H_2O	160	330	-	65	88
H_3PO_4 (0.4 M)	Xylose (1 wt%)	H_2O	180	30	-	43	33
H_3PO_4 (0.4 M)	Xylan (1 wt%)	H_2O	180	30	-	40	33
HNO_3 (0.1 M)	Xylose (1 wt%)	H_2O	180	30	-	5	33
HNO_3 (0.1 M)	Xylan (1 wt%)	H_2O	180	30	-	46	33
FA (0.08 M)	Xylose (8 wt%)	H_2O	180	30	-	70	88
FA (pH 1.12)	Xylose (1 wt%)	H_2O	180	30	-	37	33
FA (pH 1.12)	Xylan (1 wt%)	H_2O	180	30	-	38	33
FA (pH 0.92)	Xylose (3 wt%)	H_2O	180	60	100	61	91
FA (13.9 M)	Xylose (2 wt%)	H_2O	170	40	93	55	92
AA (pH 1.12)	Xylose (1 wt%)	H_2O	180	30	-	24	33
AA (pH 1.12)	Xylan (1 wt%)	H_2O	180	30	-	34	33
Maleic acid (0.25 M)	Xylose (1 wt%)	H_2O	200	28	100	67	93
Maleic acid (0.25 M)	Hydrolysate (1 wt%)	H_2O	200	15	92	61	93
Maleic acid (0.25 M)	Hydrolysate (1 wt%)	H_2O	200	28	91	56	93

CyH: cyclohexane

Organic Acids

Due to their lower corrosivity and the less environmentally harmful salt fractions produced after neutralization, organic acids offer advantages over mineral acids. Furthermore, formic and acetic acid are byproducts in the provision of biomass hydrolysates. For these reasons, various studies have been conducted to describe the behavior of organic acids in the dehydration of pentoses. As previously mentioned, Yemiş and Mazza were able to demonstrate that mineral acids are superior to organic ones at the same pH.[33] However, this study did not investigate temperature or time dependencies. Thus, Yang et al., who examined the use of formic, sulfuric, and phosphoric acids, were able to show that the use of formic acid can lead to significantly better furfural yields, but this requires higher reaction temperatures (Table 2.3).[88]

Seungmin and Seok recently demonstrated the same by investigating sulfuric and formic acid at different concentrations and temperatures.[94] They also showed that the strong mineral acid could accelerate the reaction by a factor of 4 to 12, but this did not lead to better yields ($Y_{FA\_5wt\%} = 54/Y_{SA\_1wt\%} = 45/Y_{SA\_2wt\%} = 48$ mol%). Promising results were also found by Kim et al., who investigated the use of maleic acid. Maleic acid not only showed excellent properties in the hydrolytic cleavage of hemicellulose from various lignocelluloses but also high furfural yields of up to 72 mol%. The authors note that the reusability of the catalyst is good, even though maleic acid slowly degrades to malic acid under the stated conditions.[93]

Lewis-Acids

In contrast to Brønsted acids, which donate protons, Lewis acids accept electron pairs. This can lead to the formation of aqua cations by metal ions when dissolved in water, as they form a complex with water molecules. The positive charge of the metal ions facilitates the loss of a proton from the water in the hydration shell, thereby weakening the OH bond. Thus, the metal ion acts as an acid according to the equation (2-3)[95]:

$$\mathrm{M(H_2O)}_X^{n+} \rightleftarrows \mathrm{M(H_2O)}_{X-1}(\mathrm{OH})^{(n-1)+} + \mathrm{H}^+_{\mathrm{aq}} \tag{2-3}$$

On the other hand, Lewis acids can catalyze the isomerization of pentoses, such as D-xylose, into more reactive intermediates (xylulose), which can then be more easily dehydrated to furfural (Figure 2.12).[89] The use of Lewis acids can also contribute to improved process economics, as they are often reusable and less corrosive than conventional acid catalysts, reducing the material requirements for reactors and processing equipment.

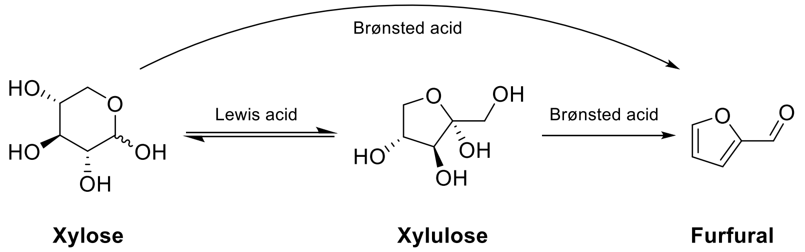

Figure 2.12 Schematic reaction pathway of Lewis- and Brønsted-acid catalyzed D-xylose dehydration to furfural.

The Lewis acids most commonly investigated in the literature are $CrCl_3$, $AlCl_3$, $FeCl_3$, $FeCl_2$, $CuCl_2$, $SnCl_4$, and NaCl. In their study, Lyu and Botte investigated the effects of four Lewis acids ($FeCl_2$, $FeCl_3$, $AlCl_3$, $CuCl_2$) and observed the highest yields for iron(III)- and aluminum(III)-chloride, followed by iron(II)- and copper(II)-chloride.[96] They were able to observe that the order of the metal ions for furfural production corresponds to the order of Lewis acid strengths (Figure 2.13). However, time-resolved concentration profiles of furfural were not determined. Therefore, it remains unclear whether the observed yields correspond to the global maxima.

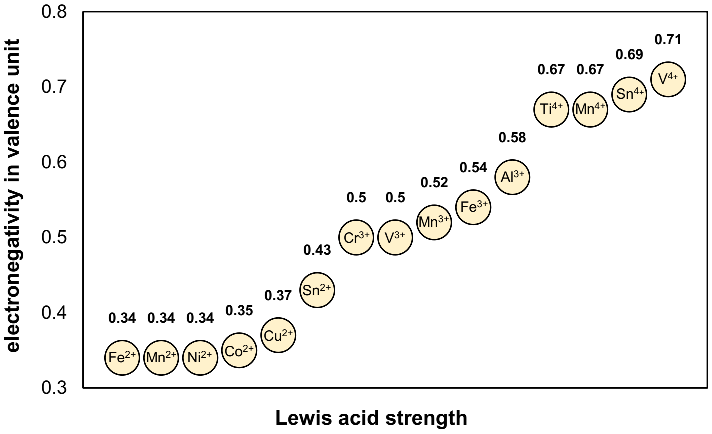

Figure 2.13 Overview of various Lewis acid strengths. Data from Hawthorne (2012).[97]

In the comprehensive study by Ershova et al., the time course of the furfural concentration was also measured.[95] In this study, they compared a total of thirteen metal chlorides in aqueous solution with regard to their catalytic properties in the dehydration of D-xylose to furfural with an HCl and autocatalytic system. The hypothesis that the yield of furfural can be increased with increasing strength of the Lewis acid could not be confirmed here. Although the highest yields were observed for $FeCl_3$, $AlCl_3$ and $CrCl_3$ showed the lowest maximum yields, as listed below according to the maximum furfural yield achieved:

$Fe^{3+} > NH_4^+ > HCl > Cu^{2+} > Li^+ > Fe^{2+} > Mn^{2+} \sim K^+ > Na^+ > Zn^{2+} > H_2O > Co^{2+} > Ca^{2+} > Cr^{3+} > Al^{3+}$.

Thus, the results indicate that the formation of furfural from D-xylose in the presence of various chlorides does not depend primarily on the metal valence but on some specific properties of the cation.

Heterogeneous Acid Catalysts

Heterogeneous catalysts exist in a different phase than the reactants, typically as solids in liquid reaction systems, which facilitates their separation and reuse after the reaction. As has been extensively described, the conversion of pentoses to furfural results in the formation of water-insoluble humins as byproducts. Therefore, heterogeneous catalysts are often used in combination with biphasic systems. This approach can reduce catalyst deposition and the associated deactivation. The most commonly studied types of heterogeneous catalysts so far are zeolites, mesoporous materials, and polymers.

Table 2.4 Overview of reported zeolite performances during dehydration of pentoses.

Catalyst	Substrate	Solvent	T (°C)	t_R (min)	X_{C5} (mol%)	Y_{Fu} (mol%)	Ref.
H-ferrierite	Xylose 3 wt%	H_2O	140	240	29	13	35
H-mordenite	Xylose 3 wt%	H_2O	140	240	30	12	35
H-mordenite	Xylose 2 wt%	H_2O:GVL	175	120	100	81	98
H-mordenite	Hydrolysate 2 wt%	H_2O:GVL	175	90	98	75	98
H-mordenite	Xylose 3 wt%	DMSO	140	240	62	24	35
H-Y	Xylose 3 wt%	H_2O	140	240	31	22	35
H-Y	Xylose 10 wt%	H_2O	160	90	76	25	99
H-ZSM-5	Xylose 3 wt%	H_2O	140	240	30	17	35
H-ZSM-5	Xylose 2 wt%	GVL	175	-	-	59	98
H-ZSM-5	Hydrolysate 16 wt%	Toluene:H_2O	190	180	91	65	32
H-β	Xylose 3 wt%	H_2O	140	240	37	19	35
H-β	Xylose 2 wt%	GVL	175	-	-	74	98

Zeolites

Zeolites are microporous, crystalline aluminosilicates with a well-defined lattice structure (Figure 2.14) that are used as catalysts, molecular sieves, and in ion exchange processes.

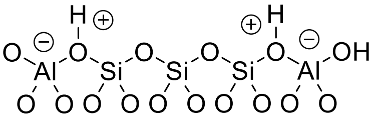

Figure 2.14 Schematic structure of a zeolite.

Due to their structure and the presence of aluminum and silicon atoms in the lattice, zeolites have acid centers, mainly Brønsted acid sites, which attract water molecules and lead to the formation of protons that can act as catalysts. The number of acid sites can be adjusted depending on the number of aluminum atoms inserted. In addition to Brønsted acid sites, zeolites also contain Lewis acid sites. Due to this property, zeolites can combine the advantages of both types of acids and are the subject of many studies. Kim et al. were the first to examine various zeolite materials and observe that the conversion of D-xylose and the furfural yield generally decrease with an increasing SiO_2/Al_2O_3 molar ratio.[35] This confirmed the findings of Weingarten et al., who explained this with a lack of accessibility to the acid sites.[99] However, promising yields can be achieved only in combination with organic solvents like GVL or DMSO, and in biphasic systems (toluene/water) (Table 2.4). Another advantage resulting from the use of organic solvents is the lower leaching of the catalysts and thus better regenerability of the catalysts.

Mesoporous Materials

Mesoporous catalyst materials are materials with pore sizes ranging from 2 to 50 nanometers. They are characterized by their large specific surface area, high pore volumes, and ability to adsorb and catalyze molecules of medium size. By modifying the surface chemistry of mesoporous materials, such as by introducing acid-functional groups, the catalytic activity can be specifically tailored to the dehydration of pentoses to furfural. Among the most well-known mesoporous materials, especially in the context of furfural production from pentoses, are MCM-41 and SBA-15 (Table 2.5).

Table 2.5 Overview of reported mesoporous catalysts performances during dehydration of pentoses.

Catalyst	**Substrate**	**Solvent**	**T (°C)**	**t_R (min)**	**X_{C5} (mol%)**	**Y_{Fu} (mol%)**	**Ref.**
MCM-41	Xylose 3 wt%	H_2O	170	2	81	30	100
MCM-41	Xylose 3 wt%	n-BuOH:H_2O	170	2	89	39	100
MCM-41-SO_3H	Xylose 3 wt%	Toluene:H_2O	140	1440	91	76	36
H-MCM-22	Xylose 10 wt%	Toluene:H_2O	170	960	98	71	101
SBA-15- SO_3H	Xylose 3 wt%	Toluene:H_2O	160	240	92	68	102
MCM-41	Xylose 3 wt%	DMSO	140	1440	86	45	36
MCM-41-SO_3H	Xylose 3 wt%	MIBK:H_2O	140	1440	84	51	36
SBA-15-(Zr)SO_3H	Xylose 2.2 wt%	GVL:H_2O	160	120	97	38	103
MCM-41-SO_3H	Hydrolysate 1 wt%	n-BuOH:H_2O	170	120	97	35	104
P-Zr-SBA-15	Xylose 1.7 wt%	Toluene:H_2O	180	60	-	80	105
P-Zr-SBA-15	Xylan 1.7 wt%	Toluene:H_2O	180	90	-	69	105
P-Zr-SBA-15	Xylose 1.7 wt%	H_2O	180	180	-	53	105
Al-SBA-15 (SA)	Xylose 3 wt%	H_2O	170	420	96	63	106

A common method to increase the acid functionality is the introduction of a sulfonic acid group (SO_3H). In this way, Dias et al. were able to achieve a yield of 76 mol% in a biphasic mixture of toluene/water.[36] By modifying an SBA-15 silica with zirconium and subsequent application of phosphorus with phosphoric acid, a P-Zr-SBA-15 catalyst could be synthesized. This also led to yields of up to 69 mol% when using xylan.[105]

Polymers

For the production of furfural from sugars such as D-xylose, various types of polymer-based catalysts are used. Two catalysts widely mentioned in the literature for the production of furfural are Nafion and Amberlyst polymers (Figure 2.15). Both catalysts are characterized by their acidic sulfonic acid groups (SO_3H), which are crucial for the dehydration of pentoses to furfural.

Figure 2.15 Structural formula of a Nafion (left) and Amberlyst (right) polymer.

In a study by Yemiş and Mazza, various polymer catalysts, including Amberlyst and Nafion, were compared with regard to their suitability for furfural synthesis from d-xylose and xylan. The best results (40 mol%) were obtained with Amberlyst-36.[107] However, when xylan was used instead of D-xylose instead, only very low yields of <3 mol% were identified, which suggests that the polysaccharide could not be sufficiently hydrolyzed by the catalysts. The group around Guenic et al. achieved very promising results using a Nafion-NR50 catalyst in the presence of NaCl in a biphasic system consisting of CPME and water. Yields of up to 80 mol% were achieved and even after four cycles of catalyst reuse, only minor activity loss was observed. Yields of > 50 mol% were also achieved when using the polysaccharide xylan.[108] The use of Amberlyst and Nafion catalysts was also successful in various organic solvents such as DMSO, achieving good results.[36,109,110] The observed reusability of the Nafion-117 catalyst used by Luong et al. is particularly noteworthy. Up to 15 repetitions without significant loss of activity were demonstrated.[109] Good results were also repeatedly shown by Amberlyst-70 during nitrogen stripping (Table 2.6).[111,112]

Table 2.6 Overview of reported performances of different polymer catalysts.

Catalyst	**Substrate**	**Solvent**	T **(°C)**	t_R **(min)**	X_{C5} **(mol%)**	Y_{Fu} **(mol%)**	**Ref.**
Amberlyst-15	Xylose 10 wt%	H_2O	170	20	-	37	107
Amberlyst-36	Xylose 10 wt%	H_2O	170	20	-	40	107
Nafion-NR50	Xylose 10 wt%	H_2O	170	20	-	28	107
DOWEX 50WX8-200	Xylose 10 wt%	H_2O	170	20	-	29	107
Nafion-NR50/NaCl	Xylose 3.8 wt%	CPME:H_2O	170	40	100	80	108
Nafion-NR50/NaCl	Xylan 3.8 wt%	CPME:H_2O	170	60	100	55	108
Nafion-117	Xylose 9.1 wt%	DMSO	150	120	91	60	109
Nafion-SAC-13	Xylose 9.1 wt%	DMSO	150	120	93	49	109
Amberlyst-15	Xylose 3 wt%	DMSO	140	240	87	59	36
Amberlyst-70	Xylose 1wt%	H_2O	175	170	82	87	111
Amberlyst-70	Xylose 13.3 wt%	DMSO	160	100	-	81	110
Amberlyst-70	Xylose 13.3 wt%	THF	160	20	-	61	110

In summary, homogeneous catalysts enable uniform reaction conditions and potentially higher reactivity due to their direct interaction with substrates. In particular, mineral acids such as sulfuric and hydrochloric acid have been extensively studied and used due to their effectiveness and cost efficiency. However, their corrosive effect, the difficulties in separating them from the reaction mixture and the environmental problems associated with the disposal of the acids limit their attractiveness. Heterogeneous catalysts, on the other hand, are in a different phase to the reactants, usually as solids in liquid systems. This phase difference facilitates the recovery and reuse of the catalyst, significantly reducing the amount of waste and improving the sustainability of the process. On the other hand, the potential deactivation of the catalyst due to surface deposits (humins) represents a challenge. The choice of homogeneous or heterogeneous catalysts in furfural production depends on a compromise between catalytic efficiency, easy separation, environmental impact, and process economics. Ongoing development of new catalysts and optimization of reaction conditions continue to improve the feasibility and sustainability of furfural production and promise to overcome the limitations of current methods.

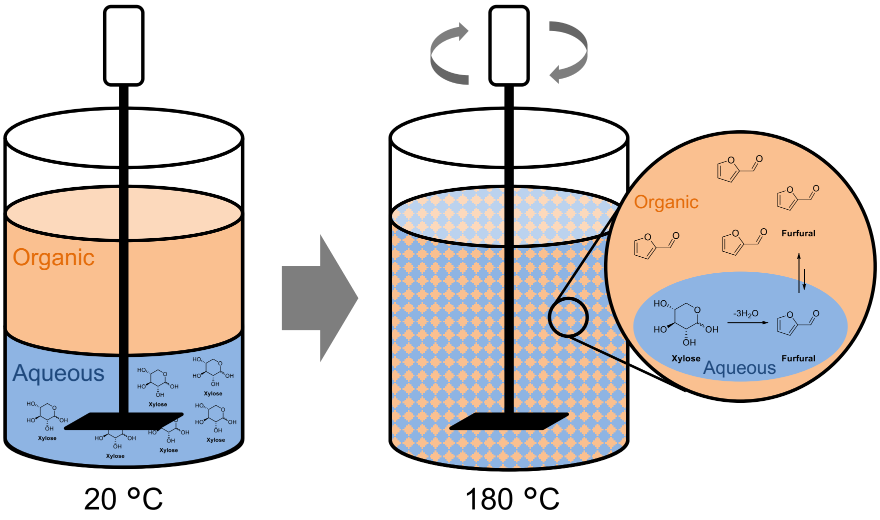

Figure 2.16 Schematic representation of a biphasic system for the reactive extraction of furfural from pentoses.

2.3.5.2 Reactive Extraction by Biphasic Systems

In biphasic systems, furfural is extracted from the organic phase immediately after its formation in the aqueous phase, thus protecting it for further degradation by interaction with sugar molecules (Figure 2.16). However, such solvents must fulfill various properties like good chemical and thermal stability, a boiling point higher than that of furfural, no azeotrope formation with furfural, low mutual solubility, and a high furfural partition coefficient, to be suitable for this procedure.[39,113] Most widely used extractants in the literature are toluene, methylisobutylketone (MIBK), cyclopentyl methyl ether (CPME), or 2-Methyltetrahydrofuran (MTHF).[31,114,115]

The use of a biphasic reaction system for the production of furfural from xylose was first described by Moreau et al. in 1998.[116] Their research primarily explored the application of zeolite catalysts (H-Y faujasite and H-mordenite) at 170 °C within water-MIBK or -toluene mixtures, achieving notable selectivities of 70 – 96 % in toluene and 50 – 60 % in MIBK. Following this, further investigations by Valente concentrated on utilizing heteropoly acids, mesoporous solid catalysts, and zeolites (MCM-41 & Nu-6(2)) in biphasic systems (water-MIBK/-toluene).[36,117,118] However, it was Dumesic who specifically focused on detailing biphasic reaction systems for synthesizing furfural and 5-HMF.[119] As of now, the method of biphasic reactive extraction has been well-established in the scientific literature (Table 2.7). Recent advancements in the field are dealing with the development of continuous reaction processes as well as the use of sustainable and green extractants.[37,120,121]

Table 2.7 Overview of reported furfural yields in biphasic reaction systems.

Extractant	**Extr.:H_2O (w/w)**	**Substrate**	***T* (°C)**	**t_R (h)**	**Cat.**	**Y_{Fu} (mol%)**	**Ref.**
MIBK	1:1	Xylose 10 wt%	160	0.5	HCl	49	38
MIBK	0.8:1	Bagasse 1 wt%	170	6	H-USY	55	122
CPME	2.6:1	Xylose 2.8 wt%	200	1	Starbon®450-SO_3H	70	123
CPME	0.86:1	Xylose 2.8 wt%	190	3	-	78	31
CPME	2.3:1	Xylose 4.5 wt%	130	6	NbO	58	124
Toluene	13:1	Xylose 10 wt%	bp[a]	5	H_2SO_4/NaCl	83	125
Toluene	1.3:1	Xylose 1.4 wt%	120	3	NbO	72	126
Toluene	1.4:1	Xylose 4.2 wt%	210	1	NbP	42	127
Toluene	0.86:1	Bagasse 1 wt%	170	6	H-USY	54	122
Isophorone	0.92:1	Xylose 2.8 wt%	190	3	-	49	31
MTHF	0.86:1	Xylose 2.8 wt%	190	3	-	71	31
Eugenol	1:1	Xylose 2 wt%	170	0.17	H_2SO_4	73	37

A notable challenge in biphasic furfural production is ensuring effective mixing of the two phases and the subsequent separation of the desired product from the extractant. In laboratory-scale reaction setups, which are commonly referenced in scientific literature (Table 2.7), achieving sufficient mixing is relatively straightforward due to the smaller volumes and more controllable mixing conditions. However, when scaling up to an industrial level, a considerable amount of the energy input is required to ensure adequate mixing. Therefore, in addition to the increased energy requirements, the design of mixers and reactors that can efficiently process the large quantities typical of industrial processes also presents a technical challenge. Moreover, the presence of impurities in the extractants can increase the solubility of water and pentoses in the organic phase. This can lead to a higher rate of furfural degradation, reducing the overall yield of the desired product. The accumulation of such impurities may require frequent replacement or regeneration of the extractant, adding operational complexity and cost. Furthermore, the increased solubility of unwanted components complicates the separation process and requires more challenging and energy-intensive purification technologies to achieve the purity required for further applications of furfural.[66]

2.3.5.3 Monophasic Solvent Mixtures

Monophasic solvent mixtures do not form a second phase with water during the entire reaction time and can be divided into volatile and non-volatile solvents (Table 2.8). Non-volatile solvents are those with a boiling point higher than 100 °C. Ethylene glycol[110,128], sulfolane[42,129,130] or γ-valerolactone (GVL)[41,130,131], as well as ionic liquids (IL), such as 1-Butyl-3-methylimidazolium-chlorid (BMIM Cl)[132] or 1-ethyl-3-methylimidazolium hydrogen sulfate (EMIM HSO_4), are typically used here. Whereas the usage of ethylene glycol, either in pure or in diluted aqueous form, results in minor furfural yields, GVL shows highly attractive results with yields up to 90 mol% independently from the examined GVL content (70 – 90 wt%).[41,131] Sulfolane, which is like GVL an aprotic solvent, shows promising furfural yield of 61 mol% without any catalyst.[130] According to Romo et al., this can be attributed to the high polarity of sulfolane. Overall, high boiling point solvents can increase the reaction rate. High boiling point solvent enables a reduction in both the reaction temperature and the residence time and thus slows down the degradation of furfural. On the other hand, furfural can be easily removed from the top of the distillation column. However, the primary challenge arises in purifying the solvent, which tends to accumulate in the distillation column's bottom along with various impurities and by-products. IL, known for their excellent ability to dissolve biomass, have been explored for their potential in furfural production as well. Studies show they can achieve high furfural yields up to 84 mol%.[133,134] Moreover, beside serving as a solvent, IL are able to act as catalyst, enhancing the efficiency of the process.[135] However, the usage of ILs must consider factors such as cost, environmental impact, and the feasibility of recycling, ensuring that their benefits outweigh the challenges.[115]

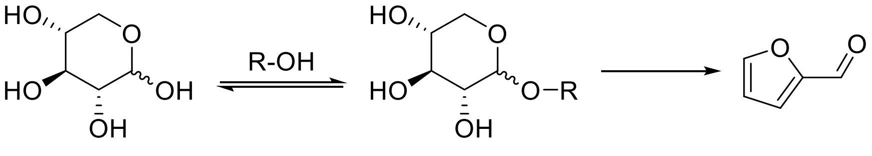

Figure 2.17 Reaction pathway of furfural production from D-Xylose in alcohols.

Low boiling point or volatile solvents are typically short-chain monovalent alcohols[40,136] or THF[110,130] are used here. Particularly promising results were achieved using alcohols. The alcohol reacts with the sugars under the formation of alkyl xyloside (alcoholysis/etherification) that subsequently can be transformed into furfural. Simultaneously, the formation of the reactive xylose carbocation can be suppressed, which is responsible for the polymerization of the sugar and furfural molecules.[40] Additionally, short-chain monovalent alcohols (C1-C4) such as ethanol or 1-butanol can be produced from biomass[137] and are well suited as co-solvent in pulping processes.[9] Moreover, the boiling point of such alcohols compared to furfural (162 °C) is low which is preferable for a cost and energy efficient product separation. Moreover, the boiling point of such alcohols compared to furfural (162 °C) is low which is preferable for a cost and energy efficient product separation. Another advantage is that problems associated with mass transfer or stirring operations are avoided due to the miscibility of such alcohol/water mixtures. From that point of view, short-chain monovalent alcohols are quite beneficial for usage as solvent in furfural synthesis. In

Table 2.8 Overview of reported furfural yields in monophasic reaction systems.

Solvent	**Solvent:H_2O (w/w)**	**Solvent type**	**Substrate**	**T (°C)**	**t_R (h)**	**Cat.**	**Y_{Fu} (mol%)**	**Ref.**
EG	1.7:1	protic, hb	Xylose 2.5 wt%	200	1	-	20	128
EG	1:0	protic, hb	Xylose 13.3 wt%	160	0[a]	A70[b]	13.5	110
GVL	1:1	aprotic, hb	Xylose 2 wt%	190	12	-	54	130
GVL	7:3	aprotic, hb	Xylose 2 wt%	225	0.03	HCl	81	41
GVL	4:1	aprotic, hb	Xylose 2 wt%	225	0.03	HCl	82.5	41
GVL	9:1	aprotic, hb	Xylose 2 wt%	225	0.03	HCl	80	41
GVL	9:1	aprotic, hb	Corn stover 6.6 wt%	170	3	H_2SO_4	63	131
GVL	9:1	aprotic, hb	Corn stover[c] 5 wt%	170	0.5	H_2SO_4	96	131
Sulfolane	1:1	aprotic, hb	Xylose 2 wt%	190	5.5	-	61	130
Sulfolane	1.9:1	aprotic, hb	Xylose 2.5 wt%	200	1	-	29	128
Sulfolane	1.9:1	aprotic, hb	Xylose 2.5 wt%	200	1	ZSM-5	50	128
Methanol	1:1	protic, lb	Xylose 5.58 wt%	150	2	A70[b]	29	40
Methanol	4.5:1	protic, lb	Xylose 5.58 wt%	170	0.66	A70[b]	52	40
Ethanol	1:1	protic, lb	Xylose 2.5 wt%	220	0.08	H_2SO_4	89.8	138
Ethanol	1:9	protic, lb	Xylose 2.5 wt%	200	0.5	H_2SO_4	60.7	138
2-Propanol	1:0	protic, lb	Xylose 4 wt%	150	5	SBA-15-Ar-SO_3H	61	136
2-Propanol	1:0	protic, lb	Xylose 13.3 wt%	160	0.66	A70[b]	52	110
2-Butanol	1:0	protic, lb	Xylose 13.3 wt%	160	0.66	A70[b]	57	110
Acetone	1.8:1	aprotic, lb	Xylose 1.5 wt%	150	0.17	H_3PO_4	54	139
THF	1:1	aprotic, lb	Xylose 2 wt%	190	12	-	51	130
THF	1:0	aprotic, lb	Xylose 13.3 wt%	160	0.33	A70[b]	62	110
THF	0.44:1	aprotic, lb	Xylose 1.25 wt%	180	1	-	41.4	140
THF	0.89:1	aprotic, lb	Maple wood 5 wt%	170	0.66	H_2SO_4	87	141
THF	2.66:1	aprotic, lb	Maple wood 5 wt%	170	0.66	H_2SO_4	87	141
THF	2.66:1	aprotic, lb	Maple wood 5 wt%	170	1	$FeCl_3$	97	142
[BMIM]Cl	1:0	IL	Xylan 2 wt%	160	0.17	$H_3PW_{12}O_{40}$	93.7	134
[BMIM]Cl	1:0	IL	Xylose 2 wt%	160	0.17	$H_3PW_{12}O_{40}$	68.4	134
[BMIM]Cl	1:0	IL	Xylose 2 wt%	160	0.03	$AlCl_3$	82.2	133
[EMIM]HSO_4	1:0	IL	Xylose 10 wt%	100	0.5	[EMIM]HSO_4	84	135

[a] Immediately after reaching the desired reaction temperature, [b] Amberlyst 70, [c] Alkaline hydrogen peroxide pretreatment
hb: high boiling point solvent, lb: low boiling point solvent

recent years, different alcohols such as methanol,[40,110,136] ethanol,[136] propanol,[110,136] or butanol[110] have been examined regarding their solvent properties in furfural synthesis. However, most of these studies used only alcohol as a solvent and did not consider or vary the proportion of water. The challenge in this approach lies in separating and purifying furfural and the solvent. Using low boiling point solvents, like THF or ethanol, results in high pressures during reaction and distillation-based purification. Additionally, furfural and other heavy components tend to accumulate in the distillation column's bottom.

2.3.5.4 Reactive Distillation

Another way to prevent furfural degradation and therefore increase the overall yield is reactive distillation, also called furfural stripping or vapor release reaction. In this process approach, furfural is removed directly from the reaction solution, thus avoiding degradation by polymerization reactions (Figure 2.18). Here, the beneficial property of furfural-water mixtures, which form a heterogeneous azeotrope with a minimum boiling point (Figure 2.6), is exploited. This means that a mixture of water and furfural has a lower boiling point than the pure substances. Organic acids such as acetic and formic acid do not form such a minimum azeotrope with furfural, hence there is no enrichment of these. The process is similar to today's industrial production process, in which biogenic residues such as corncobs, bagasse or oat husks are treated with huge amounts of superheated steam (25 – 35 ton/ton furfural).[66,70] Subsequently, formed furfural is stripped by the steam. The disadvantage of this process is that injected and condensing vapor is thermodynamically not able to bring the reaction medium in a boiling state due to soluble sugars and acids that increase the boiling point. However, the boiling state is important to transfer the furfural into the vapor phase.

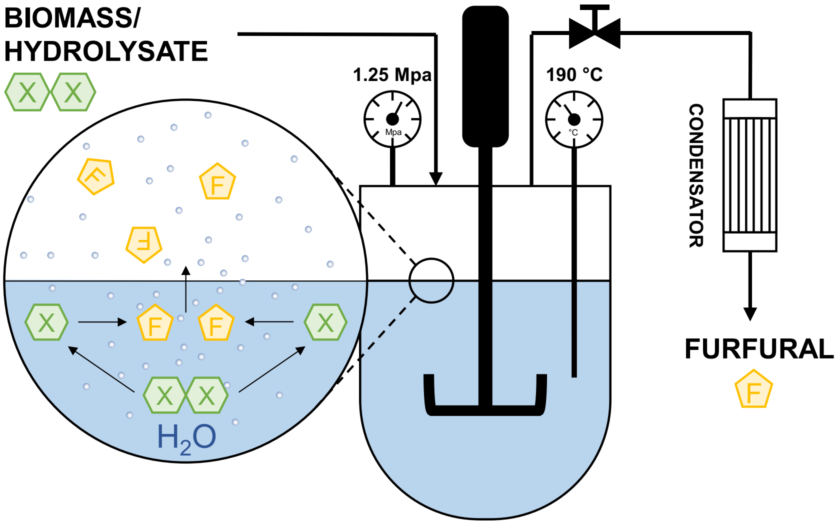

Figure 2.18 Schematic representation of a reactive distillation of furfural from pentoses.

In the case of reactive distillation, the reaction medium remains in the boiling state over the entire reaction period, since the reaction system is closed and only a small part of the vapor is removed at the top. By removing this steam, the volatile furfural can leave the reactor. The approach is similar to the SUPRAYIELD process. Although here the boiling state is maintained by lowering the temperature from 240 to 180 °C and the process has to be repeated several times until no more furfural is obtained. During the heating phase, side reactions can occur which reduce the overall furfural yield.[24]

Over the last few years, reactive distillation has been extensively studied based on D-xylose as a model substance (Table 2.9).[27,42,43,111,112,143–147] The investigations focused on the suitability of various catalysts. In particular, the use of amberlyst-70 and sulfuric acid have shown promising results. The use of stripping agents such as nitrogen has also been sufficiently investigated, particularly around the Agirrezabal-Telleria group. Krzelj et al. have shown in their modeling study that stripping agents have a large energy saving potential.[143] However, especially heterogeneous catalysts are limited for real biomass substrates due to lack of accessibility of the acid centers. So far, less attention has been paid in reactive distillation studies to the use of real biomass substrates or hydrolysates from biorefineries (Table 2.10).[27,90,146–148] Mandalika and Runge were able to show that even higher yields can be achieved, when starting from biomass or hydrolysates than from D-xylose. They attribute this to successive provision of pentoses for furfural production.[147] Therefore, side reactions due to increased furfural-pentose interactions can be reduced in this way. Liu et al. have carried out experiments with hydrolysates without the addition of any catalyst.[27] They were able to demonstrate that the organic acids already contained in the hydrolysate achieve a sufficient catalytic effect.

Table 2.9 Overview of reactive distillation studies for the production of furfural based on D-xylose as starting material.

feed	***T*** (°C)	***t*$_R$** (min)	**catalyst**	**condensate rate** (mL/min)	**stripping rate** (mL/min)	**stripping agent**	**operating mode**	***Y*$_{Fu}$**[1] (mol%)	**ref.**
D-xylose (1 wt%)	170	120	H_2SO_4 (0.5 wt%)		150	N_2	batch	54.0	108
		120			300			66.0	
		100			500			56.6	
D-xylose (2 wt%)	170	390	no	1.15		water vapor	batch	70.0	109
	200	240		1.88				63.0	
D-xylose (5 wt%)[2]	175		H-mordenite 10 g			N_2/water vapor	continuous	75.0	91
D-xylose (1 wt%)	160	180	MgF_2 (M-71) 3 g	7	150	N_2	batch	37.8	110
	180							59.2	
D-xylose (3 wt%)	180							65.7	
D-xylose (2 wt%)	180	180	SBA-12Nb	7	150	N_2	batch	50.4	111
D-xylose (1 wt%)	180	240	Amberlyst-70	5	150	N_2	batch	73	112
D-xylose (3 wt%)								59	
D-xylose (10 wt%)								25	
D-xylose (1 wt%)	175	170	Nb_2O_5/Cabosil		150	N_2	batch	78	69
			Amberlyst-70					87	
D-xylose (3 wt%)	175	150	Amberlyst-70	7	150	N_2	batch	55	70
	200							68	
D-xylose (1 wt%)	175	300					fed-batch	79	
	200							74	
D-xylose (0.5 wt%)	168.5	50	H_2SO_4 (1.6 wt%)	4		water vapor	batch	75.0	113
D-xylose (1 wt%)	175	200	Amberlyst-70		150	N_2	batch	70	114
D-xylose (3 wt%)								52	
D-xylose (5 wt%)								45	
D-xylose (7 wt%)								31	
D-xylose (10 wt%)								25	

[1] Based on initial xylose or pentosan concentration

[2] Glas tube filled with catalyst, feed is added on the top, stripping agent comes from the bottom

Table 2.10 Overview of reactive distillation studies for the production of furfural based on biomass and biomass hydrolysates as starting

feed (pentose content in wt%)	***T*** (°C)	***t_R*** (min)	**catalyst**	**condensate rate** (mL/min)	**stripping rate** (mL/min)	**stripping agent**	**operating mode**	***Y_{Fu}***[1] (mol%)	**ref.**
hardwood hydrolysate (2 wt%)	200	180	no	2.5		water vapor	batch	75.0	109
hardwood hydrolysate (11.2 wt%)	180	20	H_2SO_4 (0.4 wt%)			water vapor	batch	41.5	45
Corncob (0.32 wt%)	180	240	Amberlyst-70	5	150	nitrogen	batch	67	112
Corncob (1 wt%)								57	
Corncob (3.2 wt%)								50	
Bagasse[2] (21 wt%)	158	378	HCl (2 wt%)		0.14	Acid-steam + N_2 as co-feed	semi-continuous	59	115
hybrid poplar hydrolysate (0.5 wt%)	168.5	50	H_2SO_4 (1.6 wt%)	4		water vapor	batch	87.7	113
corn stover hydrolysate (0.5 wt%)								85.1	
miscanthus hydrolysate (0.5 wt%)								94.4	
switchgrass hydrolysate (0.5 wt%)								93.5	
hybrid poplar (0.5 wt%)								79.8	

[1] Based on initial xylose or pentosan concentration

[2] Glas tube reactor filled with bagasse, acid steam flows through the bed from below

3 Material and Methods

The following section provides a comprehensive description and explanation of all materials and experimental setups used in this dissertation. Additionally, it includes a detailed overview of all calculations, kinetic modeling, and analytical methods utilized. For detailed descriptions of the methods and materials, please refer to Papers 1, 2, and 4.

3.1 Materials

3.1.1 Chemicals

D-Xylose (Sigma-Aldrich, >99%) was utilized for experimental investigations (Paper 1-2) and for HPLC calibration (Paper 1 – 4). Furfural (Sigma-Aldrich, ≥98%) was employed in decomposition studies (Paper 1) and also for HPLC calibration (Paper 1 – 4). Sulfuric acid (≥96%), obtained from Sigma-Aldrich, was used as an analytical standard and served as the homogeneous acid catalyst during the first and second experimental series. In the third experimental series, phosphoric acid (85%, Carl Roth, Germany) was used as the homogeneous acid catalyst for all experiments. Additional chemicals used for analytical purposes included D-glucose (Merck, >99%), D-fructose (Alfa Aesar, >99%), L-(+)-arabinose (Alfa Aesar, >99%), D-(+)-galactose (≥99%, Sigma-Aldrich), 5-hydroxymethylfurfural (≥99%, Sigma-Aldrich), and calcium carbonate ($CaCO_3$, ≥99%, Carl Roth).

3.1.2 Organosolv Hemicellulose

Samples of the hemicellulose fraction were provided by the lignocellulose biorefinery pilot plant at the Fraunhofer Center for Chemical-Biotechnological Processes CBP (Leuna, Germany). These spent liquors were produced through the fractionation of industrial debarked beech wood (Fagus sylvatica) chips using an ethanol–water pulping process in a batch operation. In each batch, 70 kg (oven-dry) of wood chips were pulped in a 540 L batch reactor with forced circulation at 170 °C for 100 minutes, using 150 kg of an ethanol/water mixture (1:1 mass ratio) and 0.8 wt% sulfuric acid (based on oven-dry wood) as a catalyst. The hemicellulose fraction was obtained by diluting the organosolv spent liquor at a 1:2 ratio with water, which precipitated the dissolved lignin. Subsequently, the precipitated lignin was filtered out from hemicellulose solution and residual ethanol was removed by rectification. To increase the sugar concentration, water was removed in a falling film evaporator at reduced pressure. For the second experimental series, a higher concentration was required. Finally, the hemicellulose solution was filtered by vacuum filtration using a paper filter (MN 619 DE, retention capacity 1–2 µm, Macherey-Nagel, Germany) to remove larger particles and impurities. The composition and pH of the hemicellulose fractions used in the three experimental series (Paper 1,2, and 4) are shown in Table 3.1.

Table 3.1 Organosolv hemicellulose (OHC) composition used for hydrothermal furfural production.

Components		**OHC-1**	**OHC-2**	**OHC-3**
glucose	g L^{-1}	4.3	20.6	3.0
glucooligosaccharide [a]	g L^{-1}	n. m.	n. m.	3.0
D-xylose	g L^{-1}	36.8	133.5	37.5
arabinose	g L^{-1}	2.6	n. m.	1.5
xylooligosaccharide [b]	g L^{-1}	33.2	93.7	24.2
5-HMF	g L^{-1}	0.8	2.6	n. d.
furfural	g L^{-1}	0.2	0.4	1.0
acetic acid	g L^{-1}	6.9	30.7	3.3
formic acid	g L^{-1}	0.0	3.7	0.4
ethanol	g L^{-1}	4.0	22.8	n. m.
pH	-	1.6	1.6	1.7

[a] β-D-glucose equivalent

[b] D-xylose equivalent

3.1.3 Spelt Husk Hydrolysate (SHH)

In the third experimental series, a biomass hydrolysate derived from spelt husks was required. To obtain a hemicellulose-rich solution from the spelt husks, hydrothermal pretreatment experiments were conducted. The goal was to optimize the process parameters to maximize the dissolution of hemicellulose into the liquid phase. To achieve this, response surface methodology (RSM) was employed, utilizing a two-factor (temperature and reaction time) face-centered central composite design (CCF). This approach allowed for the systematic exploration of the optimal conditions for hemicellulose extraction. A comprehensive description of the hydrothermal pretreatment experiments, including the specific parameters and procedures used, is provided in the methodology section (3.2.2.3). The resulting composition of the spelt husk hydrolysate (SHH) is detailed in (Table 3.2), offering insight into the effectiveness of the pretreatment process and the characteristics of the hydrolysate produced.

Table 3.2 Composition and pH of produced spelt husk hydrolysate.

Components		**Spelt husk hydrolysate**[1)]
Glucose	g L^{-1}	4.0
Oligoglucose	g L^{-1}	1.7
D-Xylose	g L^{-1}	10.4
Oligoxylose	g L^{-1}	n.d.
Arabinose	g L^{-1}	1.7
Furfural	g L^{-1}	1.0
5-HMF	g L^{-1}	0.3
Formic acid	g L^{-1}	0.2
Acetic acid	g L^{-1}	1.8
pH	-	2.6

3.1.4 Biomasses

For reactive distillation experiments in the third experimental series, spelt husks (Triticum spelta) were provided from Schapfen Mühle GmbH & Co. KG (Ulm-Jungingen, Germany). Debarked beech wood shavings (Fagus sylvatica) were obtained from Abalon Hardwood Hessen GmbH (Schwalmstadt-Treysa, Germany) and also used for reactive distillation experiments (Series 3). The biopolymer composition of the spelt husks (SH) and beech wood shavings (BWS) is detailed in (Table 3.3).

Table 3.3 Biopolymeric composition, ash content, and dry matter of used feedstocks.

Constituents	**Sugar monomer**	**Spelt husks, SH (wt%)**	**Beech wood shavings, BWS (wt%)**
Cellulose	Glucose	40.0	42.6
Hemicellulose	Xylose	24.5	16.8
	Arabinose	2.8	0.5
	Mannose	0.2	1.1
	Galactose	1.1	0.8
	Rhamnose	0.1	0.4
Lignin	-	15.7	22.4
Ash (550 °C)	-	4.7	0.7
Dry matter	-	92.5	90.4

3.2 Methods

3.2.1 Analytical Methods

3.2.1.1 High Performance Liquid Chromatography

To determine the oligo- and monosaccharides along with the furans, all samples from the first experimental series were analyzed using an Agilent HPLC system (1200 series, Agilent Technologies, Santa Clara, USA). HPLC analysis for the second and third experimental series were performed on an AZURA HPLC system (Knauer, Berlin, Germany) equipped with a binary pump system (AZURA P 6.1L), an autosampler (3950), a column oven, a diode array detector (DAD), and a refractive index detector (RID). While sugars were detected by RID, furan determination was conducted over a DAD set at 280 nm. The autosampler, tempered to 10 °C, injected 15 µL of the sample into a MetaCarb 87P column (300 × 7.8 mm, Agilent Technologies, Santa Clara, CA, USA) equipped with a precolumn (30 × 7.8 mm) heated to 70 °C. For both HPLC systems the same column was used. However, the equipped precolumn (50 × 4.6 mm) for the Agilent HPLC system has slightly different geometries and was tempered at 80 °C. Ultrapure water was taken as mobile phase under isocratic conditions and a flow rate of 0.35 mL min^{-1}. Before starting the analysis, each sample was separated two times from insoluble particles by centrifugation. First, without filter for 10 min at 10 °C and a speed of 10 000 rpm and then with a filter inlet (0.2 µm) under the same conditions.[149]

Oligosaccharide concentrations were determined according to NREL methodology.[150] The sample (4.2 mL) was fully hydrolyzed with 0.15 mL of 72 % sulfuric acid and heated to 121 °C for 40 min in a digital dry bath heater (Dual Block 230 V, Corning LSE). Afterward, the sample was cooled for 30 min at 30 °C in a refrigerated heating circulator (FP 50-MS, Julabo, Seelbach, Germany) and adjusted to a pH 7 with $CaCO_3$ (≥99 %, Carl Roth GmbH, Karlsruhe, Germany). Finally, the hydrolyzed samples were analyzed by HPLC in terms of D-xylose concentration. All HPLC measurements were conducted at least in duplicate.

3.2.1.2 Gas Chromatography – Flame Ionization Detector (GC-FID)

The analysis of carboxylic acids, after derivatization into methyl esters, was conducted using a 7890A gas chromatograph equipped with a flame ionization detector (FID), both supplied by Agilent Technologies. This setup was complemented by a Turbomatrix110 headspace autosampler from Perkin Elmer, USA. The temperatures set for the headspace sampler were 85 °C for the oven, 100 °C for the needle, and 110 °C for the deactivated transfer line, respectively. The analysis protocol included a 25 min vial equilibration period, 3 min for pressurization, 0.1 min for injection, and a 0.5 min dwell time. The system operated with a carrier pressure of 32 psi and a vial pressure of 28.5 psi, using a 1:10 split injection mode. The injector temperature was maintained at 220 °C. Chromatographic separation was achieved on a DB-FFAP column (60 m × 0.25 mm × 0.5 µm, Agilent Technologies), with an initial oven temperature of 40 °C held for 20 min, followed by a linear temperature increase of 10 °C min^{-1} to 200 °C, which was then maintained for 10 min. The FID for data acquisition was set at 260 °C. For each analysis, a 20 mL headspace vial was prepared with 0 mL of the sample, 1 mL of an internal standard (2-methyl butyric acid, 184 mg L^{-1}), 0.5 mL of methanol, and 2.5 mL of sulfuric acid (diluted 1:5), and sealed with an aluminum crimp cap fitted with a PTFE/silicone septum. Each analysis was replicated three times.[151]

3.2.1.3 Borate−AEC Analysis

The borate anion exchange chromatography (AEC) method was employed for determining the biopolymeric composition (cellulose, hemicellulose, lignin) and was carried out at the University of Hamburg (Prof. Bodo Saake). Initially, samples were air-dried and ground to fine powder using a disk mill (T-1000, Siebtechnik GmbH, Mülheim an der Ruhr, Germany). The analysis proceeded with a two-stage hydrolysis process. In the first stage, 200 mg of the ground sample was mixed with 2 mL of 72 % sulfuric acid and incubated at 30 °C for 60 min. The reaction was quenched by adding 6 mL of deionized water. Then, the mixture was diluted with 50 mL of deionized water in 100 mL flasks and subjected to a second hydrolysis in an autoclave at 120 °C (0.12 MPa) for 30 min. The suspension was filtered through a G4 sintered glass frit. The acid-insoluble residue, comparable to Klason lignin, was washed with distilled water and its weight was determined gravimetrically after drying at 105 °C. For carbohydrate content analysis, the filtrate was subjected to borate-anion exchange chromatography (Borate-AEC) using a Dionex Ultimate 3000 system (Thermo Fisher Scientific, Waltham, MA, USA). The analysis column (5 mm × 20 mm) was filled with MCI Gel CA08F anion exchange resin (Mitsubishi Chemical, Tokyo, Japan) and operated at 65 °C. This approach to biopolymer composition analysis, specifically employing the borate-AEC method, is detailed in the study by Lorenz et al., published in 2016.[152]

3.2.2 Experimental Methods

3.2.2.1 Kinetic Investigations on Continuous Furfural Production

Hydrothermal conversion experiments with organosolv hemicellulose (OHC-1, Table 3.1) were carried out at different temperatures (160, 180, and 200 °C). Based on these results, experiments with D-xylose (5 wt% → 0.37 mol L^{-1}), and furfural (1 wt% → 0.1 mol L^{-1}) were conducted additionally. The residence time was varied at four stages between 150 and 1400 s. D-Xylose and furfural solutions were acidified with 1.5 mL concentrated sulfuric acid (96 %), resulting in a pH of 1.6. An overview of the performed experiments is listed in (Table 3.4).

For the experiments, a coiled tube reactor as illustrated schematically in (Figure 3.1) was used. The reactor, made of stainless steel (AISI 316Ti), has a total length of 6.8 m (dotted line, Figure 3.1) with an internal diameter of 7 mm. This results in a reaction volume of 260 mL. The aqueous reaction solutions were provided through the reactor by a membrane pump (MfS 35/10 Prominent, Heidelberg, Germany) and first heated up by an electrically driven preheater. Afterwards, the reactants passing the reaction zone (dotted line, Figure 3.1). The reactor tube is coiled around a heating

Table 3.4 Overview of performed kinetic experiments for the first experimental series.

trial	reactants	xylose (mol L^{-1})	furfural (mol L^{-1})	T_R (°C)	catalysts	pH
1	furfural	-	0.1	160	H_2SO_4	1.6
2		-	0.1	180		
3		-	0.1	200		
4	D-xylose	0.37	-	160	H_2SO_4	1.6
5		0.37	-	180		
6		0.37	-	200		
7	organosolv hemicellulose[a]	0.38[b]	3.9×10^{-4}	160	H_2SO_4/ carboxylic acids	1.6
8		0.38[b]	3.9×10^{-4}	180		
9		0.38[b]	3.9×10^{-4}	200		

[a] OHC-1 (Table 3.1), [b] Sum of xylose and xylooligosaccharide

cartridge over a length of 800 mm and isolated from environment. The reactions temperature was kept constant by a temperature controller. After leaving the reactor, process liquor was cooled to ambient by a water-cooled heat exchanger. To avoid a transfer of the aqueous reaction solutions to the vapor phase, the back-pressure regulator was set to 50 bar, to ensure complete liquid operation.

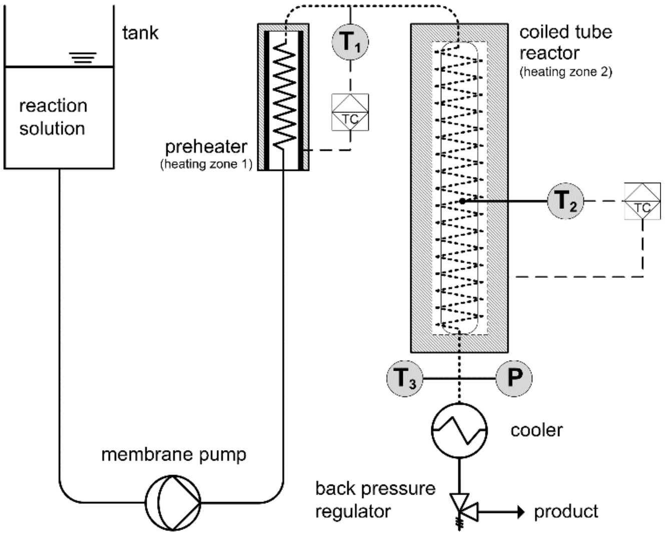

Figure 3.1 Schematic representation of coiled tube reactor used for kinetic investigation on hemicellulose solution, D-xylose, and furfural experiments.

3.2.2.2 Batch Experiments in Water/Ethanol Mixtures

The experiments were conducted in a thermostatically heated stirred batch reactor (BR-500, Berghof Products + Instruments, Germany) at three temperatures (180, 200, and 220 °C). As the reaction solvent, water/ethanol mixtures with different mass ratios (9:1, 4.5:1, and 1:1) as well as pure water were used. To avoid the heat up phase, the reactants were added to the reactor by a liquid charging pipet after the desired temperature was reached. In a typical experiment, 25 g of D-xylose was dissolved with water in a 100 mL volumetric flask and transferred in the liquid charging pipet. The water/ethanol mixture (395.5 mL) as well as the acid catalyst (4.5 mL of 1.8 M H_2SO_4) were loaded into the reactor, resulting in a pH of 1.6. Then, the reactor was purged by nitrogen for 5 min and subsequently heated to 15 K above the respective reaction temperature. The agitation rate during the total process was set at 300 rpm. Finally, the pressurized (6 MPa, nitrogen) charging pipet was opened, and the reactant solution pressed into the reactor. Immediately after addition, the first sample was taken by a liquid sample valve with a dip tube. Five more samples (10 mL) followed after 5, 15, 30, 60, and 180 min. Afterward, the reactor was cooled to ambient temperature by a thermostat (4.5 K min^{-1}). Subsequently, the insoluble humins were separated from the reaction medium by vacuum filtration and dried for 24 h at 105 °C in a drying oven. Humin residues on the agitator and reactor wall were also considered. For experiments with organosolv hemicellulose, 100 mL of the concentrated liquor (OHC-2, Table 3.1) was loaded in the charging pipet. Pretests have shown that 20 mL of 1.8 M sulfuric acid is needed to adjust the pH of the total reaction solution at 1.6.

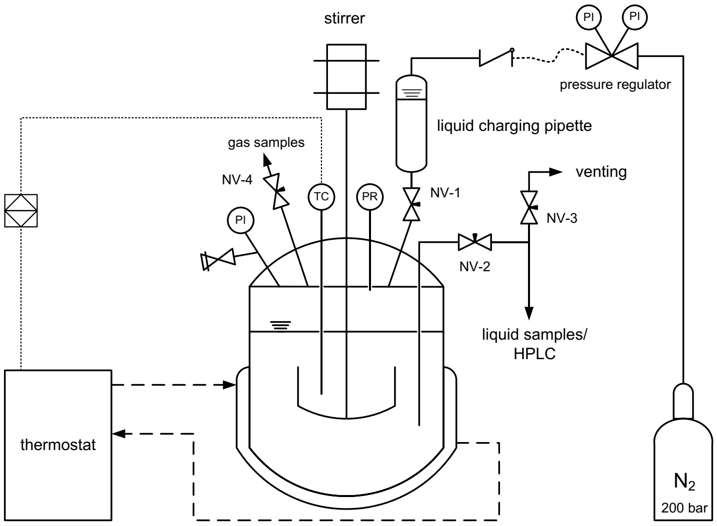

Figure 3.2 Schematic representation of experimental setup of the stirred-tank reactor equipped with a liquid charging pipet and a dip tube for liquid sampling.

3.2.2.3 Hydrothermal Pretreatment

For the provision of spelt husk hydrolysate (SHH), hydrothermal pretreatment experiments were carried out. Hereby a response surface methodology (RSM) was used by creating a two-factor (temperature and reaction time) face-centered central composite design (CCF). While the reaction temperature varied between 140, 160, and 180 °C, the reaction time was 30, 60, and 90 min, respectively. The factorial points were performed once and the center point were repeated three times (Figure 3.3). For statistically evaluation and creation of an empirical model, to predict appropriate process parameters to reach maximum hemicellulose yields in the liquid phase, the software design expert (State-Ease Inc., Version 11) was used.

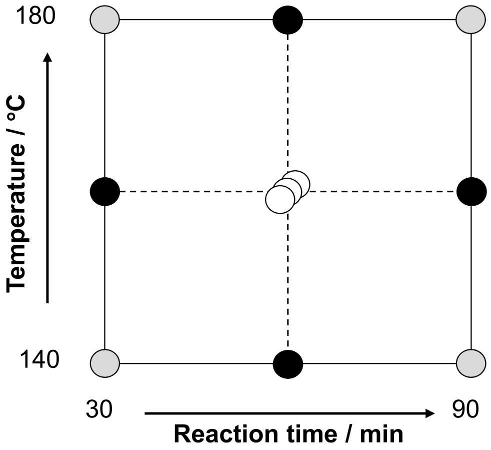

Figure 3.3 Schematic representation of the experimental design: face-centered central composite, α=1.

For a typical experiment, 28 g of spelt husks were loaded into an electrically heated stirred tank reactor (BR-500, Berghof Products + Instruments, Germany) and filled with 420 mL of distilled water, resulting in a water to biomass ratio of 15. Subsequently, 0.019 mol phosphoric acid was added, obtaining a pH of 2. The reactor was then sealed and heated up to the respective temperature with steady stirring (100 rpm) at a heating rate of 2 K min^{-1}. The reaction time was started only after the target temperature was reached. At the end of the reaction time, the electric heating was switched off and the reactor was cooled down to ambient temperature (~ 24 h). Finally, the cooled solid/liquid mixture was separated by vacuum filtration, and the liquid phase was analyzed by HPLC and GC-FID regarding hexoses, pentoses, furans, and organic acids. To provide SHH for the hydrothermal reactive distillation (HRD) experiments, three additional experiments were conducted under the determined optimal experimental conditions. The final composition and pH of those SHH used for HRD experiments are listed in Table 3.2.

3.2.2.4 Hydrothermal Reactive Distillation

HRD experiments were carried out on a 0.5 L stainless steel stirred tank reactor (BR-500, Berghof Products + Instruments, Germany) equipped with a reflux condenser (Figure 3.4). In contrast to prehydrolysis experiments, this reactor was heated with a high-temperature thermostat from Lauda (XT 4 HW, Lauda, Herzogenrath, Germany). An overview of the conducted HRD experiments can be taken from Table 3.5.

Table 3.5 Overview of the performed hydrothermal reactive distillation experiments.

Run	Feedstock	m_{Feed} 1) (g)	$V_{Feed/H2O}$ (mL)	Pentose content (wt%)	T (°C)	t_R (min)	catalyst	pH
1 2)	Spelt husks	12.7	379	0.9	170	150	H_3PO_4	2.0
2 2)					190			
3 2)					210			
4	Beech wood shavings	12.7	379	0.6	170	150	H_3PO_4	2.0
5					190			
6					210			
7	Spelt husk hydrolysate	-	330	1.2	170	150	H_3PO_4	2.0
8					190			
9					210			
10	Organosolv hemicellulose	-	380	6.3	170	150	H_2SO_4	1.7
11					190			
12					210			

1) without water content; 2) was performed twice

A typical experiment with SH or BWS was carried out as follows. The empty reactor was filled with the appropriate amount of biomass and water, resulting in a mass ratio of water to biomass of 30. The residual moisture of the biomass was taken into account. Then, a pH of 2.0 was adjusted by adding phosphoric acid (0.013 mol). The reactor was subsequently sealed and the headspace was purged with nitrogen for 3 min. To heat up the reactor to the target temperature of 170, 190, and 210 °C, respectively, a heating rate of 3 K/min was selected for each experiment. After the desired temperature was reached, a fine control valve (NV-1, Figure 3.4) was opened at the head of the reactor to release the steam. The discharged steam was channeled into the reflux condenser and completely condensed. The condensate was collected continuously (1 mL min^{-1}) in a measuring cylinder. In order to better follow the course of the reaction, a new measuring cylinder was placed underneath every 30 min. In this way, a total of five samples with 30 mL each were obtained over the reaction period of 150 min. After the end of the reaction period (150 min), a sump sample was also taken from the reactor using a dip tube. A stirring speed of 300 rpm was set for all phases of the experiment (heating, reaction, and cooling phases). The hydrolysate experiments were performed analogously, whereas only 330 instead of 380 mL per experiment were available for the SHH. Furthermore, the pH of the SHH was lowered from 2.6 to 2 by adding 0.014 mol H_3PO_4. The pH of the OHC was 1.7 and is mainly caused by the sulfuric acid used in the organosolv process. A pH adjustment was consciously omitted in order not to add any additional cations to the solution.

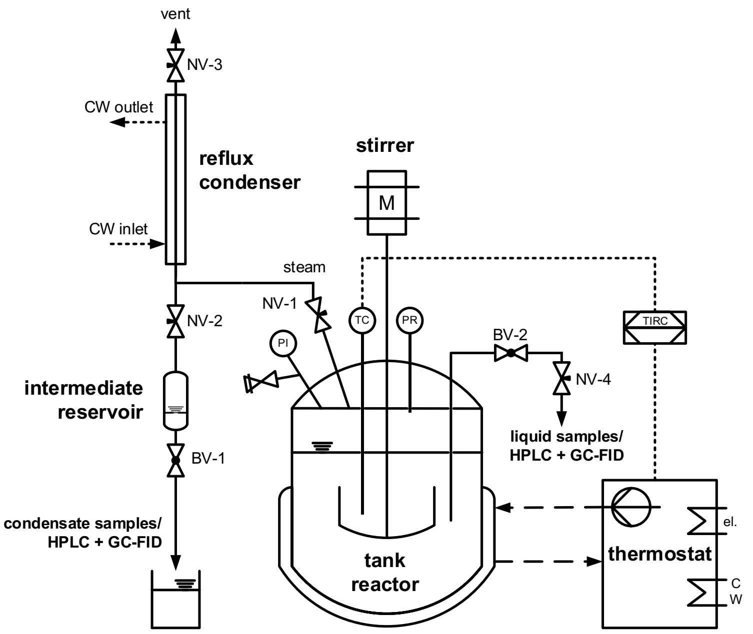

Figure 3.4 Schematic representation of experimental set-up of the stirred-tank reactor equipped with a reflux condenser and a dip tube for liquid sampling.

3.2.3 Kinetic Modeling

3.2.3.1 Kinetic Investigations on Continuous Furfural Production

In the literature, several kinetic models for acid-catalyzed production of furfural are described.[92,153,154] However, the kinetic models often characterize either the hydrolysis of hemicellulose[57,155–157] or the dehydration of D-xylose to furfural including different side reactions.[34,91,92] In this study, combinations of both models are investigated. Three different D-xylose conversion mechanisms are coupled with a simple hemicellulose hydrolysis step (Scheme 3.1). In the literature, a fast and a slow conversion step for hemicellulose is suggested. Since in our study dissolved hemicellulose was used, a simple hydrolysis step starting from xylooligosaccharide $[\mathrm{Xos}]$ was preferred. All mechanisms are depicted in Scheme 3.1 and differ mainly in terms of their side reactions. Mechanism 1 is following a first order reaction kinetic. Whereby furfural is degraded only by self-polymerization and D-xylose is decomposed directly. In mechanism 2, furfural degradation is additionally influenced by cross-polymerization between D-xylose and furfural. Mechanism 3 considers the furfural dehydration via an intermediate species and its cross-polymerization with furfural. The cross polymerization in mechanism 2 and 3 following a second order reaction kinetic.

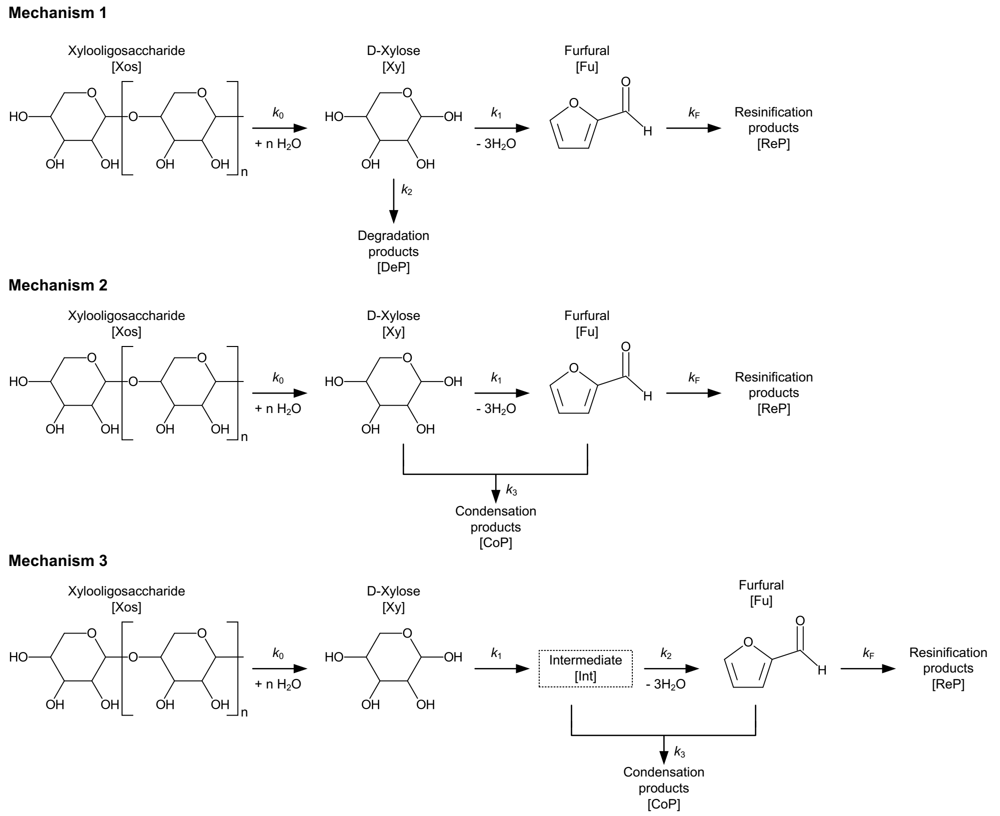

Scheme 3.1 Reaction mechanisms for conversion of xylooligosaccharide [Xos] to D-xylose [Xy], furfural [Fu], and resinification [ReP] as well as degradation [DeP] and condensation [CoP] products.

Based on these reaction mechanisms, the following reaction rate equations (Eq. (3.1)-(3.8)) for modeling reaction kinetics were formulated:

Hydrolytic splitting of xylooligosaccharide [Xos]:

$$\frac{d[\mathrm{Xos}]}{dt} = -k_0[\mathrm{Xos}] \tag{3.1}$$

Mechanism 1:

$$\frac{d[\mathrm{Xy}]}{dt} = k_0[\mathrm{Xos}] - k_1[\mathrm{Xy}] - k_2[\mathrm{Xy}] \tag{3.2}$$

$$\frac{d[\mathrm{Fu}]}{dt} = k_1[\mathrm{Xy}] - k_{\mathrm{F}}[\mathrm{Fu}] \tag{3.3}$$

Mechanism 2:

$$\frac{d[\mathrm{Xy}]}{dt} = k_0[\mathrm{Xos}] - k_1[\mathrm{Xy}] - k_3[\mathrm{Xy}][\mathrm{Fu}] \tag{3.4}$$

$$\frac{d[\mathrm{Fu}]}{dt} = k_1[\mathrm{Xy}] - k_3[\mathrm{Xy}][\mathrm{Fu}] - k_{\mathrm{F}}[\mathrm{Fu}] \tag{3.5}$$

Mechanism 3:

$$\frac{d[\mathrm{Xy}]}{dt} = k_0[\mathrm{Xos}] - k_1[\mathrm{Xy}] \tag{3.6}$$

$$\frac{d[\mathrm{Int}]}{dt} = k_1[\mathrm{Xy}] - k_2[\mathrm{Int}] - k_3[\mathrm{Int}][\mathrm{Fu}] \tag{3.7}$$

$$\frac{d[\mathrm{Fu}]}{dt} = k_2[\mathrm{Int}] - k_3[\mathrm{Int}][\mathrm{Fu}] - k_\mathrm{F}[\mathrm{Fu}] \tag{3.8}$$

Whereby k_0, k_1, k_2, k_3, and k_F are the rate constants and [Xos], [Xy], [Int], and [Fu] are the concentrations (mol L^{-1}) for xylooligosaccharide, D-xylose, intermediate species, and furfural. To calculate the rate constant for furfural destruction k_F, furfural degradation experiments were conducted. Therefore, the analytical solution of (Eq. (3.10)) were fitted to the experimental captured data.

$$\frac{d[\mathrm{Fu}]}{dt} = -k_\mathrm{F}[\mathrm{Fu}] \tag{3.9}$$

Afterwards, the system of ordinary differential equations (Eq. (3.1)-(3.9)) was solved numerically by Matlab. As solver ODE15S was used. The rate constants were estimated by using the LSQCURVEFIT function. For determination of activation energy E_i and the pre-exponential factor $A_{0,i}$ a modified Arrhenius expression (Eq. (3.10)) was used, that take into account the temperature influence as well as the acid concentration:

$$k_i = A_{0,i}[\mathrm{H}^+]^{m_i} \exp\left(-\frac{E_i}{RT}\right) \tag{3.10}$$

Where E_i is the activation energy (kJ mol^{-1}), T the temperature (K), R the universal gas constant (8.3143×10^{-3} kJ mol^{-1} K^{-1}), $A_{0,i}$ the pre-exponential factor (s^{-1}), [H^+] the hydrogen ion concentration (mol L^{-1}) and m_i the acid concentration exponent (unitless). The activation energy and the pre-exponential factor could be determined by linear fitting of logarithmic expression (Eq. (3.11)) of (Eq. (3.10)):

$$\ln k_i = \ln A_{0,i} + \ln[\mathrm{H}^+]^{m_i} - \frac{E_i}{R}\frac{1}{T} \tag{3.11}$$

The acid concentration exponent m_i was set to 1 for all rate constants and kinetic models.

3.2.3.2 Batch experiments in water/ethanol mixtures

For kinetic modeling, a simplified reaction mechanism, depicted in Scheme 3.2, was used that ignored the second order reaction between furfural and D-xylose or D-xylose intermediates. As described in our previous study, such model shows sufficiently accurate results and is well suited to describe the reaction course.[158]

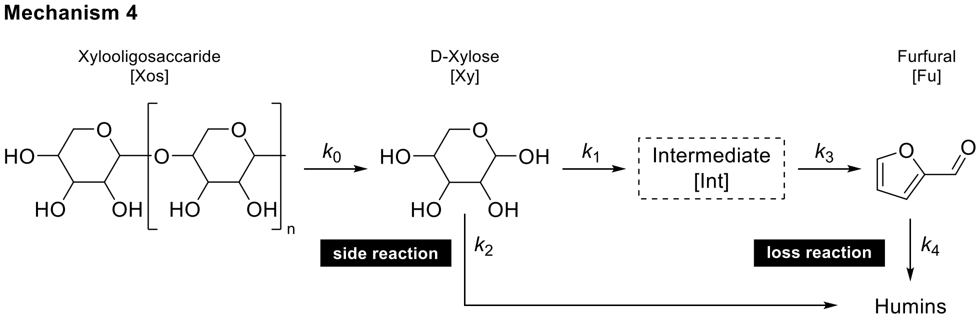

Scheme 3.2 Reaction mechanism for the conversion of xylooligosaccharide [Xos] to furfural [Fu] via D-xylose [Xy] and a reactive intermediate [Int], including side and loss reactions.

Based on the reaction mechanism 4, the following reaction rate equations (3.12) – (3.15) for kinetic modeling were formulated:

$$\frac{\mathrm{d[Xos]}}{\mathrm{d}t} = -k_0[\mathrm{Xos}] \tag{3.12}$$

$$\frac{\mathrm{d[Xy]}}{\mathrm{d}t} = k_0[\mathrm{Xos}] - (k_1 + k_2)[\mathrm{Xy}] = k_0[\mathrm{Xos}] - k'[\mathrm{Xy}] \tag{3.13}$$

$$\frac{\mathrm{d[Int]}}{\mathrm{d}t} = k_1[\mathrm{Xy}] - k_3[\mathrm{Int}] \tag{3.14}$$

$$\frac{\mathrm{d[Fu]}}{\mathrm{d}t} = k_3[\mathrm{Int}] - k_4[\mathrm{Fu}] \tag{3.15}$$

where k_0, k_1, k_2, k_3, and k_4 are rate constants (min^{-1}). According to Bodenstein's formulated quasi-stationary state approximation, where the intermediate concentration does not change or almost does not change ($\mathrm{d[Int]}/\mathrm{d}t \triangleq 0$), these differential equations can be analytical solved (detailed explanation can be found in the Supporting Information of the second paper[138]). By implementing the analytical solutions of equations (3.12) – (3.15) in the data analysis and graphing software OriginPro 2019 the kinetic rate constants could be determined by means of the Levenberg-Marquardt iteration algorithm. To calculate the activation energy and the pre-exponential factor, the modified Arrhenius expression (3.10) that consider the hydrogen ion concentration, was applied by linear fitting of logarithmic expression (3.11).

3.2.4 Calculations

3.2.4.1 Stoichiometry

The stoichiometry of converting D-xylose to furfural involves the dehydration of D-xylose, where each molecule of D-xylose is transformed into one molecule of furfural and three molecules of water (3.16).

$$\mathrm{C_5H_{10}O_5 \rightarrow C_5H_4O_2 + 3H_2O} \tag{3.16}$$

Therefore, the theoretical maximum mass yield of furfural from D-xylose can be calculated based on the molar masses of D-xylose (150.13 g mol^{-1}) and furfural (96.08 g mol^{-1}). The yield is the ratio of the molar mass of furfural to the molar mass of D-xylose and amounts 64 wt%. For this reason, all stoichiometric calculations in this work were carried out using molar concentrations.

D-Xylose conversion (X_{Xy}), furfural yield (Y_{Fu}), and furfural selectivity (S_{Fu}) were calculated according to equations (3.17), (3.18), and (3.19), respectively:

$$X_{\mathrm{Xy}} = \frac{([\mathrm{Xos}]_0 + [\mathrm{Xy}]_0) - ([\mathrm{Xos}]_1 + [\mathrm{Xy}]_1)}{[\mathrm{Xos}]_0 + [\mathrm{Xy}]_0} \times 100\ \% \tag{3.17}$$

$$Y_{\mathrm{Fu}} = \frac{[\mathrm{Fu}]_1 - [\mathrm{Fu}]_0}{[\mathrm{Xos}]_0 + [\mathrm{Xy}]_0} \times 100\ \% \tag{3.18}$$

$$S_{\mathrm{Fu}} = \frac{Y_{\mathrm{Fu}}}{X_{\mathrm{Xy}}} \times 100\ \% \tag{3.19}$$

where $[\mathrm{Xos}]$, $[\mathrm{Xy}]$, and $[\mathrm{Fu}]$ represent the concentration (mol L^{-1}) for xylooligosaccharide, D-xylose, and furfural before (0) and after the reaction (1).

Yield of dissolved hemicellulose in the hydrolysate was calculated according to equation (3.20):

$$Y_{\mathrm{HC}} = \frac{[\mathrm{Xos}]_1 + [\mathrm{Xy}]_1 + [\mathrm{Ara}]_1 + [\mathrm{Fu}]_1}{[\mathrm{HC}]_0} \times 100\ \% \tag{3.20}$$

Here $[\mathrm{HC}]_0$ stands for the amount of hemicellulose in the starting material and $[\mathrm{Ara}]_1$ are the amounts of dissolved arabinose after the hydrolysis.
Yield of dissolved glucose in the hydrolysate was calculated according to equation (3.21):

$$Y_{Glu} = \frac{[\mathrm{Glu}]_1}{[\mathrm{CE}]_0} \times 100\ \% \tag{3.21}$$

Whereby $[\mathrm{CE}]_0$ stands for the amount of cellulose in the starting material and $[\mathrm{Glu}]_1$ for the amount of dissolved glucose in solution.

The following outlines the stoichiometric calculations for cumulative yields from the third experimental series. It includes the method for determining the cumulative yield of furfural found in the condensate, as well as the overall furfural yield, which is the sum of the amounts in both the condensate and the sump:

$$Y_{\mathrm{Fu},j} = \frac{\left(\sum_{i=1}^{j}[\mathrm{Fu}]_j\right) + [\mathrm{Fu}]_{\mathrm{S},1} - [\mathrm{Fu}]_0}{[\mathrm{HC}]_0} \times 100\ \% \tag{3.22}$$

Here $[\mathrm{Fu}]_j$ corresponds to the dissolved amount of furfural in the condensate and $[\mathrm{Fu}]_0$ the amount of dissolved furfural in the hydrolysate. For experiments starting from biomass, this term can be neglected. The running index *j* stands for the corresponding condensate samples 1 – 5. $n_{\mathrm{Fur(s)1}}$ represents the amount of furfural in the sump after 150 min of reaction time and is only introduced to calculate the total furfural yield. In any other case this term must be neglected. $n_{\mathrm{HC,0}}$ stands for the amount of hemicellulose in the starting material. The yield of by-products (5-HMF or levulinic acid) in the reactor sump starting from the cellulose/hexose fraction was calculated as follows:

$$Y_{\mathrm{BP}} = \frac{[\mathrm{BP}]_1 - [\mathrm{BP}]_0}{[\mathrm{CE/Hex}]_0} \times 100\ \% \tag{3.23}$$

Whereby $[\mathrm{BP}]_1$ represents the dissolved amount of cellulose/hexose-based by-products in the sump after 150 min of reaction time and $[\mathrm{BP}]_0$ corresponds to the dissolved amount in the untreated hydrolysate. Based on biomass, this term can be neglected. $[\mathrm{CE/Hex}]_0$ denotes the amount of cellulose or hexose in the untreated biomass and hydrolysate, respectively. The selectivity of furfural in the condensate as well as of the overall process was calculated as below:

$$S_{\mathrm{Fu},j} = \frac{\left(\sum_{i=1}^{j}[\mathrm{Fu}]_j\right) + [\mathrm{Fu}]_{\mathrm{S},1} - [\mathrm{Fu}]_0}{[\mathrm{HC}]_0 - [\mathrm{Xy}]_1 - [\mathrm{Ara}]_1} \times 100\ \% \tag{3.24}$$

Where $[\mathrm{Xy}]_1$ and $[\mathrm{Ara}]_1$ corresponds to the dissolved amount of D-xylose and arabinose in the sump after the reaction. The calculation of the selectivity of by-products (5-HMF or levulinic acid) in the reactor sump starting from the cellulose/hexose fraction was carried out as shown in the following:

$$S_{\mathrm{BP}} = \frac{[\mathrm{BP}]_1 - [\mathrm{BP}]_0}{[\mathrm{CE/Hex}]_0 - [\mathrm{Hex}]_1} \times 100\ \% \tag{3.25}$$

Based on biomass, the selectivity cannot be calculated due to the fact that the remaining amount of cellulose and hemicellulose in the biomass residue after the end of the reaction (150 min) cannot be quantified.

3.2.4.2 Regression Model

For the evaluation of the hydrothermal pretreatment after RSM, the following quadratic regression model (3.26) was used for the predicted yield of dissolved hemicellulose:

$$\hat{Y}_{\mathrm{HC}} = \beta_0 + \beta_{\mathrm{T}} x_{\mathrm{T}} + \beta_{\mathrm{t}} x_{\mathrm{t}} + \beta_{\mathrm{Tt}} x_{\mathrm{T}} x_{\mathrm{t}} + \beta_{\mathrm{T}} x_{\mathrm{T}}^2 + \beta_{\mathrm{t}} x_{\mathrm{t}}^2 \tag{3.26}$$

Wherein β represents the regression coefficients and x the variables. The indices T denotes the temperature, while t describes the reaction time.

4 Results and Discussion

In the following chapter, the results and discussions of the scientific investigations underlying this work are presented. These include (**Paper 1**) Kinetics of Hydrothermal Furfural Production from Organosolv Hemicellulose and D-Xylose, (**Paper 2**) Conversion of D-Xylose and Hemicellulose in Water/Ethanol Mixtures, and (**Paper 4**) Hydrothermal Reactive Distillation of Biomass and Biomass Hydrolysates for the Recovery and Separation of Furfural and Its Byproducts.

4.1 Kinetic Investigations on Continuous Furfural Production

In this study, on the basis of three reaction models, kinetics of an aqueous organosolv hemicellulose and D-xylose conversion into furfural was examined at temperatures between 160 and 200 °C using a continuous tube reactor. Furthermore, furfural degradation was investigated to consider the self-polymerization. Results were compared with previous studies and differences are discussed.

4.1.1 Furfural Destruction

Under the given reaction conditions, in addition to the formation, furfural is degraded by consuming reactions:[24]

(i) furfural resinification (furfural reacts with itself, self-polymerization)

(ii) furfural condensation (furfural reacts with D-xylose or D-xylose intermediates, cross-polymerization).

For estimating the rate constant (k_F) for furfural resinification, a furfural solution (0.1 mol L^{-1}) was hydrothermally treated in the absence of D-xylose and xylooligosaccharide to avoid the influence of cross-polymerization. Since the degradation of furfural is influenced by the acid catalyst, sulfuric acid (0.025 mol L^{-1}) was added to the reaction solution. Figure 4.1 shows the decrease in furfural concentration with time for destruction experiments under hydrothermal conditions.

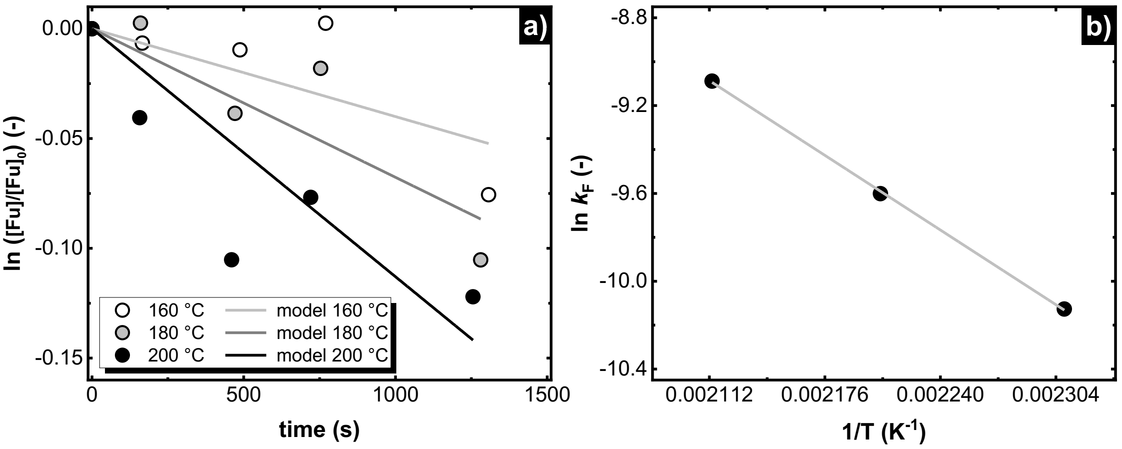

Figure 4.1 Kinetics of furfural degradation as a function of residence time at 160, 180, and 200 °C (a) and the respective Arrhenius plot for the degradation of furfural (b).

By using the analytical solution of (Eq. (3.9)), the experimental data could be fitted, and the respective rate constants were estimated by that procedure. The rate constants for furfural destruction as well as the kinetic parameters are listed in Table 4.1. Activation energy and the pre-exponential factor were determined by the modified Arrhenius equation (Eq. (3.10)).

As depicted in Figure 4.1a, the degradation of furfural shows a strong dependency on the temperature. The degradation rate increases with rising temperature (Table 4.1). This influence was already described in previous studies.[159–162] The dispersion of experimental data, especially for 160 °C, can probably attributed to the used tube reactor, which tends to be due to a missing plug flow to an inhomogeneous concentration distribution of furfural.

Table 4.1 Determined kinetic parameters for furfural degradation.

T (°C)	k_F (s^{-1})	R^2 (-)	E_F (kJ mol^{-1})	ln ($A_{0,F}$) (-)
160	$4.001 \times 10^{-5} \pm 1.305 \times 10^{-5}$	0.7015		
180	$6.766 \times 10^{-5} \pm 1.297 \times 10^{-5}$	0.8719	44.16 ± 0.80	5.82 ± 0.21
200	$1.129 \times 10^{-4} \pm 2.009 \times 10^{-5}$	0.8876		

Nevertheless, the estimated activation energy in this study are in the similar range as the values reported in the literature (Table 4.2). Williams and Dunlop[161], as well as Root et al.,[81] using H_2SO_4 as catalyst, reported higher activation energies of 83.7 and 92.3 kJ mol^{-1}, respectively. In contrast, when using HCl as homogeneous catalyst, Rose et al.[160] and Weingarten et al.[38] have estimated values of 48.1 and 67.6 kJ mol^{-1}, correspondingly. Without the influence of any catalyst, Jing and Lü[26] obtained an activation energy of 58.8 kJ mol^{-1}.

Table 4.2 Overview of activation energies (E_F) for furfural destruction.

Ref.	**Solvent**	**$[Fu]_0$ (mol L^{-1})**	**Catalyst (mol L^{-1})**	**Reactor**^{a}	***T* (°C)**	**E_F (kJ mol^{-1})**
Williams[161]	H_2O	0.01-0.02	0.1 (H_2SO_4)/0.05 (HCl)	sealed tubes	150-210	83.7
Root[81]	H_2O	0.048	0.05-0.8 (H_2SO_4)	sealed tubes	160-240	92.4
Marcotullio[163]	H_2O	0.06-0.073	0.036-0.145 (H_2SO_4)	PFR	150-200	125.1
Jing[26]	H_2O	0.034	none	DSTR	180-220	58.8
Rose[160]	H_2O	0.1	0.1 (HCl)	DSTR	150-170	48.1
Weingarten[38]	H_2O	0.156	0.1 (HCl)	DSTR (microwave)	140-160	67.6
Danon[162]	H_2O	0.05	0.05 (HCl)/0.5 (NaCl)	DSTR	160-200	102.1
Lamminpää[159]	H_2O	0.05-0.16	0.44-6.52 (HCOOH)	sealed tubes	160-200	110.3
Dussan[92]	H_2O	0.1	6.41-21.29 (HCOOH)	sealed tubes	130-170	81.7
Chen[164]	H_2O	0.21	0.17 (CH_3COOH)	DSTR	170-210	63.4

^{a} PFR: plug flow reactor; DSTR: discontinuously tank reactor

One reason for this deviation might be attributed to the short residence time present in this study. With longer reaction times the degradation in furfural is more pronounced, which leads to a lower influence of measurement inaccuracies on the estimated rate constants. Moreover, we did not take in to account the variation of hydrogen ion concentration with temperature, how Marcotullio et al.[163] or Lamminpää et al.[159] have proposed this.

Table 4.3 Determined rate constants and kinetic parameters of corresponded reaction models for acid-catalyzed D-xylose conversion.

	model 1			**model 2**			**model 3**		
***T*(°C)**	**160**	**180**	**200**	**160**	**180**	**200**	**160**	**180**	**200**
k_1 (s^{-1})	9.71×10^{-5}	5.81×10^{-4}	1.43×10^{-3}	2.03×10^{-4}	8.11×10^{-4}	1.84×10^{-3}	3.14×10^{-4}	1.06×10^{-3}	2.38×10^{-3}
E_1 (kJ mol^{-1})		116.5 ± 18.6			94.8 ± 11.4			86.5 ± 8.0	
ln $A_{0,1}$ (s^{-1})		26.9 ± 5.0			21.6 ± 3.0			19.7 ± 2.1	
R^2		0.9751			0.9857			0.9916	
k_2 (s^{-1})	2.17×10^{-4}	4.95×10^{-4}	9.36×10^{-4}	-	-	-	1.08×10^{-3}	4.60×10^{-3}	9.19×10^{-3}
E_2 (kJ mol^{-1})		61.4 ± 4.0			-			91.8 ± 16.4	
ln $A_{0,2}$ (s^{-1})		12.3 ± 1.1			-			22.4 ± 4.4	
R^2		0.9957			-			0.9691	
k_3 (L mol^{-1} s^{-1})	-	-	-	5.70×10^{-3}	3.45×10^{-3}	4.42×10^{-3}	1.23×10^{-2}	1.29×10^{-2}	1.97×10^{-2}
E_3 (kJ mol^{-1})		-			-12.7 ± 17.0			19.8 ± 9.5	
ln $A_{0,3}$ (s^{-1})		-			-5.1 ± 4.5			4.7 ± 2.5	
R^2		-			0.3567			0.8131	

4.1.2 Conversion of D-Xylose

Additional to furfural destruction experiments, investigation with D-xylose solutions (0.37 mol L^{-1}) were conducted to compare the results with literature values and for validation of the experimental method. A D-xylose concentration was used, which corresponded the total D-xylose concentration inside the organosolv hemicellulose liquor. Additionally, sulfuric acid (0.025 mol L^{-1}) was added as catalyst. To calculate the rate constants, the differential equation (Eq. (3.2) – (3.10)) without the xylooligosaccharide term were implemented in a MATLAB environment and numerically solved by using the experimental captured data. The rate constants as well as the respective kinetic parameters for each reaction model are listed in Table 4.3.

Table 4.4 Overview of activation energies (E_i) for D-xylose conversion to furfural and side products.

Ref.	Solvent	$[Xy]_0$ (mol L^{-1})	Catalyst (mol L^{-1})	Reactor	T (°C)	E_1 (kJ mol^{-1})	E_2 (kJ mol^{-1})	E_3 (kJ mol^{-1})
[26]	H_2O	0.072	none	DSTR	180-220	111.5[a]	143.1[a]	-
[165]	H_2O	0.02-0.5	0.05-0.8 (H_2SO_4)	CTR	140-240	76.6[a]	-	-
[166]	H_2O	0.01	0.001-1.0 (H_2SO_4)	sealed tubes	150-200	120.0[c]	-	-
[38]	H_2O	0.002-0.25	0.1 (HCl)	DSTR	130-170	123.9[b]	-	72.5[b]
[164]	H_2O	0.13-0.8	0-1.5 (CH_3COOH)	DSTR	170-210	108.6[b]	-	105.0[b]
[92]	H_2O	0.1	6.5-13.9 (HCOOH)	sealed tubes	130-170	136.0[a]	140.5[a]	-
[92]	H_2O	0.1	6.5-13.9 (HCOOH)	sealed tubes	130-170	137.6[b]	-	128.7[b]
[92]	H_2O	0.1	6.5-13.9 (HCOOH)	sealed tubes	130-170	140.3[c]	82.9[c]	91.5[c]
[91]	H_2O	0.067-0.2	1.5-6.5 (HCOOH)	sealed tubes	130-200	152.0[a]	161.0[a]	-
[91]	H_2O	0.067-0.2	1.5-6.5 (HCOOH)	sealed tubes	130-200	153.0[c]	144.0[c]	143.0[c]

[a] based on model 1
[b] based on model 2
[c] based on model 3

A comparison of the activation energy among each other shows a decrease for E_1 from model 1 (116.5 kJ mol^{-1}) to model 3 (86.5 kJ mol^{-1}). The deviation can be attributed to different conversion routes of D-xylose. While model 1 and 3 are described by a first order kinetic, model 2 following a second order approach. The difference between model 1 and 3 lays on the amount of D-xylose conversion routes, whereas model 1 contains two and model 3 only one. Consequently, the rate constants were differently influenced which led to the fluctuations of activation energy. Previous studies have shown similar results in the same range like our values (Table 4.4). Jing and Lü[26] could calculated an activation energy E_1 of 111 kJ mol^{-1} for model 1. However, the activation energy for the D-xylose decomposition (k_2) is much higher than our value, 143 kJ mol^{-1} in comparison to 62 kJ mol^{-1}. Kim et al.[165], who have also conducted the experiments in a tubular reactor, have determined a value of 76.6 kJ mol^{-1} for E_1 and model 1. Other research groups have calculated slightly higher activation energies than ours. Oefner et al.[166] have calculated activation energies of 120 kJ mol^{-1} independent from sulfuric acid concentration. Basis of their calculation was reaction mechanism 3 (Scheme 3.1). On the basis of model 2, Weingarten et al.[38] calculated a value of 124 kJ mol^{-1} for E_1. Dussan et al.[92], who have explored the same reaction mechanisms like this study, determined a value for E_1 of approximately 140 kJ mol^{-1} for each model and Lamminpää et al.[91] have even received values for E_1 of 153 kJ mol^{-1} based on model 1 and 3. A reasonable cause for the deviation can be attributed to the used reactor type. In contradiction to the most previous studies, a continuous tube reactor was used for this investigation. Therefore, the received experimental data strongly depend on the flow profile and the appropriate backmixing, which influenced the residence time.

In Figure 4.2, the experimental captured data from D-xylose conversion are shown. The diagrams depicted D-xylose and furfural concentration as well as the resulted model curves from reaction mechanism with time. In the examined area, D-xylose concentration decreases faster with increasing temperature. On the other hand, maximum furfural concentration increases with increasing temperature from 0.04 to 0.2 mol L^{-1}. All estimated model curves, implemented in the diagrams (Figure 4.2), show a good prediction of the experimental data. However, a closer consideration to the model curves shows that especially the course of furfural concentration is better represented by model 3, following by model 1 and finally model 2. Regarding to the course of D-xylose concentration, each of the models seems to be in good accordance. For a detailed assessment of the goodness of fit, the coefficient of determination (R^2) was calculated according to the following:

$$R^2 = 1 - \frac{\sum_{i=1}^{n}(c_i - \hat{c}_i)^2}{\sum_{i=1}^{n}(c_i - \bar{c})^2} \tag{4.1}$$

where c_i is the experimental received concentration of D-xylose or furfural, $\hat{c}_i$ is the predicted value calculated by the kinetic model, $\bar{c}$ represent the mean of observed data, and n indicates the number of experimental data.

The coefficient of determination for each model at the respective temperature is depicted in Figure 4.2. A comparison of these values indicates that the models reach a good prediction in terms of the D-xylose concentration course. Moreover, the coefficient of determination of model 1 and model 3 for D-xylose shows nearly no difference. This is because for both models a D-xylose conversion according a first order reaction kinetic was implemented. Therefore, a simple addition of k_1 and k_2 from model 1 leads to the rate constant k_1 of model 3. In model 2 the conversion of D-xylose is following a second order kinetic. However, how it is shown in Figure 4.2 only a slight difference regarding model 1 and 3 can be identified. Interestingly the coefficient of determination for furfural concentration of model 2 shows for 160 and 180 °C a poorly and for 200 °C a good prediction. The deviation can be attributed to reaction mechanism 2 (Scheme 3.1), where it is assumed that furfural consumption take place from the beginning with d-xylose by a second order reaction. At 200 °C the reaction is more advanced due to the faster reaction rate. Therefore, only a slight deviation between the estimated and the real furfural concentration can be observed, which leads overall to a better R^2 factor of the model.

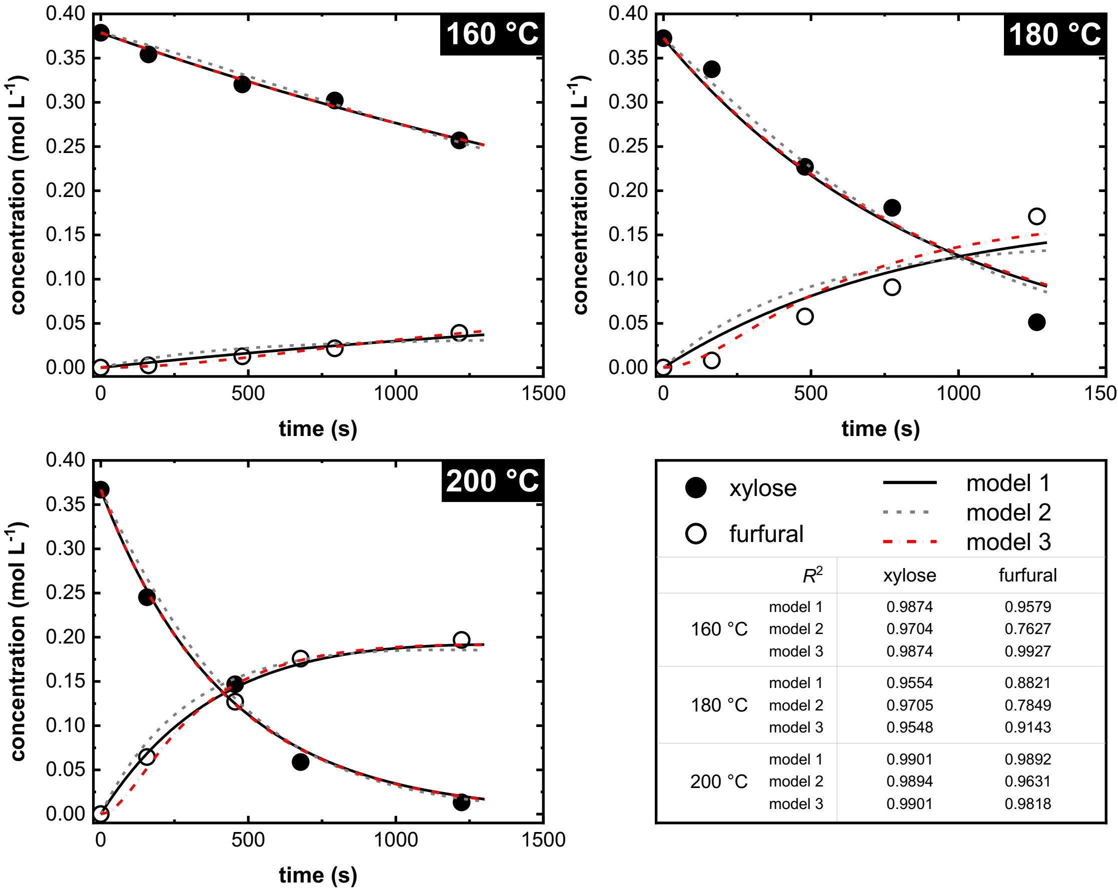

	R^2	xylose	furfural
160 °C	model 1	0.9874	0.9579
	model 2	0.9704	0.7627
	model 3	0.9874	0.9927
180 °C	model 1	0.9554	0.8821
	model 2	0.9705	0.7849
	model 3	0.9548	0.9143
200 °C	model 1	0.9901	0.9892
	model 2	0.9894	0.9631
	model 3	0.9901	0.9818

Figure 4.2 Experimental data from D-xylose conversion and the resulting curves of different reaction models for 160, 180, and 200 °C.

In Figure 4.3, D-xylose conversion (a) as well as the furfural yield (b) are represented with time. Furthermore, the different kinetic models are implemented and extrapolated to a residence time of 6000 s. In terms of D-xylose conversion, it becomes clear that all kinetic models represent the experimental data in good accordance. Only for model 2, a slight increase in D-xylose conversion rate can be seen in comparison to model 1 and 3. The experimental data of D-xylose conversion are comparable with H_2SO_4 catalyzed results from Marcotullio and Jong[34], who also used a tubular reactor and an initial D-xylose concentration of 0.35 mol L^{-1}. Whereas Marcotullio and Jong observed a total D-xylose conversion after a residence time of 1000 s, we found 95 % after 1200 s.

Possibly, that can be attributed to a higher sulfuric acid concentration. Kim et al.[165], who also used a tubular reactor, have received a maximum D-xylose conversion of 30, 50, and 70 % after a residence time of 13,200 s for 160, 180, and 200 °C, respectively. Here, no catalyst was added to the reaction solution. Oefner et al.[166], who also explored the conversion of D-xylose to furfural with and without the aid of sulfuric acid, have observed, after a reaction time of 1200 s and a sulfuric acid concentration of 0.01 M, a D-xylose degradation of 60 % at 190 °C. By increasing the acid concentration to 0.1 M, 80 % of D-xylose were converted already after a reaction time of 600 s.

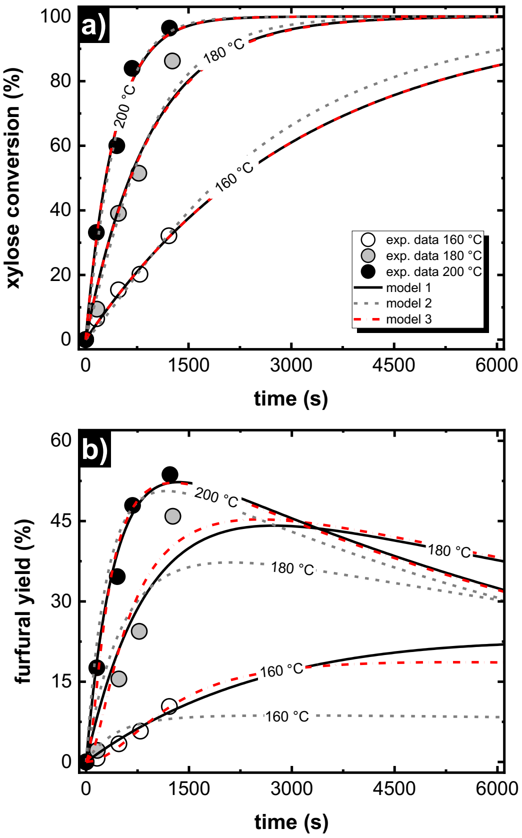

Figure 4.3 D-Xylose conversion (a) and furfural yield (b) of the experimental as well as kinetic modeled data.

Regarding the furfural yield, the experimental results are in good accordance with previous studies. Compared to the maximum furfural yield (61.4 %) reported by Marcotullio and Jong[34], we could observed a maximum yield of 53.7 % for 200 °C. For the mentioned temperatures and residence time Kim et al.[165] have determined a maximum yield of 15, 30, and 55 %, respectively. Oefner et al.[166] have determined a maximum yield between 35 % (0.01 M, H_2SO_4) and 50 % (0.1 M, H_2SO_4) at 190 °C and a reaction time of 1200 s. Concerning to the reaction mechanism, model 1 and 3 describe the experimental calculated yields in a good accordance. However, model 2 is less suitable and shows an underestimated furfural yield. In contrast to the other mechanisms, furfural is directly converted under D-xylose consumption by a condensation reaction. The stronger deviation of mechanism 2 could indicates an incorrect dependency regarding D-xylose and furfural, because a fast D-xylose decomposition inevitable leads to lower furfural yields. Our investigations have shown that the results are in good accordance with values reported by previous studies. Probably, differences can be attributed to the used reactor type as well as different dimensions. Furthermore, deviations in the initial reactant and acid concentration can also lead to different results.

4.1.3 Conversion of Organosolv Hemicellulose

Beside D-xylose and furfural experiments, hydrothermal conversion of organosolv hemicellulose was examined to assess and compare the validity of the models with literature and D-xylose experiments in this study. In addition to D-xylose, organosolv hemicellulose contains unhydrolyzed D-xylose polymers (xylooligosaccharide). To consider the conversion of xylooligosaccharide to D-xylose monomers, a simple first order reaction was implemented in all reaction mechanism (Scheme 3.1). In Table 4.5, all rate constants as well as the respective kinetic parameters are listed.

Table 4.5 Determined rate constants and kinetic parameters of the corresponded reaction models for organosolv hemicellulose conversion.

	model 1			**model 2**			**model 3**		
***T*(°C)**	**160**	**180**	**200**	**160**	**180**	**200**	**160**	**180**	**200**
k_0 (s^{-1})	6.22 x 10^{-3}	1.34 x 10^{-2}	2.75 x 10^{-2}	5.91 x 10^{-3}	1.24 x 10^{-2}	2.52 x 10^{-2}	6.24 x 10^{-3}	1.38 x 10^{-2}	3.02 x 10^{-2}
E_0 (kJ mol^{-1})	63.4 ± 0.3			61.8 ± 0.9			67.1 ± 1.4		
ln $A_{0,0}$ (s^{-1})	16.2 ± 0.1			15.7 ± 30.2			17.2 ± 0.3		
R^2	0.9999			0.9998			0.9995		
k_1 (s^{-1})	1.43 x 10^{-4}	3.24 x 10^{-4}	9.88 x 10^{-4}	3.08 x 10^{-4}	4.85 x 10^{-4}	1.20 x 10^{-3}	4.77 x 10^{-4}	6.65 x 10^{-4}	1.45 x 10^{-3}
E_1 (kJ mol^{-1})	82.2 ± 9.4			57.6 ± 12.5			47.1 ± 12.2		
ln $A_{0,1}$ (s^{-1})	17.6 ± 2.5			11.5 ± 3.3			9.0 ± 3.2		
R^2	0.9871			0.9548			0.9369		
k_2 (s^{-1})	3.33 x 10^{-4}	3.36 x 10^{-4}	4.60 x 10^{-4}	-	-	-	6.33 x 10^{-4}	1.38 x 10^{-3}	9.37 x 10^{-3}
E_2 (kJ mol^{-1})	13.6 ± 7.9			-			114.0 ± 30.9		
ln $A_{0,2}$ (s^{-1})	-0.6 ± 2.1			-			27.8 ± 8.2		
R^2	0.7493			-			0.8628		
k_3 (L mol^{-1} s^{-1})	-	-	-	5.78 x 10^{-3}	3.24 x 10^{-3}	2.34 x 10^{-3}	0	1.11 x 10^{-3}	1.52 x 10^{-2}
E_3 (kJ mol^{-1})	-			-38.7 ± 5.2			[a]-		
ln $A_{0,3}$ (L mol^{-1} s^{-1})	-			-12.2 ± 1.3			[a]-		
R^2	-			0.9822			-		

[a] Determination via Eq. 13 was not feasible.

The highest rate constants could be observed during the xylooligosaccharide conversion kinetic, k_0. Regarding these values, only slight differences between each model have surrendered. A comparison of the rate constants (Table 4.3) based on D-xylose experiments, with those from organosolv hemicellulose exhibit that the most values decreases concerning to the D-xylose experiments. One reason for that behavior could be attributed to hydrolytic splitting of xylooligosaccharide. Thereby, D-xylose is continuously provided for subsequent conversion. On the other side, impurities inside the organosolv hemicellulose could inhibit reactions that led decrease the rate constants. In the literature, kinetic experiments with hemicellulose liquors made by organosolv process are not known. Therefore, previous studies were utilized as reference, which have investigated kinetic parameters on the basis of lignocellulosic biomasses or xylan. Morinelly et al.[157] have treated aspen, balsam, and switchgrass under hydrothermal conditions and estimated the rate constants by a straight first order kinetic.

Along the conversion path from biomass to furfural, rate constants within the range of $1.8 \times 10^{-4} – 3.0 \times 10^{-2}$ s^{-1} were determined for D-xylose formation from xylooligosaccharide at 160 °C. Whereby the values depend on the sulfuric acid concentration as well as the feedstock. Kim et al.[167] have converted a xylooligosaccharide solution obtained from steam pretreated mixed hardwood at 140 to 180 °C using sulfuric acid as catalysts. For kinetic modeling, they have applied an overall kinetic, equal to model 1 of this study. The rate constants calculated by Kim et al.[167] are smaller by a factor of 2 to 10 but show similar trends. Possibly, the higher acid concentration used in this study is responsible for this deviation.

Furthermore, in Table 4.5 the activation energies for the corresponding rate constants and kinetic models are listed. For the conversion of xylooligosaccharide to D-xylose an activation energy of 62 to 67 kJ mol^{-1} were determined depending on the applied model. Compared with previous studies, these results are slightly lower. Kim et al.[167] have determined an activation energy of 89 ± 11 kJ mol^{-1}. The higher activation energy can possibly be attributed to the used substrate. Whereas the hemicellulose solution engaged by Kim et al.[167] contains a big part of unhydrolyzed xylooligosaccharide, in this study a solution with a higher D-xylose content were used. A higher xylooligosaccharide concentration indicates longer D-xylose polymer chains, therefore the hydrolysis of xylooligosaccharide needs more time. Lau et al.[168] investigated the depolymerization of D-xylose oligomers with different chain length. Thereby they have estimated activation energies of 38 – 90 kJ mol^{-1}. The same accounts for the identified activation energies (69 – 89 kJ mol^{-1}) by Morinelly et al.[157]. However, in contradiction to this study, the activation energy for xylooligosaccharide conversion were determined on the basis of lignocellulosic biomass.

The activation energies E_1, E_2, and E_3 are dependent on the applied kinetic model and not comparable with each other. Therefore, an individual discussion is necessary. For model 1, which represents one of the most examined reaction mechanisms, activation energy for D-xylose conversion (E_1) is in good agreement with previous studies (50 kJ mol^{-1} Lau et al.[168], 77 kJ mol^{-1} Kim et al.[165], 116 kJ mol^{-1} Kim et al.[167], 136 kJ mol^{-1} Dussan et al.[92], 155 kJ mol^{-1} Lamminpää et al.[91]). Differences may have resulted due to the usage of various reactors or catalysts.

Model 2 describes a more complex reaction mechanism, where D-xylose degradation was combined with furfural loss. For D-xylose conversion, a lower activation energy occurred compared to former studies (124 kJ mol^{-1} Weingarten et al.[38], 138 kJ mol^{-1} Dussan et al.[92]). Surprisingly, the activation energy, E_2, for condensation polymerization of D-xylose and furfural (model 2), resulted in a negative value. A negative activation energy means that with increasing temperature the reaction rate decrease. During D-xylose conversion experiments, a similar result was obtained. With increasing temperature, the rate constant k_2 for the respective temperatures was nearly constant. These results are not consistent with those from Dussan et al.[92] and Weingarten et al.[38], who were estimated an activation energy of 129 kJ mol^{-1} and 72 kJ mol^{-1}, respectively. The deviation could be due to the longer reaction time (up to 130 min), where the temperature influence on D-xylose decomposition was more pronounced.

In case of model 3, D-xylose conversion passes over an intermediate to furfural. The activation energy for D-xylose conversion E_1 shows a significant smaller value (47 ± 12 kJ mol^{-1}) relating to 83 kJ mol^{-1}Dussan et al.[92] or 153 kJ mol^{-1}Lamminpää et al.[91]. However, for furfural formation, starting from intermediate, the activation energy (E_2) are comparable (92 kJ mol^{-1}Dussan et al.[92], 144 kJ mol^{-1} Lamminpää et al.[91]). The activation energy for furfural loss by cross polymerization could not be estimated, since no rate constant (k_3) at 160 °C could be determined.

In contrast to the determined activation energies for D-xylose conversion experiments, all activation energies are smaller with exception to E_2 in model 3. The reduction of activation energy indicates either the catalytically influence of organic acid contained inside the hemicellulose solution[91,92,167] or due to continuously formation of new D-xylose molecules from xylooligosaccharide hydrolysis.

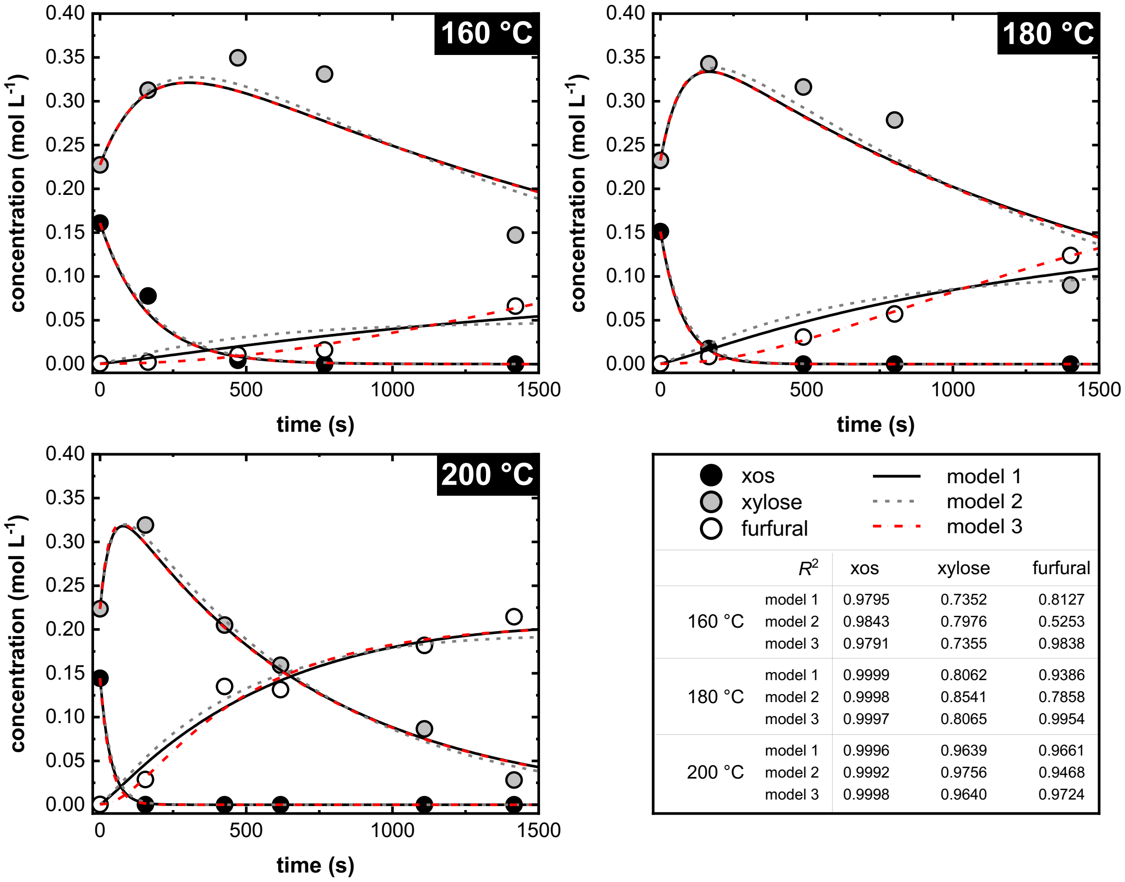

	R^2	xos	xylose	furfural
160 °C	model 1	0.9795	0.7352	0.8127
	model 2	0.9843	0.7976	0.5253
	model 3	0.9791	0.7355	0.9838
180 °C	model 1	0.9999	0.8062	0.9386
	model 2	0.9998	0.8541	0.7858
	model 3	0.9997	0.8065	0.9954
200 °C	model 1	0.9996	0.9639	0.9661
	model 2	0.9992	0.9756	0.9468
	model 3	0.9998	0.9640	0.9724

Figure 4.4 Experimental data from organosolv hemicellulose conversion and the resulting curves of different reaction models for 160, 180, and 200 °C.

In Figure 4.4 experimental captured concentration of xylooligosaccharide, D-xylose, and furfural as well as the predicted course based on the kinetic models are depicted. Moreover, the coefficient of determination indicates the goodness of fit for each model. Results show that xylooligosaccharide concentration was totally converted for all temperatures over the examined residence time. The D-xylose concentration first increase, due to xylooligosaccharide hydrolysis and was after passing a maximum degraded. Whereas the maximum was shifted to shorter residence times with increasing temperatures. The furfural concentration depends strongly from temperature. The measured maximum increases from 0.07 to 0.21 mol L^{-1} for 160 and 200 °C, respectively. Independent by the applied kinetic model, the predicted course of xylooligosaccharide conversion fits well without strong deviations. On the other hand, the mechanisms for D-xylose degradation differ but show only slight departures among each other. Regarding the coefficient of determination, mechanism 2 describes D-xylose dehydration most suitable. Furthermore, the goodness of fit shows better results at higher reaction temperatures. The same accounts for furfural concentration but in contradiction with D-xylose, the predicted courses differ stronger. Similar to D-xylose experiments (Figure 4.2), for 160 and 180 °C, respectively, model 2 shows a poorly and for 200 °C a good prediction, which can be attributed to the second order consumption of furfural in conjunction with D-xylose. Ordered according the coefficient of determination, model 3 describes the furfural formation and degradation most suitable, followed by model 1 and 2. This behavior could be also observed for D-xylose conversion experiments.

Figure 4.5 represents the conversion of xylooligosaccharide, D-xylose, as well as the yield of furfural with time calculated by experimental captured data. Simultaneously an extrapolated course for each model and temperature was implemented. As already mentioned from previous discussion, the models for xylooligosaccharide conversion do not show significant differences. Regarding D-xylose conversion, only model 2 shows a slightly faster conversion in relation to the other models. Overall it could be shown, that increasing temperatures were increase the rate of xylooligosaccharide and D-xylose conversion. Concerning to furfural yield, differences between each model were most pronounced, especially at low temperatures. Depicted by diagram (c) in Figure 4.5, it becomes clear that model 3 fit the experimental data most suitable. However, the extrapolated course of model 3 at 160 and 180 °C shows a questioning progression. The yields further increase with time and reach significant higher maximums (70 %) compared to model 1 and 2. This behavior can be explained by the determined rate constant for cross polymerization (k_3) of intermediate and furfural, which are obviously lower regarding the results from D-xylose conversion experiments. For model 3, the rate constant (k_3) at 160 °C was not considered because the calculation returned no value. Therefore, degradation of furfural was only influenced by the slow furfural self-polymerization. Model 1 and 2 show a more realistic courses comparable with previous studies,[38,167] where higher yields were achieved at higher temperatures. However, the degradation of furfural also increases with increasing temperature and therefore, the reaction time decreases until the maximum furfural yield is reached (Figure 4.5).

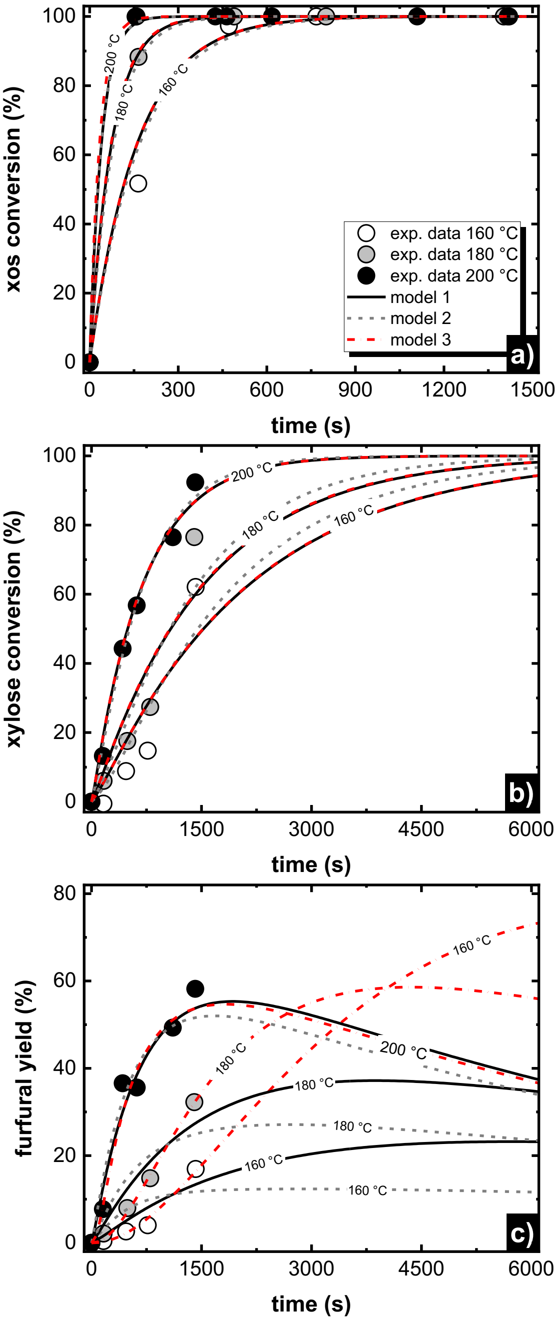

Figure 4.5 Xylooligosaccharide conversion a), D-Xylose conversion b), and furfural yield c) of the experimental as well as kinetic modeled data.

4.2 D-Xylose and Organosolv Hemicellulose Conversion in Water/Ethanol Mixtures

Short-chain alcohols, like ethanol, are able to suppress furfural-consuming side reactions. Therefore, in this study, acid-catalyzed xylose conversion in different water/ethanol mixtures was examined to evaluate the alcohol influence.

4.2.1 Influence of Ethanol Content on D-Xylose Conversion

Experimental results and the corresponding modeled courses of xylose dehydration in three different water/ethanol mixtures as well as in water are depicted in Figure 4.6. Reaction time started immediately after xylose injection. Results suggest that ethanol content up to a mass proportion of 50 % does not influence the D-xylose conversion rate. According to the Arrhenius equation, only a temperature increase leads to an acceleration of D-xylose conversion.

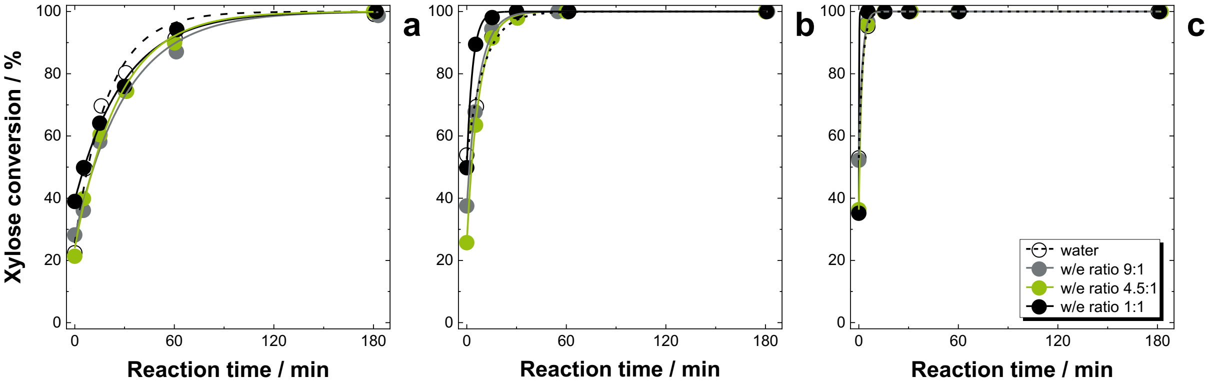

Figure 4.6 Experimentally determined D-xylose conversion and the respective modeled courses for different water/ethanol ratios at (a) 180, (b) 200, and (c) 220 °C.

This finding is in contrast to previous study from Hu et al. (2012) who varied the methanol mass ratio at moderate temperature (150 °C).[40] Hu et al. have shown a significant decline in D-xylose conversion rate with decreasing methanol proportion. Furthermore, they found that at low temperatures D-xylose conversion is mainly dominated by alcoholysis, accompanied with the formation of methyl xyloside. Logically, an increasing alcohol ratio leads to faster D-xylose conversion, due to the increasing interaction between methanol and D-xylose molecules. However, above 150 °C these alcohol/sugar intermediates are not stable and show a fast conversion to furfural and the corresponding furfural acetal.[40,136] Due to the high temperatures used in this study, the influence of the alcohol ratio is not apparent since the degradation of the formed ethyl xylosides (Scheme 4.1) and the subsequent formation of furfural are dominated.

Conversely, considering the reaction rate coefficients for D-xylose conversion (k_1 and k_2) an influence of the ethanol proportion can be seen. Kinetic rate constants, estimated by OriginPro 2019, are listed in Table 4.6 and plotted as natural logarithm against the inverse temperature in Figure 4.7. As can be clearly seen from Figure 4.7, the rate constant for D-xylose dehydration (k_1) increases with rising ethanol proportion and temperature. The influence of the alcohol is more pronounced with increasing temperature. The same accounts for the kinetic reaction rate coefficients of the side reactions k_2. However, in contrast to k_1, at 180 °C k_2 decreases with rising ethanol proportions. Only with climbing temperatures, this behavior turns again and the coefficients getting bigger with growing ethanol proportions (Figure 4.7). Summarizing, reaction coefficients of side reactions are less influenced by the addition of ethanol than the reaction rates of D-xylose dehydration.

Table 4.6 Kinetic constants k_i (min^{-1}) for the kinetic model described by equations Eq. (3.12), (3.13), and (3.15) on the basis of the experimentally determined data.

Entry	**H_2O/EtOH mass ratio**	**T (°C)**	**k_0 (min^{-1})**	**k_1 (min^{-1})**	**k_2 (min^{-1})**	**k_4 (min^{-1})**
1	H2O	180	-	0.01758 ± 0.00119	0.0326 ± 0.00732	0.00285 ± 0.00089
2		200		0.03142 ± 0.00447	0.0640 ± 0.01535	0.00685 ± 0.00301
3		220		0.13794 ± 0.01812	0.2780 ± 0.01956	0.01474 ± 0.00534
4	9:1	180	-	0.01391 ± 0.00084	0.0186 ± 0.00330	0.00251 ± 0.00071
5		200		0.06069 ± 0.00195	0.0797 ± 0.00889	0.00443 ± 0.00057
6		220		0.18397 ± 0.01274	0.2989 ± 0.01341	0.00736 ± 0.00174
7	4.5:1	180	-	0.01721 ± 0.00082	0.0206 ± 0.00383	0.00164 ± 0.00054
8		200		0.06234 ± 0.00254	0.0736 ± 0.00541	0.00276 ± 0.00059
9		220		0.20912 ± 0.01248	0.3134 ± 0.01295	0.00756 ± 0.00152
10	1:1	180	-	0.02047 ± 0.00079	0.0133 ± 0.00251	0.00131 ± 0.00042
11		200		0.15122 ± 0.00959	0.1332 ± 0.02113	0.00184 ± 0.00088
12		220		0.51969 ± 0.01873	0.4055 ± 0.01874	0.00457 ± 0.00069
13	H2O	200	0.51304 ± 0.00050	0.14272 ± 0.00862	0.45778 ± 0.00972	0.01072 ± 0.00176
14	9:1		0.36040 ± 0.00267	0.10595 ± 0.00977	0.35655 ± 0.01440	0.00686 ± 0.00196
15	4.5:1		0.42126 ± 0.00122	0.10882 ± 0.00966	0.41520 ± 0.01205	0.00617 ± 0.00168
16	1:1		0.05835 ± 0.01504	0.02119 ± 0.00158	0.13879 ± 0.02166	0.00109 ± 0.00062

By plotting the natural logarithm of the kinetic rate constants against the inverse temperature, the corresponding activation energies could be estimated by linear regression (Figure 4.7). Results are listed in Table 4.7.

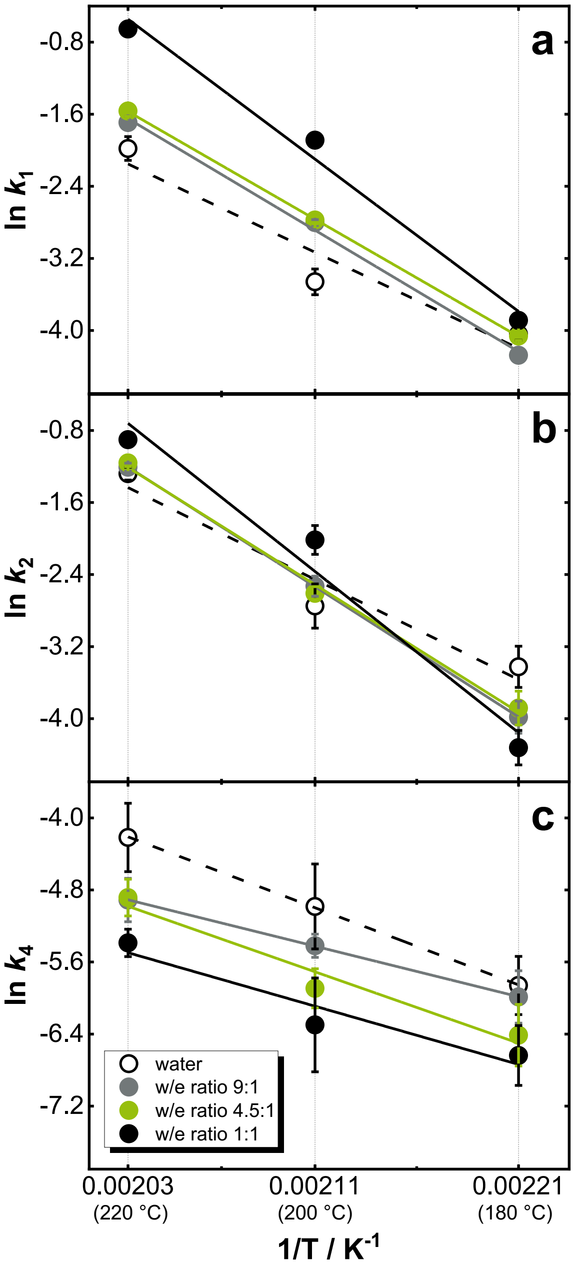

Figure 4.7 Arrhenius plots for (a) dehydration and (b) degradation of D-xylose as well as (c) furfural loss reaction at different water/ethanol (w/e) ratios.

Interestingly, the activation energies (E_1 and E_2) increase with rising ethanol proportions. As is known, increasing activation energy inhibits the reaction rate. With regard to D-xylose conversion, this finding shows that ethanol does not act as a catalyst. A plausible explanation for this behavior is that D-xylose is less consumed by side reactions in the presence of ethanol. Ethanol is able to react with D-xylose by Fischer glycosidation,[169] which suppresses the formation of the highly reactive D-xylose carbocation and reduces the subsequent uncontrollable cross-polymerization (Scheme 4.1).[110]

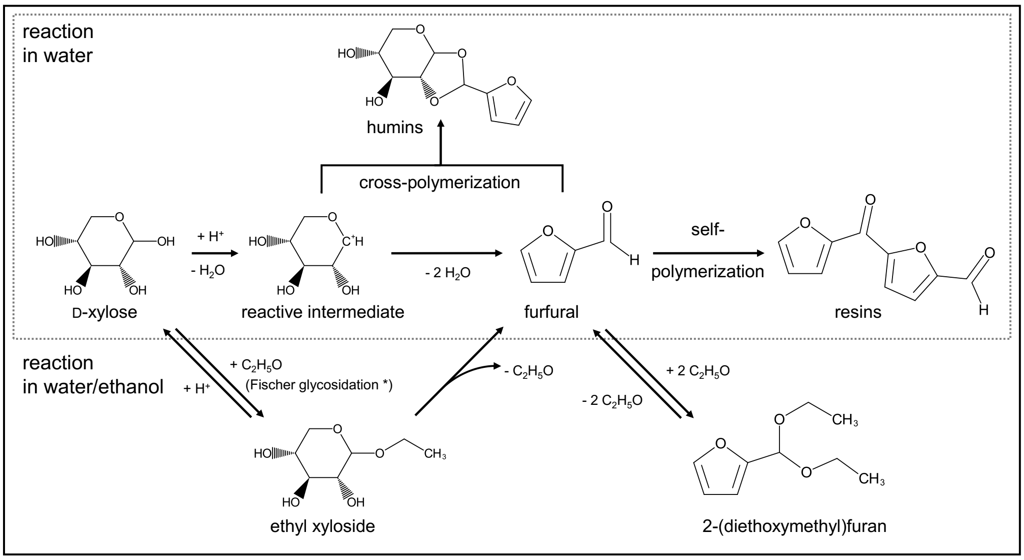

* also referred as: alcoholysis or esterification

Scheme 4.1 Possible reaction pathway of acid-catalyzed D-xylose dehydration to furfural in water and in water/ethanol mixtures.

Overall, this can lead to a deceleration of D-xylose conversion and explain the increase in the activation energies E_1 and E_2. Moreover, the reaction pathway from ethyl xyloside to furfural is unknown but might be required more energy than the dehydration of D-xylose.

Table 4.7 Activation energies for D-xylose dehydration to furfural in different water/ethanol mixtures.

solvent	**E_1 (kJ mol^{-1})**	**ln($A_{0;1}$) (-)**	**R^2**	**E_2 (kJ mol^{-1})**	**ln($A_{0;2}$) (-)**	**R^2**	**E_4 (kJ mol^{-1})**	**ln($A_{0;4}$) (-)**	**R^2**
water	95.1 ± 26.4	25.2 ± 6.7	0.93	99.0 ± 23.7	26.8 ± 6.0	0.95	76.4 ± 1.1	18.5 ± 0.3	0.99
9:1	120.1 ± 6.8	31.8 ± 1.7	0.99	128.9 ± 0.4	34.4 ± 0.1	0.99	50.0 ± 0.4	11.4 ± 0.1	0.99
4.5:1	116.0 ± 0.8	30.8 ± 0.2	0.99	126.3 ± 7.7	33.7 ± 2.0	0.99	70.6 ± 14.8	16.4 ± 3.8	0.96
1:1	150.6 ± 16.9	40.3 ± 4.3	0.99	159.5 ± 28.1	42.3 ± 7.2	0.97	57.6 ± 16.7	12.7 ± 4.3	0.92

4.2.2 Influence of Ethanol Content on Furfural Formation

In Figure 4.8 the furfural yields, as well as the corresponding modeled courses over the reaction time at temperatures between 180 and 220 °C for different water/ethanol mass ratios are presented. The diagrams show that high ethanol mass ratios have a positive effect on furfural yield. While the maximum yield in pure water was about 36 – 52 %, in the presence of ethanol it could be increased to 83 – 90 % (Table 4.8).

These results are in good agreement with Hu et al. (2012).[40] They found the highest yields at a water/alcohol mass ratio of 1:1 and the lowest for a ratio of 4.5:1 and 1:10, which corresponds the smallest and highest alcohol proportion in their study. However, in contrast to Hu et al. (2012), maximum yield in this study is two to three times higher. A similar result could be found by Grisel et al. (2013), who received higher furfural yields for ethanol during alcoholysis of wheat straw than for methanol.[170] Possibly this can be explained on the one hand due to the more drastic reaction conditions used in this examination and on the other hand by the different behavior of H_2SO_4 in methanol and ethanol.[170]

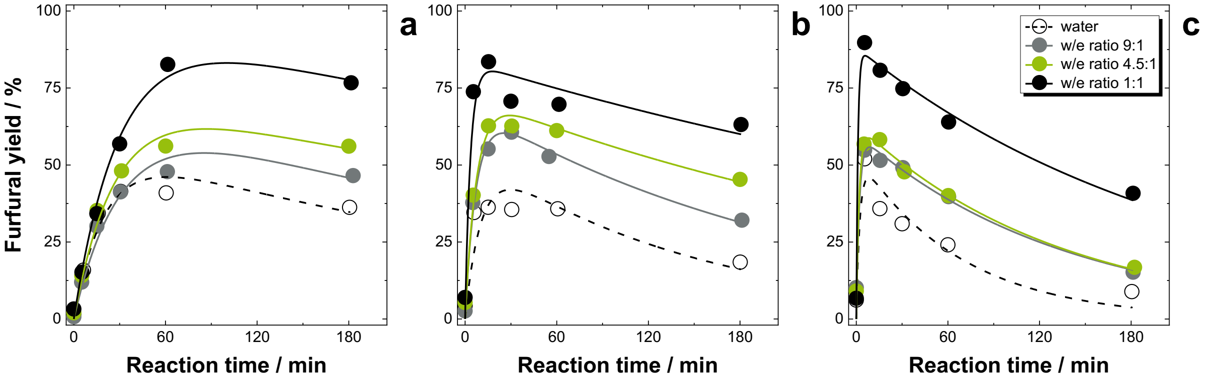

Figure 4.8 Experimentally determined furfural yield and the respective modeled courses for different water/ethanol ratios at (a) 180, (b) 200, and (c) 220 °C.

Furthermore, according to Arrhenius, with increasing reaction temperature formation of furfural and the subsequent degradation runs faster. Therefore, maximum furfural concentration is shifted to shorter reaction times. After passing the maximum concentration, furfural is starting to degrade which is more pronounced with increasing temperatures. Surprisingly, despite the high furfural yield in the presence of ethanol, the addition of the alcohol does not seem to affect the furfural degradation rate. According to our proposed reaction pathway (Scheme 4.1), an increasing ethanol content leads to a rising etherification of D-xylose under the formation of ethyl xyloside. Due to this, cross-polymerization between the reactive deprotonated D-xylose and furfural is suppressed and should lead to a deceleration of furfural degradation. However, the activation energy E_4, which is a measure of that furfural conversion rate, does not show a clear trend with

Table 4.8 Experimental determined maximum furfural yield ($Y_{\text{max, Fu}}$) as well as the corresponding reaction time ($t_{Y\text{max}}$), D-xylose conversion (X_{Xy}), and furfural selectivity (S_{Fu}).

Entry	H_2O/EtOH mass ratio	T (°C)	$Y_{\text{max, Fu}}$ (mol%)	$t_{Y\text{max}}$ (min)	X_{Xy} (mol%)	S_{Fu} (%)
1	H_2O	180	41.4	30	80.3	51.5
2		200	36.3	15	91.8	39.5
3		220	52.0	5	95.2	54.6
4	9:1	180	47.8	60	87.1	54.9
5		200	60.7	30	98.5	61.6
6		220	54.8	5	96.6	56.7
7	4.5:1	180	56.2	60	89.9	62.5
8		200	62.7	15	91.5	68.5
9		220	58.2	15	100	58.2
10	1:1	180	82.7	60	94.2	87.7
11		200	83.6	15	98.1	85.2
12		220	89.8	5	100	89.8

rising ethanol proportion (Table 4.7). The addition of ethanol is not associated with a significant decrease in E_4. From that finding, ethanol seems to have no influence on the degradation of furfural although an acetalization of furfural by ethanol to 2-diethoxymethylfuran (Scheme 4.1) is reported in the literature.[40,136,171] Hu et al. (2012) have reported that already temperatures of 150 °C are sufficient to form the acetal. However, this acetalization is an equilibrium reaction[171] and the gradual degradation of furfural by polymerization reactions shifts the equilibrium with increasing residence time and temperature to the aldehyde under the consumption of the acetal.

4.2.3 Conversion of Organosolv Hemicellulose in Water/Ethanol Mixtures

After the first series of experiments with D-xylose as the reactant, experiments were repeated at 200 °C with an organosolv hemicellulose fraction. Results of this second series are presented in (Figure 4.9) and show that xylooligosaccharide hydrolysis to D-xylose is inhibited at an ethanol proportion of 50 % (Figure 4.9a). Consequently, this behavior negatively affects the availability of D-xylose, as shown in (Figure 4.9b). However, larger differences were observed in terms of the furfural yields (Figure 4.9c). In contrast to our first series of experiments, ethanol does not increase the maximum furfural yield. An ethanol proportion of 50 % even leads to a significant reduction in the maximum yield. Moreover, the addition of ethanol seems to decelerate the furfural degradation.

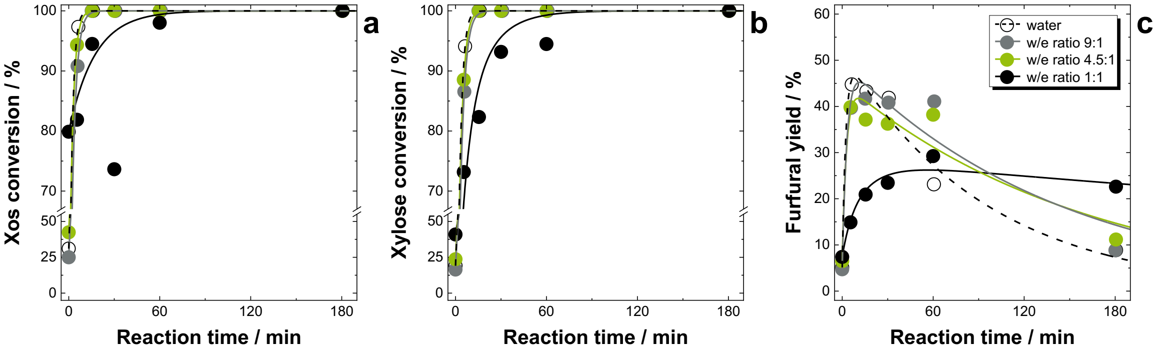

Figure 4.9 Experimentally determined xylooligosaccharide (Xos) conversion a), D-xylose conversion b), furfural yield c) and the corresponding modeled courses for hydrothermal treatment of organosolv hemicellulose at 200 °C and different water/ethanol mass ratios.

Lower furfural yields can possibly be attributed to the fact that instead of hydrolysis also alcoholysis of xylooligosaccharides (Xos) under formation of ethyl oligoglycosides takes place when ethanol is added to the reaction.[172,173] The resulting intermediates are unable to be converted to furfural.[174] While in aqueous solutions the Xos are fully available for furfural formation, they can only partially converted after the addition of ethanol. This would also explain the course of the furfural yield at a water/ethanol mass ratio of 1:1. Due to the alcoholysis of Xos, D-xylose monomers are not immediately available, which can lead to a deceleration in furfural formation. Therefore, the result leads to a seemingly slower degradation of furfural.

4.2.4 Effect of Ethanol Proportion on Humin Formation

In addition to D-xylose conversion and furfural yield, mass of the formed humins was determined after a reaction time of 180 min (Figure 4.11). The evaluation of the results is shown in Figure 4.10. As can be clearly seen, two statements can be made. First, rising temperatures lead to higher amounts of humins and second, with increasing proportion on ethanol humin formation can be suppressed. These findings are consistent with the results published by Hu et al. (2011) and Hu et al (2012).[40,175] As it was already mentioned above, the reactive carbocation, as shown in Scheme 4.1, is able to react with D-xylose or furfural under formation of water insoluble humins. In presence of ethanol, the amount of free available carbocations decreases which can consequently lead to a suppression of humin formation. Furthermore, furfural is able to react with the ethanol under formation of 2-diethoxymethylfuran by acetalization. Due to acetalization, the carbonyl group of furfural is protected and stabilized with regard to polymerization reactions. Additionally, if organosolv hemicellulose is used instead of D-xylose, the amount of humin almost doubles (Figure 4.10). However, high ethanol contents (50 wt%) decreased polymerization about 3 times.

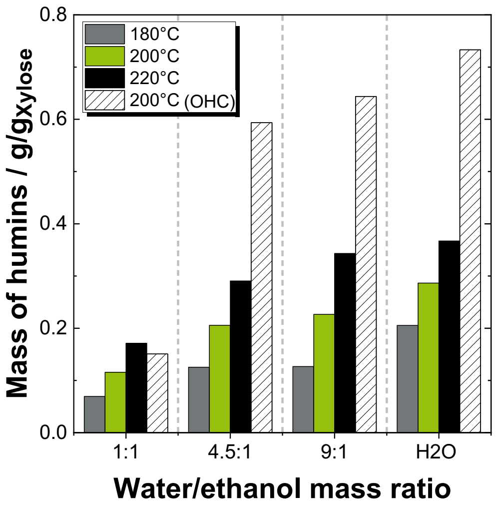

Figure 4.10 Mass of humins formed after 180 min at 180 to 220 °C during the experiments with D-xylose and organosolv hemicellulose (OHC) based on the initial amount of D-xylose.

Figure 4.11 Humins formed after 180 min at 200 °C during the experiment with organosolv hemicellulose (OHC) in water/ethanol (w/w 1:1).

One explanation could be that in contrast to D-xylose experiments, used OHC liquor is more heterogeneous containing beside hexoses and pentoses, carboxylic acids, as well as lignin residues.[176] The potential for possible side reactions is thereby noticeably increased. The drastically decline of humin mass at high ethanol concentration could be attributed on the one hand to etherification and acetalization of sugars and furans, whereby the reactive hydroxyl and carbonyl groups are stabilized and lowered their tendency to polymerize.[175] On the other hand, as already mentioned, the hemicellulose could not be completely hydrolyzed, which has led to a reduction of the available D-xylose.

4.3 Hydrothermal Reactive Distillation for the Recovery and Separation of Furfural

This section explores hydrothermal reactive distillation for producing furfural, using two types of biomass and biomass hydrolysates with varying temperatures and reaction times. The experiments compare how these factors affect the efficiency and success of furfural production, helping to identify the optimal conditions for maximizing yield.

4.3.1 Hydrothermal Pretreatment for Hydrolysate Provision

To determine a suitable combination of parameters leading to a maximum yield of dissolved hemicellulose in the hydrolysate, a quadratic regression model was constructed using RSM (Table 4.9). All components that can be allocated from this fraction, thus all oligopentoses and monopentoses as well as furfural, were considered as dissolved hemicellulose (Eq. (3.26)). Although, furfural is a degradation product of pentose, but since it is also a target product in this study, it was assigned to dissolved hemicellulose. The calculated p-values were used to test the significance of the regression coefficients. p-values < 0.05 are considered significant. As can be seen in Table 4.9, this significance criterion does not apply except for reaction time (p = 0.1333) and the quadratic influence of reaction time (p = 0.9172). From the analysis of variance (ANOVA), it can be seen that the quadratic model is highly significant overall, as shown by the F-test with a very low p-value (0.0016). Furthermore, the coefficient of determination indicates a good agreement between experimental and predicted values of dissolved hemicellulose yield.

Table 4.9 Significance of regression coefficient for dissolved hemicellulose yield.

Variables	**Regression coefficient**	**F-value**	**p-value**	**R^2**	**R^2_{Pred}**
Intercept/Model	71.29	40.91	0.0016	0.9808	0.8674
x_T	3.54	16.03	0.0161		
x_t	1.66	3.53	0.1333		
$x_T x_t$	-4.17	12.13	0.0253		
x_T^2	-11.93	114.82	0.0004		
x_t^2	-0.12	0.01	0.9172		

The graphical illustration of the regression model is shown in Figure 4.12. It shows the dependence of the dissolved hemicellulose on the two process parameters temperature and reaction time. As can be seen from Figure 4.12, there is a pronounced range between 150 and 175 °C in which the hemicellulose can be transferred very effectively into the aqueous phase. Below 150 °C it can be assumed that the process intensity is not sufficient to dissolve the hemicellulose out of the spelt husks and above

175 °C a rapidly progressing degradation of the pentose is observed and is in good accordance with similar studies.[177] The strong influence of temperature is also supported by a high significance ($p = 0.0161$). In contrast to reaction temperature, reaction time shows only a weak influence on the yield of dissolved hemicellulose, which has already been shown in previous studies.[178,179] This is also underlined by a low significance ($p = 0.1333$). However, it can be stated as a tendency that with longer reaction times the reaction temperature can be lowered and thus the yields of hemicellulose can be increased.

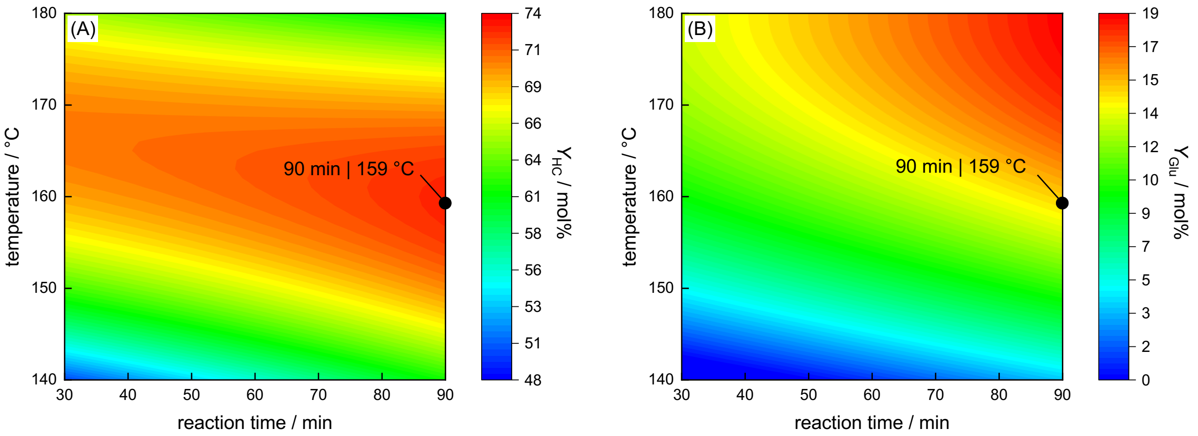

Figure 4.12 Contour plots of (A) dissolved hemicellulose and (B) glucose yields from hydrothermal pretreatment of spelt husks. Black dot represents the optimized process conditions for maximum yield of hemicellulose according to the regression model.

For the determination of suitable process parameters for the provision of SHH with a high content of dissolved hemicellulose, the optimized process conditions were calculated based on the quadratic regression model with the aid of the desirability function. The process parameters calculated in this way are plotted in the contour diagram (Figure 4.12, black dot). Based on these parameters, hydrothermal pretreatment experiments were carried out with spelt husks to provide the SHH. The composition of the SHH thus obtained can be taken from Table 3.2.

4.3.2 Furfural Production

The cumulative yield of furfural of each feedstock is shown in Figure 4.13 over the entire course of reaction, as a function of temperature. The furfural yield indicates the amount of hemicellulose sugars converted to the target product. The yield at the end of the reaction time (150 min) corresponds to the total amount of furfural that could be transferred to the condensate.

Results indicate that yields in the condensate of 35.5 – 83.5 mol % can be achieved, depending on the experimental conditions, as well as feedstock, and are in good accordance with previous studies (Table 2.10). Overall, it can be observed that a moderate reaction temperature (170 °C), especially when biomasses are used, leads to significantly lower overall yields (40.7 – 60.0 mol %). Because of the lower temperature, the hydrolysis of the hemicellulose and the afterward dehydration of the monopentoses proceed more slowly. As a result, the formation rate of furfural is low and, therefore, the proportion of furfural that can be released via the vapor phase also is small. In comparison, hydrolysate experiments show slightly higher furfural yields, and the gap to the maximum yield at 190 °C is smaller. This is also expressed in higher selectivities (Table 4.10). Equally evident is the fact that, at 170 °C, the increase in cumulative yield flattens only slightly and a total yield of 5 – 7 mol% remained in the sump of the reactor at the end of the experiment (Table 4.10). This indicates an incomplete reaction and suggests that by extending the reaction times, the yield can be further increased.

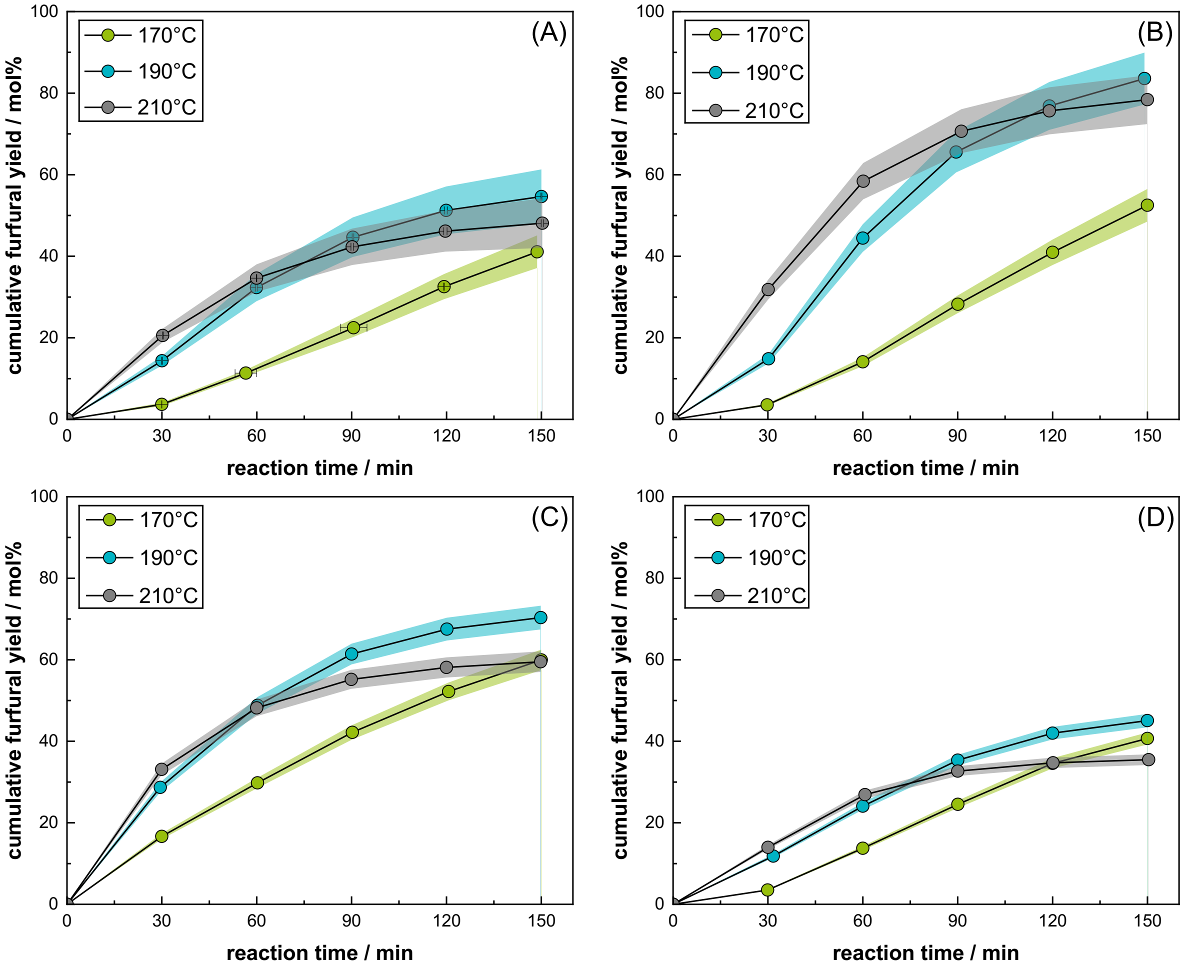

Figure 4.13 Cumulative furfural yields of (A) spelt husks (SH), (B) beechwood shavings (BWS), (C) spelt husk hydrolysate (SHH), and (D) organosolv hemicellulose (OHC), relative to the original pentose content of the feedstock.

The highest yields (45.0 – 83.5 mol%) across all experiments were observed at a reaction temperature of 190 °C. The formation and release rates of furfural seem to be in a suitable ratio under these conditions. The increase in cumulative yield flattens out with increasing reaction time and, depending on the substrate, no or only small amounts (<3 mol%) could be identified in the sump of the reactor (Table 4.10). Increasing the reaction temperature to 210 °C could not lead to any further increase in the overall yield (35.5 – 78.4 mol%) (Table 4.10). The strong flattening of the cumulative yield with increasing reaction time indicates that the hemicellulose is almost completely converted and, thus, increasing the reaction time does not lead to a further boost in furfural yield. Although high temperatures lead to a very fast release of furfural at the beginning of the reaction, they also increase the amount of undesired side and degradation reactions, which may contribute to a decrease in furfural yield.[180] In contrast to the observations by Mandalika and Runge[147] (Table 2.10) based on the results presented in Figure 4.13, no statement can be made regarding a better suitability of reactive distillation process for hydrolysates or biomasses. The highest yields were observed for BWS, followed by SHH, SH, and OHC. This is probably due to the different pentose contents of the hydrolysates, the used catalyst, and the biomasses in this study. A comparison of the hydrolysate and biomass experiments with each other shows that the substrates with the lower pentose content achieve higher yields. Reducing the pentose content directly affects the intermolecular interactions, which reduces the probability for byproducts.[180] The lignin content of the biomass (SH < BWS) has an influence on the total furfural yield insofar as the accessibility of hemicellulose decreases with increasing lignin content.[181] Therefore, the higher yields observed with BWS can be attributed to the slower supply of hemicellulose. The situation for the hydrolysates is different. Since lignin is present here in dissolved form, it has a negative influence due to intramolecular interactions between the lignin fragments and reactants of the furfural production.[28,90,182] Against this

Table 4.10 Overview of furfural (Fu) yield and selectivity of the condensate phase and overall after a reaction time of 150 min.

Feed	T_R (°C)	Y_Fu 1) (mol%)	Y_Fu 2) (mol%)	S_Fu 1) (%)	S_Fu 2) (%)
Spelt husks	170	41.1 ± 4.0	48.1 ± 5.2	46.6 ± 5.5	54.6 ± 7.1
	190	54.6 ± 6.7	57.3 ± 6.8	54.6 ± 6.7	57.3 ± 6.8
	210	48.1 ± 6.1	48.1 ± 6.1	48.1 ± 6.0	48.1 ± 6.0
Beech wood shavings	170	52.5 ± 4.0	59.7 ± 4.3	76.0 ± 7.3	86.5 ± 8.0
	190	83.5 ± 6.4	83.5 ± 6.4	83.5 ± 6.4	83.5 ± 6.4
	210	78.4 ± 6.0	78.4 ± 6.0	78.4 ± 6.0	78.4 ± 6.0
Spelt husk hydrolysate	170	60.0 ± 2.5	64.9 ± 2.5	71.7 ± 3.0	77.6 ± 3.1
	190	70.3 ± 2.9	70.3 ± 2.9	70.3 ± 2.9	70.3 ± 2.9
	210	59.9 ± 2.5	59.9 ± 2.5	59.5 ± 2.5	60.0 ± 2.5
Organosolv hemicellulose (OHC-3)	170	40.7 ± 1.5	47.4 ± 1.5	51.2 ± 1.9	59.7 ± 1.9
	190	45.0 ± 1.6	46.8 ± 1.7	45.2 ± 1.7	47.0 ± 1.7
	210	35.5 ± 1.3	35.5 ± 1.3	35.6 ± 1.3	35.6 ± 1.3

1) Related to the total condensate fraction
2) Related to the condensate and sump fraction

background, the lower yield and selectivity of furfural for OHC, compared to SHH, can be attributed to the fact that the amount of dissolved lignin in organosolv-based hydrolysates is usually much higher than that in hydrothermally provided ones. However, the catalyst used may also be responsible for the lower yields in OHC. Strong acids such as sulfuric acid tended to increase the formation of byproducts.

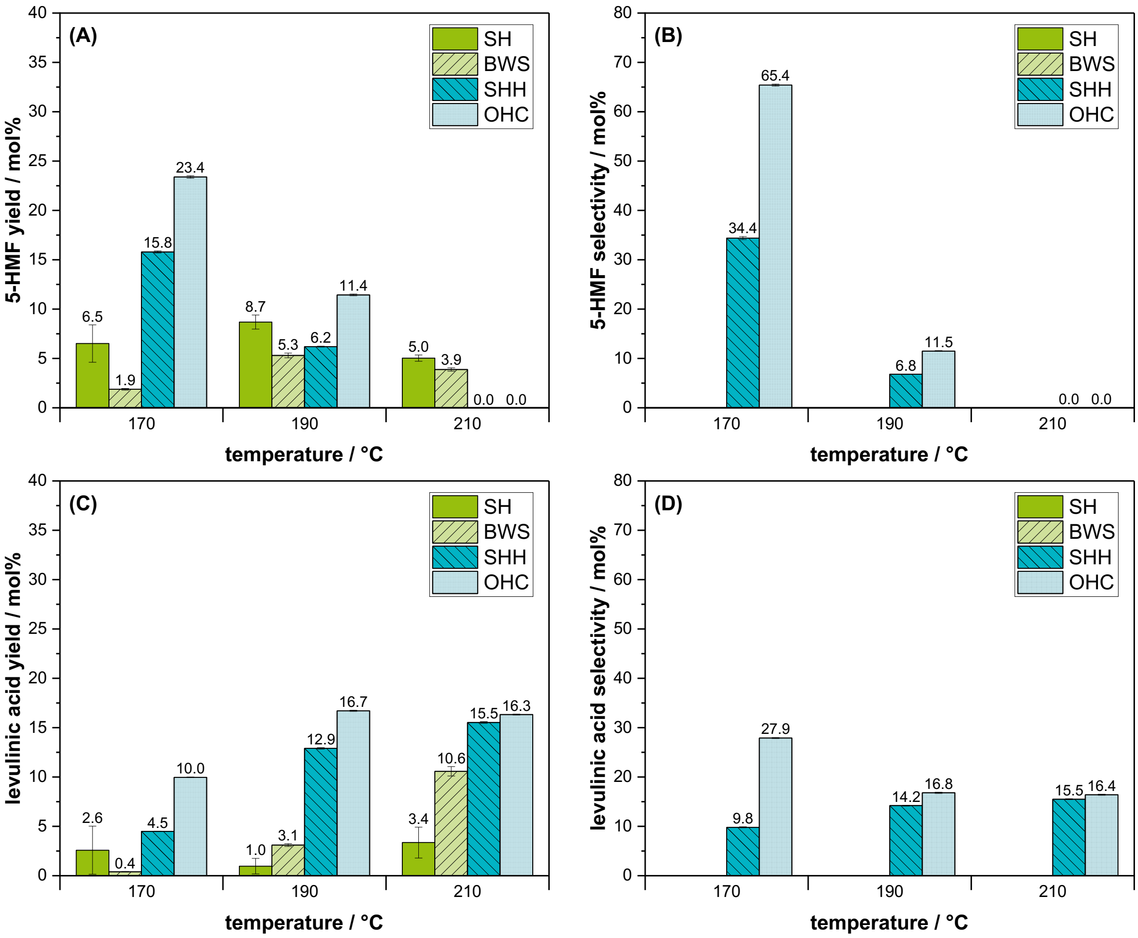

Figure 4.14 (A) 5-HMF yields and (B) selectivity, as well as (C) LA yield and (D) selectivity in the sump after 150 min related to the initial cellulose/hexose content of spelt husk (SH), beechwood shavings (BWS), spelt husk hydrolysate (SHH), and organosolv hemicellulose (OHC-3).

4.3.3 Byproducts in the Sump

In Figure 4.14, the yields and selectivities of 5-hydroxymethylfurfural (5-HMF) and levulinic acid (LA) are depicted. The formation of 5-HMF and LA can be attributed to the hexoses (Scheme 4.2). Here, 5-HMF is initially formed by dehydration of glucose. However, under the given experimental conditions, 5-HMF is not stable and can be rehydrated to LA in the presence of a Brønsted acid. Moreover, the mineral acids used in this study have low volatility, which leads to their accumulation in the sump and thereby reduces the pH. Therefore, the rehydration of 5-HMF to LA is accelerated with progressing reaction.[183] Based on the data, it is evident that, compared to the biomasses, significantly higher yields and selectivities of 5-HMF and LA are obtained starting from hydrolysates (Figure 4.14). This is related to the availability of the hexoses in the starting material. While hexoses are readily available in the hydrolysate, they must be first dissolved in the biomasses. Since, starting from biomass, the proportion of dissolved cellulose increases as the reaction temperature increases, the yield of LA also increases. For the hydrolysates, it is noticeable that, with rising reaction temperature, the 5-HMF yield decreases, while the LA yield increases. Yields of up to 23.4 mol % for 5-HMF and 16.7 mol % for LA are promising and represent a possibility for the simultaneous provision of 5- HMF/LA and furfural. HMF can be separated by MIBK extraction, followed by vacuum evaporation or from the sump solution by vacuum distillation.[184,185] Levulinic acid can be separated by several approaches, such as extraction or pervaporation, or by means of adsorption materials.[186–188] Selectivities of 5-HMF and LA from biomasses could not be calculated (Figure 4.14), because the hexose/cellulose remaining in the solid residue after the reaction could not be determined. Beside HMF and levulinic acid, humins as polycondensation product of furans and sugar molecules can be observed after the reaction in the sump.

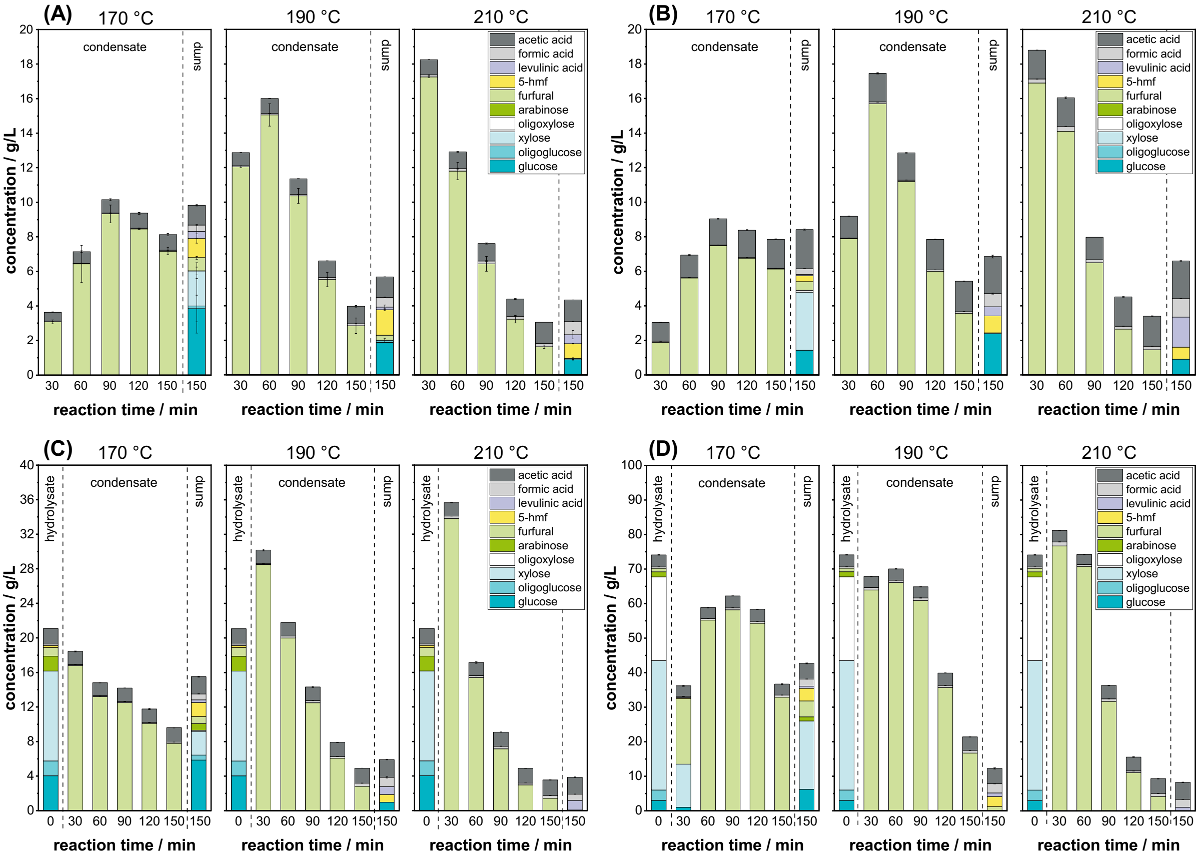

Figure 4.15 Composition of condensate, hydrolysate, and sump samples of (A) spelt husks (SH), (B) beechwood shavings (BWS), (C) spelt husk hydrolysate (SHH), and (D) organosolv hemicellulose (OHC) depicted over the reaction time.

4.3.4 Temperature Influence on Byproducts

Figure 4.15 compares the compositions of the respective condensates, hydrolysates and sump residues. Based on the data, the course of the reaction as well as the composition of the corresponding fractions can be described. Overall, the following relationships apply across all experiments. In addition to water and furfural, FA and AA are also transferred out of the reactor via the vapor phase. The reaction temperature as well as the availability of the pentoses (bound in the hydrolysate or in the biomass) significantly determine the release rate of furfural. As the temperature increases, more furfural is discharged at the beginning of the reaction. Neither monosugars and oligosugars nor 5-HMF and LA could be identified in the condensate, with the exception of the condensate sample (30 min/170 °C/OHC). Here, a partial discharge of the liquid phase occurred after opening the vapor release valve. It was also observed that FA and AA were not completely separated via the vapor phase and could always be found as residue in the sump of the reactor.

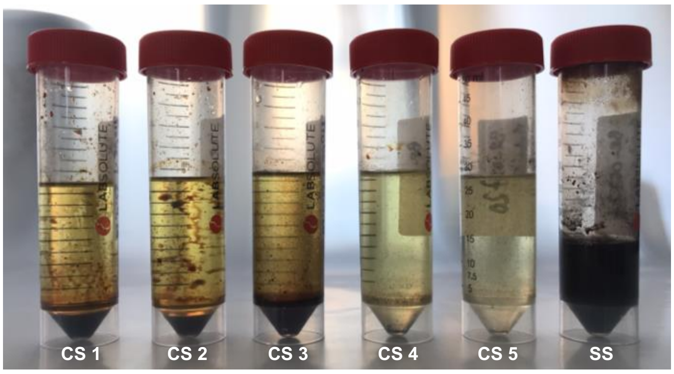

Figure 4.16 Picture of sample fraction after hydrothermal reactive distillation (HRD) of organosolv hemicellulose at 210 °C (CS 1 – 30 min, CS 2 – 60 min, CS 3 – 90 min, CS 4 – 120 min, CS 5 – 150 min, SS – 150 min). The dark brown phase at the bottom of samples CS 1 to CS 3 shows the separated organic phase consisting of furfural.

Furthermore, no transition of humins into the condensate phase could be observed (Figure 4.16). A comparison of the different feedstocks shows that the discharge of furfural is greatest at the beginning when hydrolysates are used and increases further with rising temperature. Moreover, it is evident from the residual D-xylose concentration of the sump samples that the dehydration reaction of the pentoses is not yet completed at 170 °C. Extending the reaction time here may lead to a further increase in the total yield of furfural. In the experiments with OHC, phase separation occurred at 210 °C due to the high starting sugar concentration in the condensate samples (Figure 4.16). The water/furfural mixture has a miscibility gap at ambient temperature between concentrations of 96 to 910 g L^{-1} (data from Aspen Properties V10, AspenTech, USA) in which water and furfural segregate. Interestingly, furfural concentrations of >96 g L^{-1} were not determined, which may be due to the fact that no representative sample could be taken for HPLC analysis. Moreover, already small amounts of formic or acetic acid significantly increase the solubility of furfural, thus reducing the miscibility gap (Figure 4.17 and Figure 4.18).

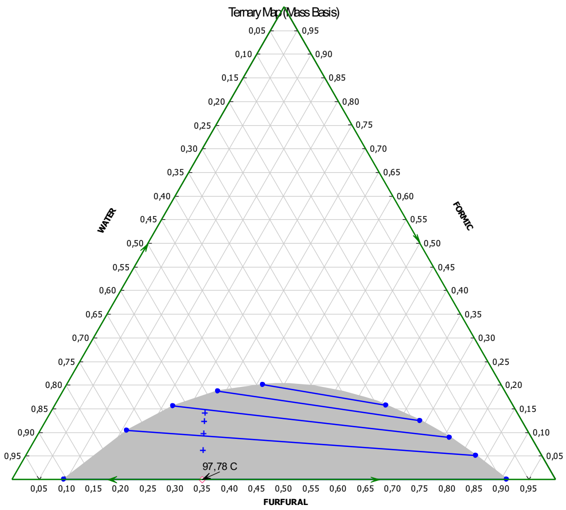

Figure 4.17 Ternary diagram for the water-formic acid-furfural mixture (mass basis) calculated by ASPEN Properties V10 on the basis of NRTL property method.

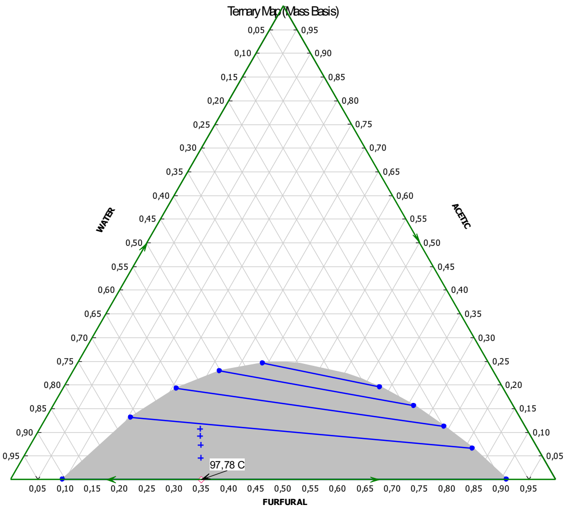

Figure 4.18 Ternary diagram for the water-acetic acid-furfural mixture (mass basis) calculated by ASPEN Properties V10 on the basis of NRTL property method.

As already mentioned above, in addition to furfural and water, FA and AA are also discharged via the vapor phase. However, both acids are also identified in the sump for all feedstocks after the reaction. On the one hand, this can be attributed to the fact that both FA and AA are degradation products of hemicellulose, sugars, and furans, respectively, and thus are formed until the end of the reaction.[83,84,166,189] Similar to furfural-water mixtures (up to the miscibility gap), mixtures of water and FA or AA have only small separation factors; however, in contrast they do not lead to a lower boiling point as in the case of furfural (Figure 4.19).[147]

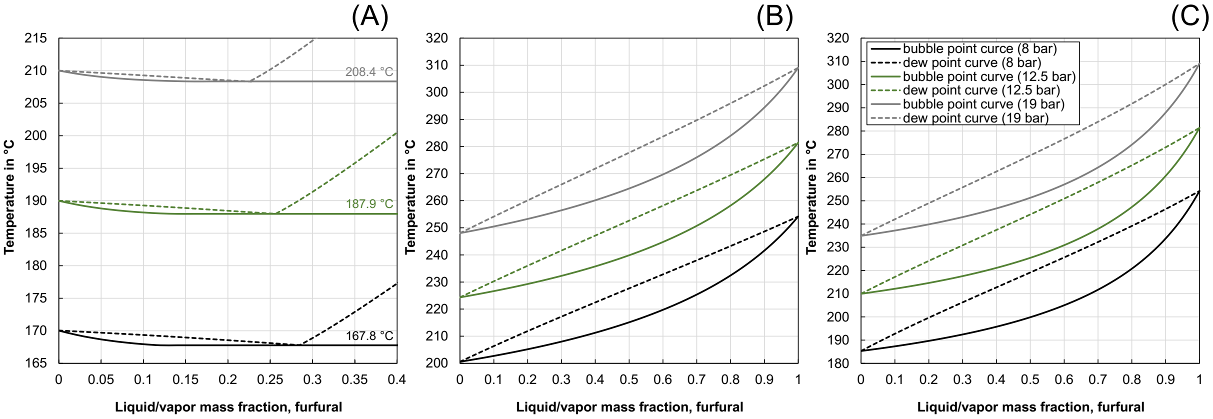

Figure 4.19 T-x,y diagrams for (A) water-furfural, (B) acetic acid-furfural, and (C) formic acid-furfural mixtures at the respective reaction conditions (8, 12.5, and 19 bar). The diagrams were created using ASPEN Properties V10 on the basis of NRTL property method.

4.3.5 Acetic/Formic Acid Ratio in the Condensate

The influence of the reaction temperature on the discharge of acetic and formic acid is shown in Figure 4.20. The discharge over the vapor phase depends on two aspects, volatility and the concentration of each component in the sump. First, it can be stated that more AA is discharged than FA across all experiments, although pure FA is more volatile then AA (Figure 4.21). This indicates a higher concentration of AA in the sump and is in good accordance with results from previous experiments.[84,190]

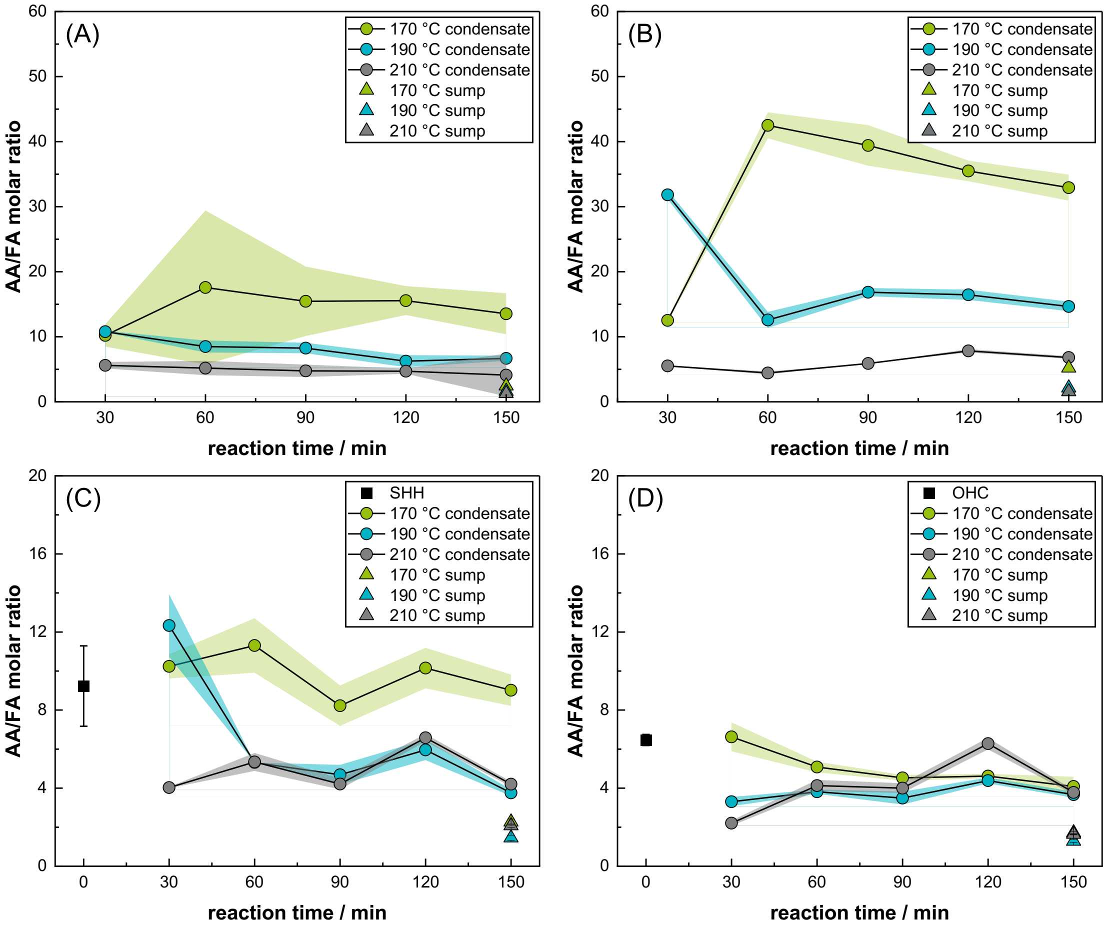

Figure 4.20 Molar ratio of acetic (AA) to formic acid (FA) in the hydrolysate, condensate, and sump before, during, and after hydrothermal reactive distillation of (A) spelt husk, (B) beechwood shavings, (C) spelt husk hydrolysate (SHH), and (D) organosolv hemicellulose (OHC), respectively.

However, the molar ratio decreases as the temperature increases. Looking at the concentrations (Figure 4.15), it is noticeable that this is due to an increase in discharge of FA. While FA is a byproduct of furan degradation, AA is mostly formed during hemicellulose and glucose degradation (Scheme 4.2).[83,189] However, as the reaction temperature increases, the degradation of the furans accelerates, so that, ultimately, more FA can be discharged via the vapor phase. This effect, coupled with the fact that steam is continuously discharged, partially preventing the degradation of FA, results in a higher discharge of FA with increasing temperature. Furthermore, as depicted in Figure 4.20, biomasses show larger molar AA/FA ratio after HRD, in comparison to hydrolysates. This can be attributed to the untreated hemicellulose in the biomass. During hemicellulose degradation, AA and FA is released from the biopolymer structure by hydrolysis of acetyl groups or formyl groups, respectively.[84,189] Meanwhile, the proportion of acetyl groups is usually 10 times greater than that of formyl groups.[24]

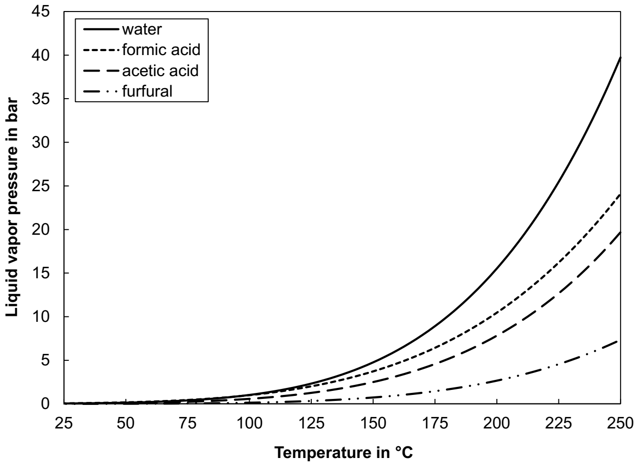

Figure 4.21 Liquid vapor pressure of water, furfural, acetic, and formic acid calculated by ASPEN Properties V10 on the basis of NRTL property method.

Beside the hemicellulose degradation, another source of AA formation is the presence of hexoses. However, the cellulose fraction is already separated from the hydrolysate and, therefore, the overall potential of formed AA in hydrolysates is lower than in untreated biomasses. From this point of view, lower process temperatures are preferred, because a lower discharge of FA is caused.

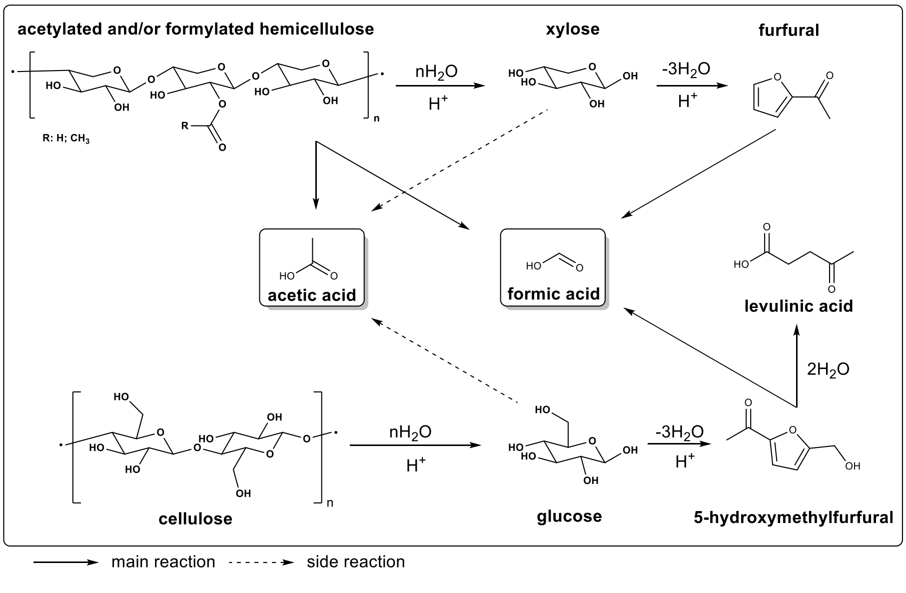

Scheme 4.2 Reaction scheme of hydrothermal degradation of hemicellulose and cellulose, respectively, based on data and referring to Refs [83,84,189].

5 Conclusion and Outlook

5.1 Conclusion

This thesis was dedicated to the conversion of hemicellulose sugars into furfural using different chemical engineering processes, with the primary aim of optimizing the yield of furfural from an aqueous hemicellulose hydrolysate of an organosolv process and determining the influence of accompanying substances in the hydrolysate. To achieve this goal, three hypotheses were formulated and their verification was presented in three scientific articles, which formed the basis of this work.

(HYP-1)	The use of advanced kinetic models, which consider sugar oligomers and furfural degradation, will significantly improve the ability to accurately predict furfural production from D-xylose and organosolv hemicellulose, leading to more effective process control and optimization.

The first experimental series examined the kinetics of hydrothermal conversion of D-xylose and organosolv hemicellulose as well as furfural degradation in a temperature range of 160–200 °C using a continuous tube reactor. The study compares three reaction models to examine the conversion of D-xylose and organosolv hemicellulose into furfural and also investigates furfural degradation to understand its self-polymerization. All the reaction mechanisms investigated involved the hydrolysis of oligopentoses and differed in terms of the mechanisms for the formation and degradation of furfural. While model 1 focuses exclusively on the self-polymerization of furfural, model 2 suggests a cross-polymerization between pentose and furfural. Model 3 expands upon this by introduces a reactive D-xylose intermediate along with the cross-polymerization process. Determined kinetic parameters for D-xylose experiments are in good accordance with previous studies. The individual models differed only slightly. Compared with D-xylose investigation, kinetic parameters from organosolv hemicellulose experiments have shown a stronger deviation, possibly influenced by the complex composition and sugar oligomers. Overall, regarding the furfural formation, model 3, which includes the formation of a D-xylose intermediate, have shown the best performance, followed by model 1 and finally model 2.

The results of this study must be viewed with caution with regard to their comparability with other studies, as it was not possible to realize a turbulent flow and thus an ideal plug flow in the flow tube reactor used. Despite considerable efforts to create a steady state, this limitation led to back-mixing, which potentially influenced the test results. This had a particular impact on the analysis of the furfural degradation reactions to determine the degradation kinetics. In addition, the use of Organosolv hemicellulose led to a significant formation of humins, which repeatedly blocked the spring-based counterflow valve at the outlet of the plant and thus changed the back pressure. This resulted in slightly varying residence times and affected the reproducibility of the results.

(HYP-2)	The introduction of ethanol as a co-solvent in the acid-catalyzed conversion of D-xylose and organosolv hemicellulose to furfural is expected to lead to a substantial increase in furfural yield while simultaneously reducing the formation of humins.

Acid-catalyzed dehydration of D-xylose to furfural using water/ethanol mixtures was studied over a temperature range of 180–220 °C. The water/ethanol mass ratio was varied between 9:1, 4.5:1, and 1:1 and compared with experiments without the addition of ethanol. Results have shown that ethanol-rich environments significantly enhance furfural yield while concurrently diminishing humin formation, a noteworthy advancement for the field of biomass conversion. Specifically, it could be demonstrated that furfural yield could be elevated from 45 to 85 mol%, accompanied by a substantial 60 wt% reduction in humin formation under certain conditions. With regard to the determined activation energies, it could be shown that rising ethanol proportions inhibit the D-xylose conversion and catalyze the furfural degradation. These findings are possibly an expression of the rapid etherification of the reactive D-xylose carbocation to the more stable ethyl xyloside and the acetylation of furfural. Experiments were repeated with organosolv hemicellulose at 200 °C. High ethanol proportions have been decelerated the xylooligosaccharide hydrolysis, which is why no increase or even a decrease (for water/ethanol mass ratio of 1:1) in furfural yield could be observed. Nevertheless, polymerization between the sugar and furfural molecules could be suppressed, which contributed to a reduction of the formed humin mass. Overall, ethanol offers a good opportunity to increase the furfural yield and to reduce humin formation. Simultaneously, a simple distillative furfural separation is possible, due to the higher boiling point compared to the solvents. However, more research attention needs to be paid to hemicellulose liquors and biomass conversion.

Unfortunately, it was not possible within the scope of this study to carry out analyses that would have allowed a detailed clarification of the side reactions caused by the use of ethanol. Such analyses would have provided potentially valuable insights and could have further supported the description of the reaction process proposed in the study.

(HYP-3) Hydrothermal reactive distillation (HRD) as a separation technique will significantly enhance furfural yield and purity by effectively minimizing side reactions during production. The continuous stripping of furfural from the reaction mixture via the vapor phase will prevent the accumulation of undesirable by-products.

Hydrothermal reactive distillation was carried out and has systematically demonstrated the efficiency of this approach for the production and separation of furfural from biogenic materials, specifically through the processing of spelt husks, beechwood shavings, and their respective hydrolysates. Operating within a temperature range of 170–210 °C, it could be successfully achieved furfural yields of up to 83 mol%, directly transferred into the condensate phase without the formation of humins. This indicates a high efficiency of the process in converting biomass to furfural, with the added benefit of facilitating easier product purification thanks to observed phase separation in high-concentration furfural samples. In addition to furfural, the process also results in the discharge of acetic and formic acids, with a notably higher proportion of acetic acid when starting from biomass rather than hydrolysates. This distinction underscores the influence of feedstock type on the distribution of reaction products. Moreover, significant quantities of nonvolatile compounds, such as 5-HMF and levulinic acid, accumulate in the sump of the reactor, reaching yields of 23 and 17 mol%, respectively. This not only showcases the potential for a broader range of valuable chemical production from the process but also highlights the necessity for optimizing separation strategies for these compounds.

The HRD was carried out using phosphoric acid as a homogeneous catalyst. However, it should be noted that different mineral acids can influence the dehydration of D-xylose to furfural to slightly varying degrees. In this study, organosolv hemicellulose acidified with sulfuric acid was used as the starting material, which poses a challenge for the direct comparability of the results. This also applies to the different initial concentrations of the sugars, which introduces an additional level of complexity in the interpretation of the data.

5.2 Outlook

The present thesis highlights the complexity and challenges in the conversion of hemicellulose sugars to furfural, and indicates the urgent need for further research to improve the economic feasibility of such processes. The investigation of various approaches showed that promising results are possible with hemicellulose model substances such as D-xylose, but the transformation to real substrates often fails due to technical hurdles or leads to significant losses in selectivity. A central problem is the formation of insoluble humins, which lead to blockages, particularly in continuous reactor systems, and make the use of heterogeneous catalysts more difficult.

The use of ethanol has shown to be a significant step in improving furfural yields and it is recommended that further studies with alcohols in different ratios are carried out along with detailed analysis of the intermediates and by-products. These could contribute to the identification and better understanding of the intermediates and by-products formed through interactions with alcohols. Additionally, exploring the potential of alcohols as hydrogen donors for further furfural valorization presents a promising approach for research, potentially enhancing the value of furfural derivatives. The use of real hemicellulose fractions from biomass pulping processes also deserves more detailed consideration, as these substrates often contain sugar oligomers whose hydrolysis can be reduced by the use of organic solvents. In addition, organosolv processes in particular work with alcohols as solvents. Concepts that allow process integration and at the same time take solvent recovery into account are desirable.

A particular focus is placed on hydrothermal reactive distillation, which offers numerous starting points for future scientific investigations. The lack of continuous processes in this area underlines the need to develop and evaluate new process designs. In order to assess the sustainability and marketability of hydrothermal reactive distillation, comprehensive techno-economic analyses and life cycle assessments are required that take environmental impact, energy efficiency and cost aspects fully into account. The integration of various technologies with reactive distillation, in particular the use of organic solvents, offers promising prospects. It is crucial to ensure that no solvent is disproportionately separated from the reaction process. Additionally, the use of packing materials coated with catalyst material could also be employed in reactive distillation to enhance reaction efficiency. In addition, further research efforts are needed into the utilization or isolation of the by-products produced such as HMF, levulinic acid and humins in the reactor sump. These efforts are essential to improve the overall efficiency and sustainability of the process. Furthermore, the successful transfer of laboratory results to technical scale through pilot studies is crucial to test the feasibility and robustness of the developed processes under real conditions. Such pilot studies are a critical step on the way to industrial application, as they not only confirm the technical feasibility but also provide valuable data for further optimization of the process.

6 References

1. United Nations Framework Convention on Climate Change, 2015, *Paris Agreement*.
2. International Energy Agency, 2018, *The Future of Petrochemicals: Towards more sustainable plastics and fertilisers*, Paris.
3. Münnich, P., Somers, J., Metz, J., Hermanns, R., Kalousdian, A., Bardow, A. and Winter, B., 2023, *Agora Industrie: Chemie im Wandel:: Die drei Grundpfeiler für die Transformation chemischer Wertschöpfungsketten*.
4. *Land use statistics and indicators statistics. Global, regional and country trends 1990–2019*, 2021, Rome.
5. Umweltbundesamt, 2017, *Biomassekaskaden: Mehr Ressourceneffizienz durch Kaskadennutzung von Biomasse – von der Theorie zur Praxis*, Dessau-Roßlau.
6. Martin Hundt, *Der AlkaPolP-Prozess als Ausgangspunkt für eine lignocellulosebasierte Bioraffinerie*, Doctoralthesis, BTU Cottbus - Senftenberg, 2015.
7. Smit, A.T., Verges, M., Schulze, P., van Zomeren, A. and Lorenz, H., 2022, Laboratory- to Pilot-Scale Fractionation of Lignocellulosic Biomass Using an Acetone Organosolv Process, *ACS Sustainable Chemistry & Engineering*, **10**(32): 10503–10513.
8. Tofani, G., Jasiukaitytė-Grojzdek, E., Grilc, M. and Likozar, B., 2024, Organosolv biorefinery: resource-based process optimisation, pilot technology scale-up and economics, *Green Chem*, **26**(1): 186–201.
9. Johansson, A., Aaltonen, O. and Ylinen, P., 1987, Organosolv pulping — methods and pulp properties, *Biomass*, **13**(1): 45–65.
10. Laure, S., Leschinsky, M., Fröhling, M., Schultmann, F. and Unkelbach, G., 2014, Assessment of an organosolv lignocellulose biorefinery concept based on a material flow analysis of a pilot plant, *Cellulose Chemistry and Technology*, **48**(9-10): 793–798.
11. Caparrós, S., Ariza, J., Garrote, G., López, F. and Díaz, M.J., 2007, Optimization of Paulownia Fortunei L. Autohydrolysis−Organosolv Pulping as a Source of

Xylooligomers and Cellulose Pulp, *Industrial & Engineering Chemistry Research*, **46**(2): 623–631.

12. F. López, A. Pérez, J.C. García, M.J. Feria, M.M. García and M. Fernández, 2011, Cellulosic pulp from Leucaena diversifolia by soda–ethanol pulping process, *Chemical Engineering Journal*, **166**(1): 22–29.
13. Sixta, H., Harms, H., Dapia, S., Parajo, J.C., Puls, J., Saake, B., Fink, H.-P. and Röder, T., 2004, Evaluation of new organosolv dissolving pulps. Part I: Preparation, analytical characterization and viscose processability, *Cellulose*, **11**(1): 73–83.
14. Ramon E. Vera, Keren A. Vivas, Fernando Urdaneta, Jorge Franco, Runkun Sun, Naycari Forfora, Ryen Frazier, Stephanie Gongora, Daniel Saloni, Larissa Fenn, J.Y. Zhu, Hou-min Chang, Hasan Jameel and Ronalds Gonzalez, 2023, Transforming non-wood feedstocks into dissolving pulp via organosolv pulping: An alternative strategy to boost the share of natural fibers in the textile industry, *Journal of Cleaner Production*, **429**: 139394.
15. Schmatz, A.A., Masarin, F. and Brienzo, M., 2022, Lignin Removal and Cellulose Digestibility Improved by Adding Antioxidants and Surfactants to Organosolv Pretreatment of Sugarcane Bagasse, *BioEnergy Research*, **15**(2): 1107–1115.
16. Terán Hilares, R., Swerts, M.P., Ahmed, M.A., Ramos, L., Da Silva, S.S. and Santos, J.C., 2017, Organosolv Pretreatment of Sugar Cane Bagasse for Bioethanol Production, *Industrial & Engineering Chemistry Research*, **56**(14): 3833–3838.
17. Anthi Karnaouri, Georgia Asimakopoulou, Konstaninos G. Kalogiannis, Angelos Lappas and Evangelos Topakas, 2020, Efficient d-lactic acid production by Lactobacillus delbrueckii subsp. bulgaricus through conversion of organosolv pretreated lignocellulosic biomass, *Biomass and Bioenergy*, **140**: 105672.
18. Esteves, B., Sen, U. and Pereira, H., 2023, Influence of Chemical Composition on Heating Value of Biomass: A Review and Bibliometric Analysis, *Energies*, **16**(10): 4226.
19. UPM, 2022, RFF will be a real game-changer, Retrieved Mar. 15, 2024, from *https://www.upm.com/articles/biochemicals/22/rff-will-be-a-real-game-changer/*
20. Statista Research Department, 2023, Global furfural market volume 2015-2030, Retrieved Mar. 14, 2024, from *https://www.statista.com/statistics/1310459/furfural-market-volume-worldwide/*

21. Bozell, J.J. and Petersen, G.R., 2010, Technology development for the production of biobased products from biorefinery carbohydrates—the US Department of Energy's "Top 10" revisited, *Green Chemistry*, **12**(4): 539.
22. Mariscal, R., Maireles-Torres, P., Ojeda, M., Sádaba, I. and Granados, M.L., 2016, Furfural: A renewable and versatile platform molecule for the synthesis of chemicals and fuels, *Energy Environ. Sci.*, **9**(4): 1144–1189.
23. Brownlee, H.J. and Miner, C.S., 1948, Industrial Development of Furfural, *Industrial & Engineering Chemistry*, **40**(2): 201–204.
24. Zeitsch, K.J., 2000, *The Chemistry and Technology of Furfural and its Many By-Products*, Vol. 13, Elsevier.
25. Marcotullio, G., *The Chemistry and Technology of Furfural Production in Modern Lignocellulose-Feedstock Biorefineries*, Dissertation, Delft University of Technology, 2011.
26. Jing, Q. and Lü, X., 2007, Kinetics of Non-catalyzed Decomposition of D-xylose in High Temperature Liquid Water, *Chinese Journal of Chemical Engineering*, **15**(5): 666–669.
27. Liu, L., Chang, H., Jameel, H. and Park, S., 2018, Furfural production from biomass pretreatment hydrolysate using vapor-releasing reactor system, *Bioresource Technology*, **252**: 165–171.
28. Jemaa, N., Mazar, A., Al Dajani, W.W. and Paleologou, M., 2017, Lignin recovery and furfural production from prehydrolysate streams.
29. Mazar, A., Jemaa, N., Al Dajani, W.W., Marinova, M. and Perrier, M., 2017, Furfural production from a pre-hydrolysate generated using aspen and maple chips, *Biomass and Bioenergy*, **104**: 8–16.
30. Qing, Q., Guo, Q., Zhou, L., Wan, Y., Xu, Y., Ji, H., Gao, X. and Zhang, Y., 2017, Catalytic conversion of corncob and corncob pretreatment hydrolysate to furfural in a biphasic system with addition of sodium chloride, *Bioresource Technology*, **226**: 247–254.
31. Gómez Millán, G., Hellsten, S., King, A.W., Pokki, J.-P., Llorca, J. and Sixta, H., 2019, A comparative study of water-immiscible organic solvents in the production of furfural from xylose and birch hydrolysate, *Journal of Industrial and Engineering Chemistry*, **72**: 354–363.
32. Gao, H., Liu, H., Pang, B., Yu, G., Du, J., Zhang, Y., Wang, H. and Mu, X., 2014, Production of furfural from waste aqueous hemicellulose solution of hardwood over ZSM-5 zeolite, *Bioresource Technology*, **172**: 453–456.

33. Oktay Yemiş and Giuseppe Mazza, 2011, Acid-catalyzed conversion of xylose, xylan and straw into furfural by microwave-assisted reaction, *Bioresource Technology*, **102**(15): 7371–7378.
34. Marcotullio, G. and Jong, W. de, 2010, Chloride ions enhance furfural formation from D-xylose in dilute aqueous acidic solutions, *Green Chemistry*, **12**(10): 1739–1746.
35. Kim, S.B., You, S.J., Kim, Y.T., Lee, S., Lee, H., Park, K. and Park, E.D., 2011, Dehydration of D-xylose into furfural over H-zeolites, *Korean Journal of Chemical Engineering*, **28**(3): 710–716.
36. Dias, A.S., Pillinger, M. and Valente, A.A., 2005, Dehydration of xylose into furfural over micro-mesoporous sulfonic acid catalysts, *Journal of Catalysis*, **229**(2): 414–423.
37. Cañada-Barcala, A., Rodríguez-Llorente, D., López, L., Navarro, P., Hernández, E., Águeda, V.I., Álvarez-Torrellas, S., Parajó, J.C., Rivas, S. and Larriba, M., 2021, Sustainable Production of Furfural in Biphasic Reactors Using Terpenoids and Hydrophobic Eutectic Solvents, *ACS Sustainable Chemistry & Engineering*, **9**(30): 10266–10275.
38. Weingarten, R., Cho, J., Conner Jr, W.C. and Huber, G.W., 2010, Kinetics of furfural production by dehydration of xylose in a biphasic reactor with microwave heating, *Green Chemistry*, **12**(8): 1423–1429.
39. Gürbüz, E.I., Wettstein, S.G. and Dumesic, J.A., 2012, Conversion of hemicellulose to furfural and levulinic acid using biphasic reactors with alkylphenol solvents, *ChemSusChem*, **5**(2): 383–387.
40. Hu, X., Lievens, C. and Li, C.-Z., 2012, Acid-catalyzed conversion of xylose in methanol-rich medium as part of biorefinery, *ChemSusChem*, **5**(8): 1427–1434.
41. Sener, C., Motagamwala, A.H., Alonso, D.M. and Dumesic, J.A., 2018, Enhanced Furfural Yields from Xylose Dehydration in the γ-Valerolactone/Water Solvent System at Elevated Temperatures, *ChemSusChem*, **11**(14): 2321–2331.
42. Metkar, P.S., Till, E.J., Corbin, D.R., Pereira, C.J., Hutchenson, K.W. and Sengupta, S.K., 2015, Reactive distillation process for the production of furfural using solid acid catalysts, *Green Chemistry*, **17**(3): 1453–1466.
43. Agirrezabal-Telleria, I., Larreategui, A., Requies, J., Güemez, M.B. and Arias, P.L., 2011, Furfural production from xylose using sulfonic ion-exchange resins (Amberlyst) and simultaneous stripping with nitrogen, *Bioresource Technology*, **102**(16): 7478–7485.

44. Holtzapple, M.T., 2003, Hemicelluloses, in: Caballero, B. (ed.), *Encyclopedia of Food Sciences and Nutrition*, 2nd edn., Elsevier, pp. 3060–3071.
45. Brunner, G., 2014, *Hydrothermal and supercritical water processes*, Vol. 5, Elsevier, Amsterdam, Boston, Heidelberg, London, New York, Oxford, Paris, San Diego, San Francisco, Singapore, Sydney, Tokyo.
46. Sixta, H. (ed.), 2006, *Handbook of pulp*, Wiley-VCH Verlag GmbH & Co. KGaA, Weinheim.
47. Waite, R. and Gorrod, A.R.N., 1959, The structural carbohydrates of grasses, *Journal of the science of food and agriculture*, **10**(6): 308–317.
48. Vassilev, S.V., Baxter, D., Andersen, L.K., Vassileva, C.G. and Morgan, T.J., 2012, An overview of the organic and inorganic phase composition of biomass, *Fuel*, **94**: 1–33.
49. Paloheimo, L., Vainio, K.A., Kero, M.-L. and Herkola, E., 1961, Analyses of plant products in greater detail, *Agricultural and Food Science*, **33**(1): 51–56.
50. van Ewijk, S., Stegemann, J.A. and Ekins, P., 2017, Global Life Cycle Paper Flows, Recycling Metrics, and Material Efficiency, *Journal of Industrial Ecology*, **22**(4): 686–693.
51. Lies, T.M., 2023, PLASTIK AUS HOLZ: Bio-Raffinerie in Leuna: Branche fernab vom Holzweg, Retrieved Mar. 05, 2024, from *https://www.mdr.de/nachrichten/sachsen-anhalt/halle/saalekreis/leuna-holz-raffinerie-112.html*
52. Grüne Chemie mit holzbasierten Biochemikalien: UPM treibt Schaffung einer Kreislaufwirtschaft durch nachwachsende Rohstoffe auf Holzbasis voran, *CHEManager*, **2023**(12): 9.
53. Aparicio, S. and Alcalde, R., 2009, Characterization of two lactones in liquid phase: an experimental and computational approach, *Physical chemistry chemical physics : PCCP*, **11**(30): 6455–6467.
54. Kato, C., Nishihara, S., Tsunashima, R., Tatewaki, Y., Okada, S., Ren, X.-M., Inoue, K., Long, D.-L. and Cronin, L., 2013, Quick and selective synthesis of Li6α-P2W18O62·28H2O soluble in various organic solvents, *Dalton transactions (Cambridge, England : 2003)*, **42**(32): 11363–11366.
55. Kruse, A. and Dinjus, E., 2007, Hot compressed water as reaction medium and reactant, *The Journal of Supercritical Fluids*, **39**(3): 362–380.
56. Kruse, A. and Dahmen, N., 2015, Water – A magic solvent for biomass conversion, *The Journal of Supercritical Fluids*, **96**: 36–45.

57. Möller, M. and Schröder, U., 2013, Hydrothermal production of furfural from xylose and xylan as model compounds for hemicelluloses, *RSC Advances*, **3**(44): 22253.

58. Garrote, G., Domínguez, H. and Parajó, J.C., 1999, Mild autohydrolysis: an environmentally friendly technology for xylooligosaccharide production from wood, *Journal of Chemical Technology & Biotechnology*, **74**(11): 1101–1109.

59. Boussarsar, H., Rogé, B. and Mathlouthi, M., 2009, Optimization of sugarcane bagasse conversion by hydrothermal treatment for the recovery of xylose, *Bioresource Technology*, **100**(24): 6537–6542.

60. Nitsos, C.K., Choli-Papadopoulou, T., Matis, K.A. and Triantafyllidis, K.S., 2016, Optimization of Hydrothermal Pretreatment of Hardwood and Softwood Lignocellulosic Residues for Selective Hemicellulose Recovery and Improved Cellulose Enzymatic Hydrolysis, *ACS Sustainable Chemistry & Engineering*, **4**(9): 4529–4544.

61. Hidalgo-Carrillo, J., Marinas, A. and Urbano, F.J., 2018, Chemistry of Furfural and Furanic Derivatives, in: Granadaos, M.L. and Alonso, D.M. (eds.), *Furfural: An Entry Point of Lignocellulose in Biorefineries to Produce Renewable Chemicals, Polymers, and Biofuels*, Sustainable Chemistry Series volume 2, World Scientific, New Jersey, pp. 1–30.

62. Hoydonckx, H.E., van Rhijn, W.M., van Rhijn, W., Vos, D.E. de and Jacobs, P.A., 2007, Furfural and Derivatives, in: *Ullmann's Encyclopedia of Industrial Chemistry*, John Wiley & Sons, Ltd.

63. Panchaksharam, Y., Kiri, P., Bauen, A., vom Berg, C., Puente, Á., Chinthapalli, R., Spekreijse, J., Vos, J., Pfau, S., Rübberdt, K., Michels, J. and König, L., 2019, *Roadmap for the Chemical Industry in Europe towards a Bioeconomy*.

64. Verfahren zur Hydrolyse pentosanhaltiger pflanzlicher Stoffe, 19-05.

65. Zeitsch, K.J., 2002, Process for the manufacture of furfural, DE19991005655;WO2000ZA00024, C07D307/50;C07D307/50.

66. Alonso, D.M. and Marcotullio, G., 2018, Past, Current Situation and Future Technologies of Furfural Production, in: Granadaos, M.L. and Alonso, D.M. (eds.), *Furfural: An Entry Point of Lignocellulose in Biorefineries to Produce Renewable Chemicals, Polymers, and Biofuels*, Sustainable Chemistry Series volume 2, World Scientific, New Jersey, pp. 31–52.

67. Fitzpatrick, S.W., 1988, Lignocellulose degradation to furfural and levulinic acid, US19880186234, C07C59/185;C07D307/48;C07D307/50;C07D307/48;C07D307/50.

68. Gravitis, J., Vedernikov, N., Zandersons, J. and Kokorevics, A., 2001, Furfural and Levoglucosan Production from Deciduous Wood and Agricultural Wastes, in: Bozell, J.J. (ed.), *Chemicals and materials from renewable resources: A symposium ... was held at the 218th National Meeting of the American Chemical Society in New Orleans, Louisiana, from August 22 to August 26, 1999*, ACS Symposium Series Vol. 784, American Chemical Society, Washington, D.C., Great Britain, pp. 110–122.

69. Jong, W. de and Marcotullio, G., 2010, Overview of Biorefineries based on Co-Production of Furfural, Existing Concepts and Novel Developments, *International Journal of Chemical Reactor Engineering*, **8**(1).

70. Win, D.T., 2005, Furfural - Gold from Garbage, *Au J. Technol*, **8**(4): 185–190.

71. Crnomarkovic, M., Panchaksharam, Y., Spekreijse, J., vom Berg, C., Puente, A. and Chinthapalli, R., 2018, Road to Bio - Business cases: Case studies on potentially attractive opportunities for bio-based chemicals in Europe, Retrieved Mar. 13, 2023, from *https://www.roadtobio.eu/uploads/publications/deliverables/RoadToBio_D12_Case_studies_bio-based_chemicals.pdf*

72. Mario Kabbour and Rafael Luque, 2020, Chapter 10 - Furfural as a platform chemical: From production to applications, in: Shunmugavel Saravanamurugan, Ashok Pandey, Hu Li and Anders Riisager (eds.), *Biomass, Biofuels, Biochemicals*, Biomass, Biofuels, Biochemicals, Elsevier, pp. 283–297.

73. Feather, M.S., Harris, D.W. and Nichols, S.B., 1972, Routes of conversion of D-xylose, hexuronic acids, and L-ascorbic acid to 2-furaldehyde, *The Journal of Organic Chemistry*, **37**(10): 1606–1608.

74. Ahmad, T., Kenne, L., Olsson, K. and Theander, O., 1995, The formation of 2-furaldehyde and formic acid from pentoses in slightly acidic deuterium oxide studied by 1H NMR spectroscopy, *Carbohydrate Research*, **276**(2): 309–320.

75. Hurd, C.D. and Isenhour, L.L., 1932, Pentose reactions. I. Furfural formation, *Journal of the American Chemical Society*, **54**(1): 317–330.

76. Bonner, W.A. and Roth, M.R., 1959, The Conversion of D-Xylose-1-C 14 into 2-Furaldehyde-α-C 14, *Journal of the American Chemical Society*, **81**(20): 5454–5456.

77. Harris, D.W. and Feather, M.S., 1974, Intramolecular C-2 --> C-1 Hydrogen Transfer Reactions during the Conversion of Aldoses to 2-Furaldehydes, *The Journal of Organic Chemistry*, **39**(5): 724–725.

78. Antal, M.J., Leesomboon, T., Mok, W.S. and Richards, G.N., 1991, Mechanism of formation of 2-furaldehyde from d-xylose, *Carbohydrate Research*, **217**: 71–85.
79. Nimlos, M.R., Qian, X., Davis, M., Himmel, M.E. and Johnson, D.K., 2006, Energetics of xylose decomposition as determined using quantum mechanics modeling, *The Journal of Physical Chemistry A*, **110**(42): 11824–11838.
80. Enslow, K.R. and Bell, A.T., 2015, The Role of Metal Halides in Enhancing the Dehydration of Xylose to Furfural, *ChemCatChem*, **7**(3): 479–489.
81. Root, D.F., Saeman, J.F., Harris, J.F. and Neill, W.K., 1959, Kinetics of the Acid-Catalyzed Conversion of Xylose to Furfural, *For. Prod. J.*, **9**(5): 158–165.
82. Jakob, A., Likozar, B. and Grilc, M., 2022, Aqueous conversion of monosaccharides to furans: were we wrong all along to use catalysts?, *Green Chem*, **24**(21): 8523–8537.
83. Poerschmann, J., Weiner, B., Koehler, R. and Kopinke, F.-D., 2017, Hydrothermal Carbonization of Glucose, Fructose, and Xylose—Identification of Organic Products with Medium Molecular Masses, *ACS Sustainable Chemistry & Engineering*, **5**(8): 6420–6428.
84. Xing, R., Qi, W. and Huber, G.W., 2011, Production of furfural and carboxylic acids from waste aqueous hemicellulose solutions from the pulp and paper and cellulosic ethanol industries, *Energy & Environmental Science*, **4**(6): 2193.
85. Cristina Sánchez, Luis Serrano, Mª Angeles Andres and Jalel Labidi, 2013, Furfural production from corn cobs autohydrolysis liquors by microwave technology, *Industrial Crops and Products*, **42**: 513–519.
86. Héctor D. Mansilla, Jaime Baeza, Sergio Urzúa, Gabriel Maturana, Jorge Villaseñor and Nelson Durán, 1998, Acid-catalysed hydrolysis of rice hull: Evaluation of furfural production, *Bioresource Technology*, **66**(3): 189–193.
87. Mittal, A., Black, S.K., Vinzant, T.B., O'Brien, M., Tucker, M.P. and Johnson, D.K., 2017, Production of Furfural from Process-Relevant Biomass-Derived Pentoses in a Biphasic Reaction System, *ACS Sustainable Chemistry & Engineering*, **5**(7): 5694–5701.
88. Yang, W., Li, P., Bo, D. and Chang, H., 2012, The optimization of formic acid hydrolysis of xylose in furfural production, *Carbohydrate Research*, **357**: 53–61.
89. Choudhary, V., Sandler, S.I. and Vlachos, D.G., 2012, Conversion of Xylose to Furfural Using Lewis and Brønsted Acid Catalysts in Aqueous Media, *ACS Catalysis*, **2**(9): 2022–2028.
90. Liu, H., Hu, H., Jahan, M.S. and Ni, Y., 2015, Improvement of furfural production from concentrated prehydrolysis liquor (PHL) of a kraft-based hardwood

dissolving pulp production process, *Journal of Wood Chemistry and Technology*, **35**(4): 260–269.

91. Lamminpää, K., Ahola, J. and Tanskanen, J., 2012, Kinetics of xylose dehydration into furfural in formic acid, *Industrial & Engineering Chemistry Research*, **51**(18): 6297–6303.
92. Dussan, K., Girisuta, B., Lopes, M., Leahy, J.J. and Hayes, M.H.B., 2015, Conversion of hemicellulose sugars catalyzed by formic acid: kinetics of the dehydration of D-xylose, L-arabinose, and D-glucose, *ChemSusChem*, **8**(8): 1411–1428.
93. Kim, E.S., Liu, S., Abu-Omar, M.M. and Mosier, N.S., 2012, Selective Conversion of Biomass Hemicellulose to Furfural Using Maleic Acid with Microwave Heating, *Energy & Fuels*, **26**(2): 1298–1304.
94. Lee Seungmin and Kim Jun Seok, 2023, Furfural Production From Xylose by Using Formic Acid and Sulfuric Acid, *Korean Chemical Engineering Research*, **61**(4): 561–569.
95. Ershova, O., Nieminen, K. and Sixta, H., 2017, The Role of Various Chlorides on Xylose Conversion to Furfural: Experiments and Kinetic Modeling, *ChemCatChem*, **9**(15): 3031–3040.
96. Xiang Lyu and Gerardine G. Botte, 2021, Investigation of factors that inhibit furfural production using metal chloride catalysts, *Chemical Engineering Journal*, **403**: 126271.
97. Hawthorne, F.C., 2012, A bond-topological approach to theoretical mineralogy: crystal structure, chemical composition and chemical reactions, *Physics and Chemistry of Minerals*, **39**(10): 841–874.
98. Gürbüz, E.I., Gallo, J.M.R., Alonso, D.M., Wettstein, S.G., Lim, W.Y. and Dumesic, J.A., 2013, Conversion of Hemicellulose into Furfural Using Solid Acid Catalysts in γ-Valerolactone, *Angewandte Chemie International Edition*, **52**(4): 1270–1274.
99. Ronen Weingarten, Geoffrey A. Tompsett, Wm Curtis Conner and George W. Huber, 2011, Design of solid acid catalysts for aqueous-phase dehydration of carbohydrates: The role of Lewis and Brønsted acid sites, *Journal of Catalysis*, **279**(1): 174–182.
100. Zhang, J., Zhuang, J., Lin, L., Liu, S. and Zhang, Z., 2012, Conversion of D-xylose into furfural with mesoporous molecular sieve MCM-41 as catalyst and butanol as the extraction phase, *Biomass and Bioenergy*, **39**: 73–77.
101. Margarida M. Antunes, Sérgio Lima, Auguste Fernandes, Martyn Pillinger, Maria F. Ribeiro and Anabela A. Valente, 2012, Aqueous-phase dehydration of xylose to

furfural in the presence of MCM-22 and ITQ-2 solid acid catalysts, *Applied Catalysis A: General*, **417-418**: 243–252.

102. Shi, X., Wu, Y., Yi, H., Rui, G., Li, P., Yang, M. and Wang, G., 2011, Selective Preparation of Furfural from Xylose over Sulfonic Acid Functionalized Mesoporous Sba-15 Materials, *Energies*, **4**(4): 669–684.
103. Cabrera-Munguia, D.A., Gutiérrrez-Alejandre, A., Romero-Galarza, A., Morales-Martínez, T.K., Ríos-González, L.J. and Sifuentes-López, J., 2023, Function of Brønsted and Lewis acid sites in xylose conversion into furfural, *RSC Adv*, **13**(44): 30649–30664.
104. Olivares, Y., Herrera, C., Seguel, J., Sepúlveda, C., Parra, C. and Pecchi, G., 2023, Stable Sulfonic MCM-41 Catalyst for Furfural Production from Renewable Resources in a Biphasic System, *Catalysts*, **13**(6): 1024.
105. Liu, P., Shi, S., Wei, R., Gao, L., Zhang, J. and Xiao, G., 2023, Dehydration of Xylose and Xylan to Furfural using P-Zr-SBA-15 Catalyst in Aqueous or Biphasic System, *ChemistrySelect*, **8**(16).
106. Rakngam, I., Osakoo, N., Wittayakun, J., Chanlek, N., Pengsawang, A., Sosa, N., Butburee, T., Faungnawakij, K. and Khemthong, P., 2021, Properties of mesoporous Al-SBA-15 from one-pot hydrothermal synthesis with different aluminium precursors and catalytic performances in xylose conversion to furfural, *Microporous and Mesoporous Materials*, **317**: 110999.
107. Yemiş, O. and Mazza, G., 2019, Catalytic Performances of Various Solid Catalysts and Metal Halides for Microwave-Assisted Hydrothermal Conversion of Xylose, Xylan, and Straw to Furfural, *Waste and Biomass Valorization*, **10**(5): 1343–1353.
108. Le Guenic, S., Gergela, D., Ceballos, C., Delbecq, F. and Len, C., 2016, Furfural Production from d-Xylose and Xylan by Using Stable Nafion NR50 and NaCl in a Microwave-Assisted Biphasic Reaction, *Molecules (Basel, Switzerland)*, **21**(8).
109. Lam, E., Majid, E., Leung, A.C.W., Chong, J.H., Mahmoud, K.A. and Luong, J.H.T., 2011, Synthesis of furfural from xylose by heterogeneous and reusable nafion catalysts, *ChemSusChem*, **4**(4): 535–541.
110. Hu, X., Westerhof, R.J.M., Dong, D., Wu, L. and Li, C.-Z., 2014, Acid-Catalyzed Conversion of Xylose in 20 Solvents: Insight into Interactions of the Solvents with Xylose, Furfural, and the Acid Catalyst, *ACS Sustainable Chemistry & Engineering*, **2**(11): 2562–2575.
111. Agirrezabal-Telleria, I., Garcia-Sancho, C., Maireles-Torres, P. and ARIAS, P.L., 2013, Dehydration of xylose to furfural using a Lewis or Brönsted acid catalyst and N2 stripping, *Chinese Journal of Catalysis*, **34**(7): 1402–1406.

112. Agirrezabal-Telleria, I., Requies, J., Güemez, M.B. and Arias, P.L., 2012, Furfural production from xylose + glucose feedings and simultaneous N2-stripping, *Green Chem*, **14**(11): 3132–3140.

113. Lin, L., Ma, S., Li, P., Zhu, T. and Chang, H., 2015, Mutual Solubilities for the Water–2- sec -Butylphenol System and Partition Coefficients for Furfural and Formic Acid in the Water–2- sec -Butylphenol System, *Journal of Chemical & Engineering Data*, **60**(6): 1926–1933.

114. Cousin, E., Namhaed, K., Pérès, Y., Cognet, P., Delmas, M., Hermansyah, H., Gozan, M., Alaba, P.A. and Aroua, M.K., 2022, Towards efficient and greener processes for furfural production from biomass: A review of the recent trends, *The Science of the total environment*, **847**: 157599.

115. Ricciardi, L., Verboom, W., Lange, J.-P. and Huskens, J., 2021, Production of furans from C 5 and C 6 sugars in the presence of polar organic solvents, *Sustainable Energy & Fuels*, **6**(1): 11–28.

116. Moreau, C., Durand, R., Peyron, D., Duhamet, J. and Rivalier, P., 1998, Selective preparation of furfural from xylose over microporous solid acid catalysts, *Industrial Crops and Products*, **7**(2-3): 95–99.

117. Dias, A.S., Pillinger, M. and Valente, A.A., 2005, Liquid phase dehydration of d-xylose in the presence of Keggin-type heteropolyacids, *Applied Catalysis A: General*, **285**(1): 126–131.

118. Lima, S., Pillinger, M. and Valente, A.A., 2008, Dehydration of d-xylose into furfural catalysed by solid acids derived from the layered zeolite Nu-6(1), *Catalysis Communications*, **9**(11-12): 2144–2148.

119. Chheda, J.N., Román-Leshkov, Y. and Dumesic, J.A., 2007, Production of 5-hydroxymethylfurfural and furfural by dehydration of biomass-derived mono- and poly-saccharides, *Green Chemistry*, **9**(4): 342–350.

120. Papaioannou, M., Kleijwegt, R.J.T., van der Schaaf, J. and Neira d'Angelo, M.F., 2019, Furfural Production by Continuous Reactive Extraction in a Millireactor under the Taylor Flow Regime, *Industrial & Engineering Chemistry Research*, **58**(35): 16106–16115.

121. Guo, W., Bruining, H.C., Heeres, H.J. and Yue, J., 2022, Efficient synthesis of furfural from xylose over HCl catalyst in slug flow microreactors promoted by NaCl addition, *AIChE Journal*, **68**(5).

122. Sahu, R. and Dhepe, P.L., 2012, A one-pot method for the selective conversion of hemicellulose from crop waste into C5 sugars and furfural by using solid acid catalysts, *ChemSusChem*, **5**(4): 751–761.

123. Millán, G.G., Phiri, J., Mäkelä, M., Maloney, T., Balu, A.M., Pineda, A., Llorca, J. and Sixta, H., 2019, Furfural production in a biphasic system using a carbonaceous solid acid catalyst, *Applied Catalysis A: General*, **585**: 117180.

124. Molina, M.J.C., Granados, M.L., Gervasini, A. and Carniti, P., 2015, Exploitment of niobium oxide effective acidity for xylose dehydration to furfural, *Catalysis Today*, **254**: 90–98.

125. Rong, C., Ding, X., Zhu, Y., Li, Y., Wang, L., Qu, Y., Ma, X. and Wang, Z., 2012, Production of furfural from xylose at atmospheric pressure by dilute sulfuric acid and inorganic salts, *Carbohydrate Research*, **350**: 77–80.

126. Gupta, N.K., Fukuoka, A. and Nakajima, K., 2017, Amorphous Nb 2 O 5 as a Selective and Reusable Catalyst for Furfural Production from Xylose in Biphasic Water and Toluene, *ACS Catalysis*, **7**(4): 2430–2436.

127. Pholjaroen, B., Li, N., Wang, Z., Wang, A. and Zhang, T., 2013, Dehydration of xylose to furfural over niobium phosphate catalyst in biphasic solvent system, *Journal of Energy Chemistry*, **22**(6): 826–832.

128. Lawanwong, R., Daorattanachai, P. and Laosiripojana, N., 2022, Effects of solvents and catalysts to furfural production from xylose dehydration reaction, *Journal of Sustainable Energy & Environment*, **13**: 9–12.

129. Fagan, P.J., Ozer, R. and Till, E.J., 2012, Process for the Production of Furfural, US201161580711P;US201161580714P, C07D307/48;B01J27/053;B01J29/82.

130. Romo, J.E., Miller, K.C., Sundsted, T.L., Job, A.L., Hoo, K.A. and Wettstein, S.G., 2019, The Effect of Solvent Polarity on Autocatalytic Furfural Production Confirmed by Multivariate Statistical Analysis, *ChemCatChem*, **11**(19): 4715–4719.

131. Alonso, D.M., Wettstein, S.G., Mellmer, M.A., Gürbüz, E.I. and Dumesic, J.A., 2013, Integrated conversion of hemicellulose and cellulose from lignocellulosic biomass, *Energy & Environmental Science*, **6**(1): 76–80.

132. Peleteiro, S., Rivas, S., Alonso, J.L., Santos, V. and Parajó, J.C., 2016, Furfural production using ionic liquids: A review, *Bioresource Technology*, **202**: 181–191.

133. Zhang, L., Yu, H., Wang, P., Dong, H. and Peng, X., 2013, Conversion of xylan, d-xylose and lignocellulosic biomass into furfural using AlCl3 as catalyst in ionic liquid, *Bioresource Technology*, **130**: 110–116.

134. Zhang, L., Yu, H. and Wang, P., 2013, Solid acids as catalysts for the conversion of D-xylose, xylan and lignocellulosics into furfural in ionic liquid, *Bioresource Technology*, **136**: 515–521.

135. Lima, S., Neves, P., Antunes, M.M., Pillinger, M., Ignatyev, N. and Valente, A.A., 2009, Conversion of mono/di/polysaccharides into furan compounds using 1-alkyl-3-methylimidazolium ionic liquids, *Applied Catalysis A: General*, **363**(1-2): 93–99.
136. Iglesias, J., Melero, J.A., Morales, G., Paniagua, M. and Hernández, B., 2016, Dehydration of Xylose to Furfural in Alcohol Media in the Presence of Solid Acid Catalysts, *ChemCatChem*, **8**(12): 2089–2099.
137. Romo, J.E., Bollar, N.V., Zimmermann, C.J. and Wettstein, S.G., 2018, Conversion of Sugars and Biomass to Furans Using Heterogeneous Catalysts in Biphasic Solvent Systems, *ChemCatChem*, **10**(21): 4805–4816.
138. Köchermann, J., Schreiber, J. and Klemm, M., 2019, Conversion of d-Xylose and Hemicellulose in Water/Ethanol Mixtures, *ACS Sustainable Chemistry & Engineering*, **7**(14): 12323–12330.
139. Wang, Q., Zhuang, X., Wang, W., Tan, X., Yu, Q., Qi, W. and Yuan, Z., 2018, Rapid and simultaneous production of furfural and cellulose-rich residue from sugarcane bagasse using a pressurized phosphoric acid-acetone-water system, *Chemical Engineering Journal*, **334**: 698–706.
140. Morais, A.R.C. and Bogel-Lukasik, R., 2016, Highly efficient and selective CO 2 -adjunctive dehydration of xylose to furfural in aqueous media with THF, *Green Chem*, **18**(8): 2331–2334.
141. Cai, C.M., Zhang, T., Kumar, R. and Wyman, C.E., 2013, THF co-solvent enhances hydrocarbon fuel precursor yields from lignocellulosic biomass, *Green Chem*, **15**(11): 3140.
142. Cai, C.M., Nagane, N., Kumar, R. and Wyman, C.E., 2014, Coupling metal halides with a co-solvent to produce furfural and 5-HMF at high yields directly from lignocellulosic biomass as an integrated biofuels strategy, *Green Chem*, **16**(8): 3819–3829.
143. Krzelj, V., van Kampen, J., van der Schaaf, J. and Neira d'Angelo, M.F., 2019, Furfural Production by Reactive Stripping: Process Optimization by a Combined Modeling and Experimental Approach, *Industrial & Engineering Chemistry Research*, **58**(35): 16126–16137.
144. Agirrezabal-Telleria, I., Guo, Y., Hemmann, F., Arias, P.L. and Kemnitz, E., 2014, Dehydration of xylose and glucose to furan derivatives using bifunctional partially hydroxylated MgF2 catalysts and N2-stripping, *Catalysis Science & Technology*, **4**(5): 1357–1368.

145. García-Sancho, C., Agirrezabal-Telleria, I., Güemez, M.B. and Maireles-Torres, P., 2014, Dehydration of d-xylose to furfural using different supported niobia catalysts, *Applied Catalysis B: Environmental*, **152**: 1–10.
146. Agirrezabal-Telleria, I., Gandarias, I. and Arias, P.L., 2013, Production of furfural from pentosan-rich biomass: Analysis of process parameters during simultaneous furfural stripping, *Bioresource Technology*, **143**: 258–264.
147. Mandalika, A. and Runge, T., 2012, Enabling integrated biorefineries through high-yield conversion of fractionated pentosans into furfural, *Green Chemistry*, **14**(11): 3175.
148. van Buijtenen, J., Lange, J.-P., Espinosa Alonso, L., Spiering, W., Polmans, R.F. and Haan, R.J., 2013, Furfural production by 'acidic steam stripping'of lignocellulose, *ChemSusChem*, **6**(11): 2132–2136.
149. Köchermann, J., Görsch, K., Wirth, B., Mühlenberg, J. and Klemm, M., 2018, Hydrothermal carbonization: Temperature influence on hydrochar and aqueous phase composition during process water recirculation, *Journal of Environmental Chemical Engineering*, **6**(4): 5481–5487.
150. Sluiter, A., Hames, B., Ruiz, R., Scarlata, C., Sluiter, J., Templeton, D. and Crocker, D., 2005, *Determination of Structural Carbohydrates and Lignin in Biomass: Laboratory Analytical Procedure (LAP)*, Vol. 1617, Golden (Colorado).
151. Görsch, K., Kröger, M. and Klemm, M., 2016, Hydrothermal Liquefaction of Biomass for Chemicals, in: *Papers of the 24th European Biomass Conference and Exhibition : Setting the course for a biobased economy,* 06.-09.06.2016, Amsterdam, pp. 1096–1098.
152. Lorenz, D., Erasmy, N., Akil, Y. and Saake, B., 2016, A new method for the quantification of monosaccharides, uronic acids and oligosaccharides in partially hydrolyzed xylans by HPAEC-UV/VIS, *Carbohydrate Polymers*, **140**: 181–187.
153. Binder, J.B., Blank, J.J., Cefali, A.V. and Raines, R.T., 2010, Synthesis of furfural from xylose and xylan, *ChemSusChem*, **3**(11): 1268–1272.
154. Dunlop, A.P., 1948, Furfural Formation and Behavior, *Industrial & Engineering Chemistry*, **40**(2): 204–209.
155. Carrasco, F. and Roy, C., 1992, Kinetic study of dilute-acid prehydrolysis of xylan-containing biomass, *Wood Science and Technology*, **26**(3): 189–208.
156. Lavarack, B.P., Griffin, G.J. and Rodman, D., 2002, The acid hydrolysis of sugarcane bagasse hemicellulose to produce xylose, arabinose, glucose and other products, *Biomass and Bioenergy*, **23**(5): 367–380.

157. Morinelly, J.E., Jensen, J.R., Browne, M., Co, T.B. and Shonnard, D.R., 2009, Kinetic Characterization of Xylose Monomer and Oligomer Concentrations during Dilute Acid Pretreatment of Lignocellulosic Biomass from Forests and Switchgrass, *Industrial & Engineering Chemistry Research*, **48**(22): 9877–9884.

158. Köchermann, J., Mühlenberg, J. and Klemm, M., 2018, Kinetics of Hydrothermal Furfural Production from Organosolv Hemicellulose and D-Xylose, *Industrial & Engineering Chemistry Research*, **57**(43): 14417–14427.

159. Lamminpää, K., Ahola, J. and Tanskanen, J., 2014, Kinetics of furfural destruction in a formic acid medium, *RSC Advances*, **4**(104): 60243–60248.

160. Rose, I.C., Epstein, N. and Watkinson, A.P., 2000, Acid-catalyzed 2-furaldehyde (furfural) decomposition kinetics, *Industrial & Engineering Chemistry Research*, **39**(3): 843–845.

161. Williams, D.L. and Dunlop, A.P., 1948, Kinetics of Furfural Destruction in Acidic Aqueous Media, *Industrial & Engineering Chemistry*, **40**(2): 239–241.

162. Danon, B., van der Aa, L. and Jong, W. de, 2013, Furfural degradation in a dilute acidic and saline solution in the presence of glucose, *Carbohydrate Research*, **375**: 145–152.

163. Marcotullio, G., Cardoso, M.A.T., Jong, W. de and Verkooijen, A.H.M., 2009, Bioenergy II: Furfural Destruction Kinetics during Sulphuric Acid-Catalyzed Production from Biomass, *Int. J. Chem. React. Eng.*, **7**: A67.

164. Chen, Z., Zhang, W., Xu, J. and Li, P., 2015, Kinetics of xylose dehydration into furfural in acetic acid, *Chinese Journal of Chemical Engineering*, **23**(4): 659–666.

165. Kim, S.B., Lee, M.R., Park, E.D., Lee, S.M., Lee, H., Park, K.H. and Park, M.-J., 2011, Kinetic study of the dehydration of d-xylose in high temperature water, *React. Kinet., Mech. Catal.*, **103**(2): 267–277.

166. Oefner, P.J., Lanziner, A.H., Bonn, G. and Bobleter, O., 1992, Quantitative studies on furfural and organic acid formation during hydrothermal, acidic and alkaline degradation of D-xylose, *Monatsh. Chem.*, **123**(6-7): 547–556.

167. Kim, Y., Kreke, T. and Ladisch, M.R., 2013, Reaction mechanisms and kinetics of xylo-oligosaccharide hydrolysis by dicarboxylic acids, *AIChE J.*, **59**(1): 188–199.

168. Lau, C.-S., Thoma, G.J., Clausen, E.C. and Carrier, D.J., 2014, Kinetic Modeling of Xylose Oligomer Degradation during Pretreatment in Dilute Acid or in Water, *Industrial & Engineering Chemistry Research*, **53**(6): 2219–2228.

169. Rybinski, W. von and Hill, K., 1998, Alkyl Polyglycosides—Properties and Applications of a new Class of Surfactants, *Angewandte Chemie International Edition*, **37**(10): 1328–1345.

170. Grisel, R., van der Waal, J.C., Jong, E. de and Huijgen, W., 2014, Acid catalysed alcoholysis of wheat straw: Towards second generation furan-derivatives, *Catalysis Today*, **223**: 3–10.

171. Rubio-Caballero, J.M., Saravanamurugan, S., Maireles-Torres, P. and Riisager, A., 2014, Acetalization of furfural with zeolites under benign reaction conditions, *Catalysis Today*, **234**: 233–236.

172. Marinkovic, S. and Estrine, B., 2010, Direct conversion of wheat bran hemicelluloses into n-decyl-pentosides, *Green Chem*, **12**(11): 1929.

173. Bouxin, F., Marinkovic, S., Le Bras, J. and Estrine, B., 2010, Direct conversion of xylan into alkyl pentosides, *Carbohydrate Research*, **345**(17): 2469–2473.

174. Bhaumik, P. and Dhepe, P.L., 2016, Solid acid catalyzed synthesis of furans from carbohydrates, *Catalysis Reviews*, **58**(1): 36–112.

175. Hu, X., Lievens, C., Larcher, A. and Li, C.-Z., 2011, Reaction pathways of glucose during esterification: effects of reaction parameters on the formation of humin type polymers, *Bioresource Technology*, **102**(21): 10104–10113.

176. Nitzsche, R., Gröngröft, A. and Kraume, M., 2019, Separation of lignin from beech wood hydrolysate using polymeric resins and zeolites–Determination and application of adsorption isotherms, *Separation and Purification Technology*, **209**: 491–502.

177. Świątek, K., Gaag, S., Klier, A., Kruse, A., Sauer, J. and Steinbach, D., 2020, Acid Hydrolysis of Lignocellulosic Biomass: Sugars and Furfurals Formation, *Catalysts*, **10**(4): 437.

178. Pu, Y., Treasure, T., Gonzalez, R., Venditti, R.A. and Jameel, H., 2013, Autohydrolysis pretreatment of mixed softwood to produce value prior to combustion, *BioEnergy Research*, **6**(3): 1094–1103.

179. Rissanen, J.V., Grénman, H., Willför, S., Murzin, D.Y. and Salmi, T., 2014, Spruce hemicellulose for chemicals using aqueous extraction: Kinetics, mass transfer, and modeling, *Industrial & Engineering Chemistry Research*, **53**(15): 6341–6350.

180. Danon, B., Hongsiri, W., van der Aa, L. and Jong, W. de, 2014, Kinetic study on homogeneously catalyzed xylose dehydration to furfural in the presence of arabinose and glucose, *Biomass and Bioenergy*, **66**: 364–370.

181. Geng, W., Narron, R., Jiang, X., Pawlak, J.J., Chang, H., Park, S., Jameel, H. and Venditti, R.A., 2019, The influence of lignin content and structure on hemicellulose alkaline extraction for non-wood and hardwood lignocellulosic biomass, *Cellulose*, **26**(5): 3219–3230.

182. Lamminpää, K., Ahola, J. and Tanskanen, J., 2015, Acid-catalysed xylose dehydration into furfural in the presence of kraft lignin, *Bioresource Technology*, **177**: 94–101.
183. Körner, P., Jung, D. and Kruse, A., 2019, Influence of the pH Value on the Hydrothermal Degradation of Fructose, *ChemistryOpen*, **8**(8): 1109–1120.
184. Motagamwala, A.H., Huang, K., Maravelias, C.T. and Dumesic, J.A., 2019, Solvent system for effective near-term production of hydroxymethylfurfural (HMF) with potential for long-term process improvement, *Energy & Environmental Science*, **12**(7): 2212–2222.
185. Wei, Z., Liu, Y., Thushara, D. and Ren, Q., 2012, Entrainer-intensified vacuum reactive distillation process for the separation of 5-hydroxylmethylfurfural from the dehydration of carbohydrates catalyzed by a metal salt–ionic liquid, *Green Chemistry*, **14**(4): 1220–1226.
186. Zhang, Z., Wu, Y., Gao, L. and Xiao, G., 2021, Pervaporation separation of levulinic acid aqueous solution by ZSM-5/PDMS composite membrane, *Journal of Applied Polymer Science*, **138**(1): 49611.
187. Kumar, A., Shende, D.Z. and Wasewar, K.L., 2020, Extractive separation of levulinic acid using natural and chemical solvents, *Chemical Data Collections*, **28**: 100417.
188. Wang, B., Cong, H., Li, X., Li, H. and Gao, X., 2022, Selective and efficient separation of biomass hydrolysate levulinic acid and formic acid from aqueous solution, *Chemical Engineering Research and Design*, **181**: 266–277.
189. Nitsos, C.K., Matis, K.A. and Triantafyllidis, K.S., 2013, Optimization of hydrothermal pretreatment of lignocellulosic biomass in the bioethanol production process, *ChemSusChem*, **6**(1): 110–122.
190. Bariani, M., Boix, E., Cassella, F. and Cabrera, M.N., 2021, Furfural production from rice husks within a biorefinery framework, *Biomass Conversion and Biorefinery*, **11**(3): 781–794.

PUBLICATIONS

Previously published reports:

DBFZ Report Nr. 52 Strategies for Demand Side Management in Biorefineries – Exploring New Frontiers in Enhancing Load Flexibility and Optimization
DBFZ Report Nr. 51 Emissionsminderungsstrategien zur umweltverträglichen Verbrennung (UVV) auf Basis von aktuellen Forschungsergebnissen
DBFZ Report Nr. 50 Biogaserzeugung und -nutzung in Deutschland - Report zum Anlagenbestand Biogas und Biomethan
DBFZ Report Nr. 49 Modellregion Bioökonomie im Mitteldeutschen und Lausitzer Revier
DBFZ Report Nr. 48 Adsorption and Membrane Filtration for the Separation and Valorization of Hemicellulose from Organosolv Beechwood Hydrolyzates – Doctoral thesis
DBFZ Report Nr. 47 WasteGui: Guideline for organic waste treatment in East Africa
DBFZ Report Nr. 46 Wasserstoff aus Biomasse
DBFZ Report Nr. 45 Status-Quo of organic waste collection, transport and treatment in East Africa and Ethiopia
DBFZ Report Nr. 44 Monitoring erneuerbarer Energien im Verkehr
DBFZ Report Nr. 43 Beitrag zur Optimierung des Pelletierverhaltens von Gärresten und Landschaftspflegeheu sowie deren Mischungen
DBFZ Report Nr. 42 Rahmenbedingungen für einen optimierten Betrieb von kleinen biomassebasierten BHKW
DBFZ Report Nr. 41 National Resource Monitoring for Biogenic Residues, By-products and Wastes – Development of a Systematic Data Collection, Management and Assessment for Germany
DBFZ Report Nr. 40 Basics of Anaerobic Digestion - Biochemical Conversion and Process Modelling
DBFZ Report Nr. 39 Optimierte Regelungsstrategien für Pellet-Solar-Kombiheizanlagen zur Steigerung der Systemeffizienz bei gleichzeitiger Minimierung der Energiekosten
DBFZ Report Nr. 38 Hydrothermal processing of biogenic residues in Germany - A technology assessment considering development paths by 2030
DBFZ Report Nr. 37 Economic assessment of biogas plants as a flexibility option in future electricity systems
DBFZ Report Nr. 36 BioplanW: Systemlösungen Bioenergie im Wärmesektor im Kontext zukünftiger Entwicklungen
DBFZ Report Nr. 35 Leitfaden zur Substrat- und Effzienzbewertung an Biogasanlagen
DBFZ Report Nr. 34 Entwicklung einer Methode zur Verwendung der Daten des Schornsteinfegerhandwerks für die energiewirtschaftliche Berichterstattung - Dissertationsschrift
DBFZ Report No. 33 Recommendations for reliable methane emission rate quantification at biogas plants
DBFZ Report Nr. 32 Wärmenutzung von Biogasanlagen
DBFZ Report Nr. 31 Die Niedertemperatursynthese von Methan in Thermoöl-temperierten Plattenreaktoren – Dissertationsschrift –
DBFZ Report Nr. 30 Anlagenbestand Biogas und Biomethan – Biogaserzeugung und -nutzung in Deutschland
DBFZ Report Nr. 29 Effiziente Bioenergie für Regionen - Ergebnisse der technisch-ökonomischen Begleitforschung zur Fördermaßname Bioenergie-Regionen 2012-2015
DBFZ Report Nr. 28 Potenziale zur Steigerung der Leistungsfähigkeit von Biogasanlagen - Energetische Effizienz von Repoweringmaßnahmen
DBFZ Report Nr. 27 Neuartiger emissionsarmer Kaminofen (DBU-NEKO)
DBFZ Report Nr. 26 Bewertung technischer und wirtschaftlicher Entwickoungspotenziale künftiger und bestehender Biomasse-zu-Methan-Konversionsprozesse - Dissertationsschrift
DBFZ Report Nr. 25 Nachrüstlösung zum katalytischen Abbau von gasförmigen organischen Emissionen aus Kaminöfen
DBFZ Report Nr. 24 Biomasse zur Wärmeerzeugung– Methoden zur Quantifizierung des Brennstoffeinsatzes
DBFZ Report Nr. 23 Technisch-ökonomische Begleitforschung des Bundeswettbewerbes „Bioenergie-Regionen“
DBFZ Report Nr. 22 Die Biokraftstoffproduktion in Deutschland – Stand der Technik und Optimierungsansätze
DBFZ Report Nr. 21 Entwicklung der Förderung der Stromerzeugung aus Biomasse im Rahmen des EEG
DBFZ Report Nr. 20 KlimaCH4 – Klimaeffekte von Biomethan
DBFZ Report Nr. 19 Hy-NOW – Evaluierung der Verfahren und Technologien für die Bereitstellung von Wasserstoff auf Basis von Biomasse
DBFZ Report Nr. 18 Kleintechnische Biomassevergasung – Option für eine nachhaltige und dezentrale Energieversorgung
DBFZ Report Nr. 17 Grünlandenergie Havelland – Entwicklung von übertragbaren Konzepten zur naturverträglichen energetischen Nutzung von Gras und Schilf am Beispiel der Region Havelland
DBFZ Report Nr. 16 Algae biorefinery – material and energy use of algae
DBFZ Report Nr. 15 Politics and Economics of Ethanol and Biodiesel Production and Consumption in Brazil
DBFZ Report Nr. 14 Holzpelletbereitstellung für Kleinfeuerungsanlagen
DBFZ Report Nr. 13 Basisinformationen für eine nachhaltige Nutzung von landwirtschaftlichen Reststoffen zur Bioenergiebereitstellung
DBFZ Report Nr. 12 Monitoring zur Wirkung des Eneuerbare-Energien-Gesetz (EEG) auf die Entwicklung der Stromerzeugung aus Biomasse
DBFZ Report Nr. 11 Monitoring Biokraftstoffsektor
DBFZ Report Nr. 10 Ermittlung des Verbrauchs biogener Festbrennstoffe im Sektor Gewerbe, Handel, Dienstleistungen (GHD-Sektor) – Endbericht
DBFZ Report Nr. 9 Analyse und Bewertung ausgewählter zukünftiger Biokraftstoffoptionen auf der Basis fester Biomasse
DBFZ Report Nr. 8 – Kompakt – Sammelband
DBFZ Report Nr. 7 Final Report – Global and Regional Spatial Distribution of Biomass Potentials – Status quo and options for specication –

Further information and free downloads:
www.dbfz.de/en/press-media-library/publication-series/dbfz-reports

DBFZ Deutsches Biomasseforschungszentrum
gemeinnützige GmbH
Torgauer Straße 116
04347 Leipzig
Phone: +49 (0)341 2434-112
E-Mail: info@dbfz.de

www.dbfz.de